The Pennsylvania State University

The Graduate School

Department of Mechanical Engineering

DEVELOPMENT OF A NEW OFF-ROAD RIGID RING MODEL FOR TRUCK TIRES USING FINITE ELEMENT ANALYSIS TECHNIQUES

A Thesis in

Mechanical Engineering

by

Jeffrey L. Slade

© 2009 Jeffrey L. Slade

Submitted in Partial Fulfillment

of the Requirements

for the Degree of

Master of Science

August 2009

The thesis of Jeffrey L. Slade was reviewed and approved* by the following:

Moustafa El-Gindy
Senior Scientist, Applied Research Laboratory
Thesis Co-Advisor

Kevin Koudela
Senior Research Associate, Applied Research Laboratory
Thesis Co-Advisor

Amanul Haque
Associate Professor of Mechanical Engineering
Thesis Reviewer

Karen Thole
Professor of Mechanical Engineering
Head of the Department of Mechanical and Nuclear Engineering

*Signatures are on file in the Graduate School.

ABSTRACT

Finite Element Analysis (FEA) is a powerful tool which allows researchers to use computers to quickly perform simulations of many complex physical objects. In this thesis, non-linear three dimensional FEA models are developed using PAM-CRASH to perform simulations of heavy truck tires running on both rigid surfaces and soils. These models include an FEA truck tire model and an elastic-plastic FEA soil model. The FEA models are then used to calculate parameters for a new semi-empirical off-road rigid ring model.

An FEA truck tire model of a Goodyear RHD 315/80R22.5 drive tire for tractor semi-trailers is generated and the properties are tuned to match the manufacturer's specifications. Simulations are performed under typical loading conditions to establish the behavior of the tire. An elastic-plastic FEA soil model, designed to represent sandy loam, is developed using material properties from published data and is validated using a number of previously published techniques. The construction of the tire and soil models and the methods used for validation are explained in detail in this thesis. A comparison between the tire running on rigid road and soft soil is made by performing various simulations for both cases.

A new semi-empirical off-road rigid ring tire model is developed as a simplified model to describe the behavior of a heavy truck tire running on soft soil. This model is a modification of the rigid ring tire model developed by Pacejka and Zegelaar and includes additional parameters to incorporate the flexibility of the soil. Rigid ring parameters for the Goodyear RHD 315/80R22.5 truck tire are calculated for both the on and off-road rigid ring models.

The results show that, in general, for a tire running on a sandy loam the motion resistance coefficient is approximately three times higher than on rigid road. The longitudinal slip stiffness is about a factor of four lower for sandy loam than for rigid road. This indicates that the available tractive force on sandy loam is about one-fourth of the available tractive force on rigid road. Interestingly, the longitudinal, or tractive force, appears to continue to increase with slip on sandy loam, while the tractive forces on rigid road level out after reaching a peak around 20% slip. When the tire and soil model is run at high slip angle it is noticed that the

soil begins to 'build up' in front on the tire, causing an additional lateral force due to the pushing of the soil.

Utilizing well validated and robust FEA models to predict the off-road behavior of tires may reduce the need to perform physical experiments, thereby reducing the cost and time required to obtain results and affect design changes. The off-road rigid ring model can be used in industry for full vehicle simulations for durability testing and structural dynamics. It is safe to assume that the use of finite element analysis in research and development will continue to rise as the available processing power of computers increases and become cheaper.

TABLE OF CONTENTS

LIST OF FIGURES

LIST OF TABLES

NOMENCLATURE

Symbol	Description	Unit
a	Half contact length between tire and road surface	m
c	Cohesion constant of soil	-
C_{10}, C_{01}	Mooney-Rivlin coefficient	kN/m^2
C_{bx}, C_{bz}	In-plane translational damping of sidewall	kN s/m
C_{by}	Out-of-plane translational damping constant	kN s/m
$C_{b\gamma}$	Out-of-plane rotational damping constant	kN m s/rad
$C_{b\theta}$	In-plane rotational damping of sidewall	kN m s/rad
C_c	Critical damping constant	kN s/m
C_l	Out-of-plane slip damping constant	kN s/m
C_{vr}	Residual damping constant	kN s/m
d	Tire deflection due to loading	m
E	Young's modulus of the soil	MPa
f	Stretching force on a single chain molecule	kN
f_r	Rolling resistance coefficient	-
F_x	Longitudinal or tractive force	kN
F_y	Lateral force	kN
f_y	Yaw oscillation frequency	Hz
F_{y_R}	Resultant lateral force	kN
F_z	Vertical or normal force	kN
F_{z_R}	Resultant vertical force	kN
G	Shear modulus of the soil	MPa
I_{ax}, I_{az}	Mass moment of inertia of wheel rim about X- and Z-axis	kg m^2
I_{ay}	Mass moment of inertia of wheel rim about Y-axis	kg m^2
I_{bx}, I_{bz}	Mass moment of inertia of tire about X- and Z-axis	kg m^2
I_{by}	Mass moment of inertia of tire about Y-axis	kg m^2
K	Bulk modulus of the soil	MPa
k_{bx}, k_{bz}	In-plane translational stiffness of sidewall	kN/m
k_{by}	Out-of-plane translational stiffness	kN/m

$k_{b\gamma}$	Out-of-plane rotational stiffness	kN m/rad
$k_{b\theta}$	In-plane rotational stiffness of sidewall	kN m/rad
k_{cx}	Longitudinal tread stiffness	kN/m
k_f	Cornering stiffness	kN/rad
k_k	Longitudinal slip stiffness	kN/slip unit
k_l	Lateral slip stiffness	kN/m
k_M	Self-aligning moment stiffness	kN m/rad
k_{tot}	Tire total vertical stiffness	kN/m
k_{vr}	Residual vertical stiffness	kN/m
m_a	Wheel rim mass	kg
m_b	Tire belt mass	kg
m_{tot}	Mass of the tire and rim ($m_a + m_b$).	kg
m_{tread}	Mass of the tread of the tire only	kg
M_x	Overturning moment	kN m
M_y	Rolling resistance moment	kN m
M_z	Vertical or aligning moment	kN m
n	Exponent from terrain values in Bekker equation	-
R	Radius of the inflated tire before loading	m
R_e	Effective rolling radius	m
R_{drum}	Drum radius	m
v, v_{tire}	Tire speed	m/s
v_{drum}	Drum speed	-
v_{tr}	Tread speed	-
Y	Yield stress of the soil	MPa
z	Sinkage of disk in Bekker equation	m
α	Slip angle	rad
δ	Log decrement	-
γ	Amplitude ratio of the output to yaw oscillation input	-
Θ_{ss}	Steady state angle value for rotation	rad
Θ_1	First peak angle used for calculating log decrement	rad
Θ_2	Second peak angle used for calculating log decrement	rad

ϕ	Phase angle	rad
ρ	Density of soil	ton/mm^3
τ	System time constant	s
τ_d	Damped period of vibration	s
ω	Wheel angular speed	rad/s
ω_d	Damped natural frequency	rad/m
ω_{drum}	Drum angular speed	rad/s
ω_n	Undamped natural frequency	rad/m
ω_{path}	Path frequency	rad/m
ω_y	Yaw oscillation frequency	rad/s
ζ	Damping ratio	-

ACKNOWLEDGEMENTS

The author expresses his appreciation to Mukesh Trivedi, Fredrik Öijer of Volvo 3P for their continuous financial and technical support through the course of this thesis research. The author also expresses his gratitude to the Applied Research Laboratory (ARL) of the Pennsylvania State University and Dr. Dick Stern, director of the E&F Graduate Assistant program for the opportunity and financial support to perform this research. Dr. Moustafa El-Gindy, my advisor and chair of my committee has provided me with a great amount of direction and support for this research. Special thanks are also owed to members of my graduate committee: Dr. Kevin Koudela, Dr. Amanul Haque, and Dr. Karen Thole.

On a personal note, I would like to give thanks to my family and friends for their continuous encouragement during the many challenges I have experienced throughout my studies.

CHAPTER 1

INTRODUCTION

This chapter will serve as an introduction to the work completed in this thesis. There are four sections to this chapter: motivation, literature survey, objectives and scope, and an outline of this thesis.

1.1 MOTIVATION

Tires and the vehicles they are mounted to comprise an inherently complex system with a large number of degrees of freedom. Due to these complexities the automotive industry is always looking to improve tire and vehicle dynamics models for use during the vehicle design phase. Models allow a designer to determine the effects of design changes far more quickly and inexpensively than by constructing and testing prototypes. There are many types of models available today ranging from empirical equations for contact forces under specific loads and speeds, such as Pacejka's magic tire formulas (Pacejka et al., 1997), to full Finite Element Analysis (FEA) models capable of modeling the tire dynamics and internal tire stresses.

FEA models have the advantage of having a relatively quick set-up time and being less expensive when compared to physical testing of tires and vehicles. Physical testing may require expensive custom machinery, equipment, and sensors, as well as large facilities to perform the tests and house the machinery. Analyzing the data from physical tests requires a significant amount of post-test processing, whereas it is simple and easy to obtain results from FEA models. In addition, errors in measurements and faulty test procedures or equipment may require repeat testing to achieve accurate results. The future of FEA computer models will allow very detailed analyses of tires and vehicles, giving rise to an increased understanding of the underlying physics in off road vehicle design, as well as accelerating research.

1.2 LITERATURE REVIEW

This literature survey presents work related to analytical modeling of tires, finite element analysis modeling of tires, and the interaction of tires with road and soil. This literature is introduced in order to provide the necessary background for understanding this thesis and to examine the current state of research in the fields of tire and soil modeling.

1.2.1 RADIAL PLY PNEUMATIC TIRE

The radial ply pneumatic tire is a complex device consisting of several different components such as rubber, steel belts, and nylon or aramid cords. The role of the pneumatic tire for wheeled vehicles is an extremely important one which greatly impacts the performance of a vehicle. Since the pneumatic tire is the only component of a vehicle that contacts the ground, it is therefore the only means for transferring forces from the vehicle to the road. In addition to transferring vehicle forces to the road for acceleration, braking, and cornering, a tire also serves as a spring and damper system to isolate the vehicle from shocks caused by sudden changes in the road profile. This is important for ride comfort as well as maintaining vehicle stability, control, and durability.

There are two main types of pneumatic tires that have been used on vehicles in recent history. Bias-ply tires were the standard design until Michelin introduced the radial-ply tire in 1946 (Michelin AG, 2009). Figure 1.1 shows the construction of a typical radial ply truck tire. Radial-ply tires are almost exclusively used now due to several advantages over bias-ply tires. Some of these advantages include decreased rolling resistance due to decreased internal friction between plies, improved contact patch due to better road conformity, and improved handling and ride comfort characteristics (Michelin AG, 2009). Both radial- and bias-ply tires have a carcass made from steel and/or nylon/aramid plies; however, the orientation of the cords and belts is different between the two tire types. In a radial-ply tire there are radially oriented cords running directly from one bead to the other. Layers of belts cross each other at a cord angle ($\pm 20°$ as in Figure 1.2) and reinforce the tread (Tönük and Ünlüsoy, 2001). Figure 1.2 shows a comparison of the cord angles for bias-ply and radial-

ply tires. Tönük and Ünlüsoy created an FEA model and performed simulations over a range of slip angles (0° to 7° slip) and vertical loads (1.5 kN to 4.5 kN) to determine lateral forces. The simulation data was compared with experimental data, and it was found that the model successfully predicted lateral forces to an acceptable degree of accuracy. This research led Tönük and Ünlüsoy to deem that FEA models were a valuable tool for tire design.

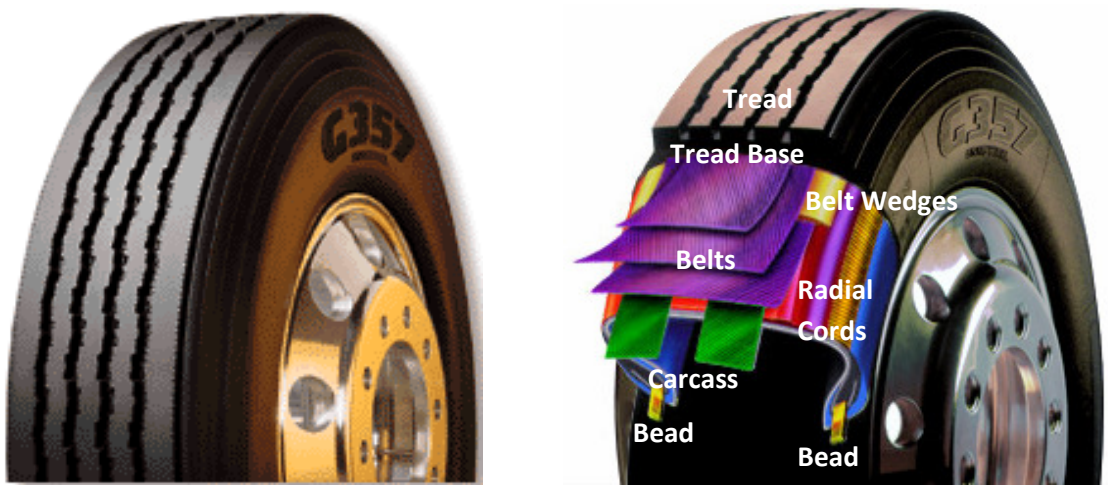

(a) 297/75R22.5 Truck Tire (b) Tire components

Figure 1.1: Radial truck tire with cutaway (retrieved from www.goodyear.com)

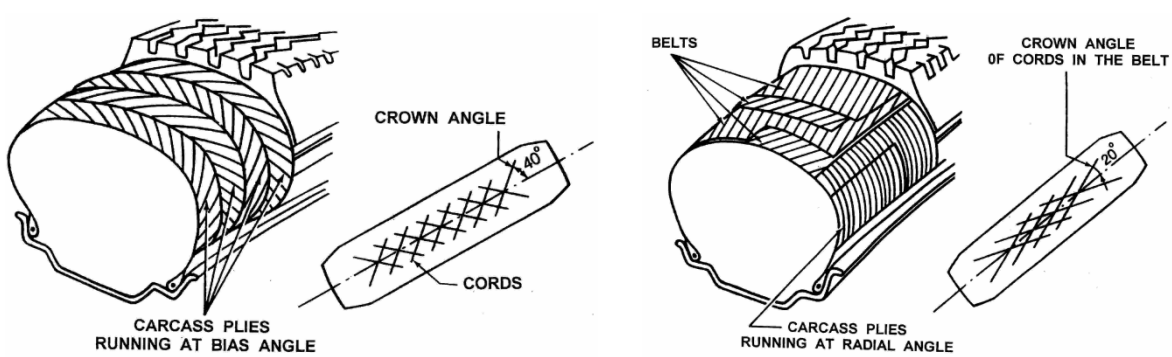

(a) Bias-ply tire (b) Radial-ply tire

Figure 1.2: Typical tire construction comparison (Wong, 2001)

1.2.2 THE RIGID RING TIRE MODEL

The rigid ring tire model is a simple analytical tire model that captures some of the tire's dynamic behavior. The model was initially developed by Zegelaar and Pacejka in 1997 and was used to model a passenger car tire. The model, shown in Figure 1.3, has five degrees of freedom and uses five sets of springs and dampers to represent the rotational stiffness, vertical stiffness, longitudinal stiffness, residual tread stiffness and longitudinal slip stiffness of the tire (Zegelaar, 1997). The tread belt of the tire is modeled as a rigid ring with the springs and dampers connecting the tread to a centrally located rigid rim. The residual vertical stiffness parameter arises because the tread's elastic properties are ignored as the tread is modeled as a simple rigid ring. This model therefore incorporates the tread's elasticity by adding a spring and damper beneath the rigid ring to represent the residual vertical stiffness and damping. Additionally, the longitudinal slip between the ground and the tire is modeled as a spring and damper to allow for velocity differences.

In order to test and validate the tire model, it was placed on a 2.5 meter diameter drum model and vertically loaded. The drum was rotationally accelerated to an equivalent linear velocity of 150 km/hr, and the vertical forces transmitted to the rim center and the effective tire rolling radius were measured. Excitations were applied to the tire in order to measure the frequency response and calculate the appropriate parameters for the rigid ring model. It was found that there is a positive relationship between the vertical force and rotational speed as well as the effective rolling radius of the tire and rotational speed (Zegelaar, 1997).

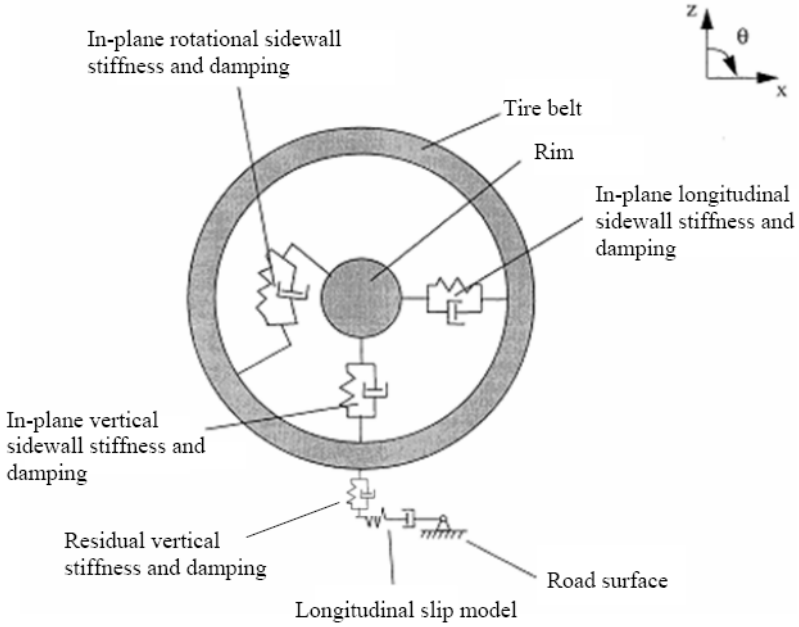

Figure 1.3: Rigid ring tire model (Zegelaar, 1997)

In 1985 Loo developed a pneumatic tire model consisting of a mass-less flexible tread band connected to a rigid center by a series of radially arranged linear springs and dampers. The model, shown in Figure 1.4, was developed to predict the rolling resistance and vertical load-deflection characteristics of the tire. The parameters for the springs and dampers were obtained by performing static load tests and contact patch size measurements on the tire model. The model was successfully validated using experimental data for comparison.

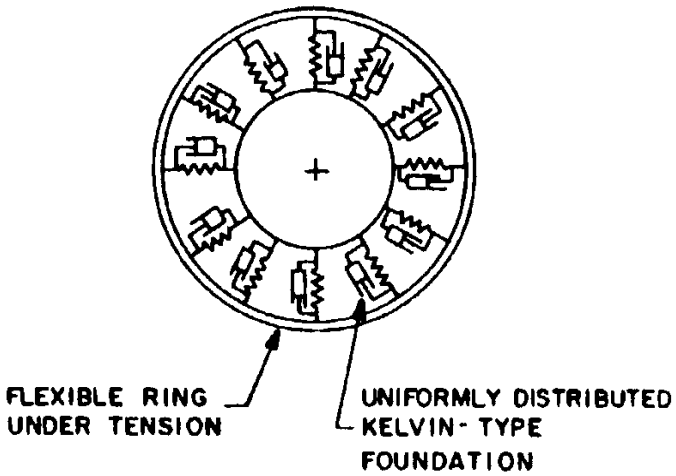

Figure 1.4: Loo's flexible ring tire model (Chang et. al, 2003)

In 1997 Bruni et al. and Allison and Sharp also utilized a rigid ring model with a rigid tread band to analyze vehicle handling and comfort. Their work focused on modeling vehicle vibrations and comfort in the low frequency range up to approximately 100 Hz. In 2004 Schmeitz et al. expanded on this work by developing a quarter-vehicle model consisting of a rigid ring tire model, a spring and damper suspension system, and a sprung mass. Elliptical cams were used to produce a road profile with vertical excitations. The model was found to predict vertical tire motion and longitudinal forces well when compared with actual measurements.

1.2.3 FINITE ELEMENT ANALYSIS TIRE MODELING

Finite Element Analysis (FEA) has proven to be a powerful tool for simulating a variety of different terramechanics problems. In 1978 Yong et al. investigated the performance of off-road pneumatic tires. A series of tests were performed to determine the stiffness of the tire carcass and the available tractive force as functions of tire inflation pressure. The laboratory and FEA tests were compared with analytical calculations and found to be in good agreement. The work determined that FEA can produce accurate tire-soil interaction results if the characteristics of the tire under load are well understood. This work was corroborated by Hiroma et al. in 1997 when FEA was used to predict the tractive forces and pressure distributions beneath a rolling wheel. Hiroma et al. found that the FEA predictions were reasonable when compared to measurements and concluded that, under low slip conditions, finite element analysis methods can be used to predict traction.

Wallentowitz et al. wrote a paper in 1999 comparing experimental testing and simulations in determining both static and dynamic tire characteristics. Tire models at the time of the paper were found to be either too simple to model dynamic behavior or were too time-consuming to be practical. A dynamic tire test rig was designed and installed at the Institut für Kraftfahrwesen Aachen, Germany with the purpose of providing data to improve tire models. Over a range of slip angles, the lateral forces, self-aligning torques, and sinusoidal steering characteristics of automobile tires were measured. This data is and has been very useful for

model tuning and validation purposes when comparing experimental data to trends obtained from FEA simulations.

1.2.4 FINITE ELEMENT ANALYSIS SOIL MODELING

Modeling of off-road vehicle dynamics is a very complex issue that has been a subject of research for some time. To properly model the performance characteristics of off-road vehicles, both the tires and soil must be accurately modeled. In addition, modeling the interaction between the tire and soil is required for accurate driving forces (such as braking and traction performance). These issues currently make tire-soil interaction analysis very difficult and time-consuming to simulate.

In order to attempt to model soil it is first necessary to determine the material properties and characteristics of soil. Properties such as density, shear modulus, bulk modulus, elastic modulus, yield stress and viscosity must be measured for the soil in question. Various equipment and techniques are used to measure these properties such as the bevameter, cone-penetrometer, cone-index, motorized rheometer (Karmakar 2006), pressure-sinkage test, and angular torque soil strain. Many authors (such as Janosi *et. al* (1965 and 1961), Wismer and Luth (1973), Brixius (1987), Wittig and Alcock (1992) and Bekker (1956, 1960 and 1969)) have developed equations to describe the behavior of soils, and the equations have been validated using material property data obtained from soil testing.

The rolling resistance of a tire on soil is heavily dependent on the amount that the tire sinks into the soil. Therefore, an important characteristic of soil behavior is the relationship between pressure and soil sinkage. An equation for the pressure-sinkage relationship of various soils was developed by Bekker in 1956 using Mohr-Coulomb failure criterion. Bekker tabulated parameters for a wide range of soil types that can be used to predict the pressure distribution under a tire. Janosi and Hanamoto developed models to predict traction characteristics on soil using a uniform pressure distribution with stress-strain relationships in 1961. In 1973 and 1987, respectively, Wismer et. al and Brixius developed equations to predict the tractive performance of tires using soil parameters such as the cone index.

Okello determined in 1991 that the bevameter technique was superior to the cone-penetrometer for determining soil properties. The bevameter technique consists of two types of basic tests to determine the surface properties of soil. The first test is a plate penetration test in which a plate of similar area to a tire is loaded on soil and the pressure-sinkage relationship is determined. The second test is a shear test which measures the shear strength of the soil by pushing a finned plate through the soil and measuring reaction forces. Figure 1.5 shows rectangular and annular shear plates. Figure 1.6 shows a cone penetrometer for determining soil properties. Okello's results were in agreement with Wittig and Alcock's tests to determine the maximum transferrable torque for a wheel loaded on soil. Wittig and Alcock also added that soil parameters such as bulk density and moisture content had a very large effect on off-road tire performance.

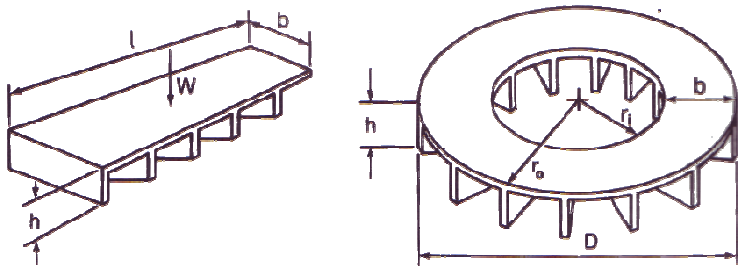

Figure 1.5: Rectangular and annular shear plates for measuring terrain shear strength parameters (Wong, 1993, pp. 104).

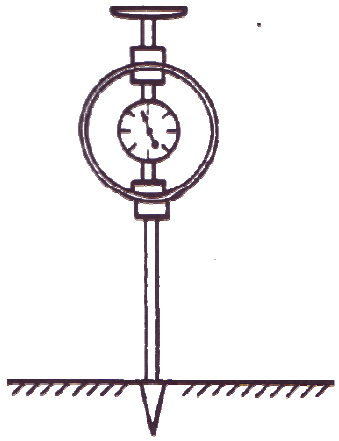

Figure 1.6: Cone penetrometer for determining the consistency and weight bearing capacity of soils (Wong, 1993, pp. 87).

Another very important phenomenon in accurately predicting tire sinkage and rolling resistance is the effect of penetration velocity. Much as a water skier is able to glide along the water surface instead of sinking into the water when traveling at high speeds, off-road vehicles encounter a similar effect. If a vehicle is traveling at high speed over a soft soil, such as sand or snow, it is able to avoid sinking into the soil. Grahn studied this effect in 1992 and developed a simplified model for testing the dynamic pressure-sinkage properties of soil. The tests were performed by pushing a plate into the soil of choice (sandy loam in this case) at various velocities and using force measurement data to calculate the pressure under the plate. The data revealed that, for a constant pressure, as penetration velocity increased the sinkage decreased. Rolling resistance therefore also decreased as penetration velocity increased since rolling resistance has an inverse relationship with tire sinkage. In addition, tests with a rigid wheel were performed and discovered that the point of highest pressure occur in front of the tire as opposed to directly beneath it.

Masad et al. developed a new critical state model in 1998 that includes parameters containing information about the soil's structure. Prior research shows that directionality (anisotropy) of the voids in clay, referred to as the "fabric" of the soil in this paper, have an effect on the stress-strain behavior of the soil. This model is an extension to the cam-clay critical state models developed by Cambridge University and includes a number of additional parameters. Their work concluded that there is a structure to some soils which collapses at a certain strain, appearing as a strain-softening effect. Once the structure of the soil is broken down, the soil follows the behavior of the original cam-clay models. The newly developed model was found to be far superior to the modified cam-clay model in capturing the stress-strain relationships of the soil.

In 2004 Fervers used the Drucker-Prager material with extended Cap-Plasticity available in ABAQUS® to model soils. Two soil types were modeled: a wet loam with high cohesion and dry sand with low cohesion. The tire was run at a constant speed on both soil types at low and high inflation pressures. It was found that, for the lower inflation pressure on the loam, the soil compacted less and pressure contours went less deep into the soil. On the sand,

however, the soil compacted more with lower inflation pressures due to the low cohesion and internal shear between soil particles.

In 2003 Al-Shayea et al. developed a soil model to predict the stress-strain behavior of isotropic post peak-stress strain-softening soils such as clays and dense sand. These types of soil exhibit a drop in stress once a certain strain is reached. The model captures this behavior by combining an elastic-plastic model and an elastic-damage model. Two methods were used for determining the plastic strain. In the first method the plastic strain was assumed to be the damage strain multiplied by some factor. In the second method the plastic strain was calculated by applying the Drucker-Prager model. The parameters used for both methods come from conventional triaxial compression (CTC) tests. However, the second method required additional parameters determined by isotropic compression tests. The first method was validated and found to produce very good stress-strain predictions.

1.3 OBJECTIVES AND SCOPE

The primary objective of this thesis is to develop a new rigid ring model for use on soft soil. Current methods of modeling tire-soil interaction require full FEA models with large numbers of solid elements and a long processing time. An efficient off-road rigid ring model is desirable to industry and would help accelerate research and development for off-road vehicles. The scope of this thesis will include the development of an FEA tire model, an elastic-plastic FEA soil model, and a new off-road rigid ring model for an RHD tire on dense sand.

1.4 OUTLINE

Chapter 2 is an introduction to the methods used for tire modeling. Chapter 3 describes the technique used to model the soft soil. Chapter 4 introduces the original rigid ring model and the new off-road rigid model and explains its development. Chapter 5 describes the theory and calculations behind obtaining the in-plane rigid ring parameters. Chapter 6 describes the theory and calculations behind obtaining the out-of-plane rigid ring parameters. Chapter 7 discusses the conclusions of this thesis as well as recommendations for future work.

CHAPTER 2

TIRE MODELING USING PAM-CRASH

2.1 TIRE CONSTRUCTION

A four-groove Finite Element Analysis (FEA) truck tire, which was originally developed by Chae in 2006, has been modified to represent the Goodyear's off-road RHD 315/80R22.5 tire. The advantages of this tire model are its computational efficiency and proven stability. The time to complete a 1.8 second yaw oscillation maneuver simulation on rigid road is about 27 hours on a dual Pentium 4 PC. The FEA tire is quite detailed and includes many different tire components. Figure 2.1 shows the basic dimensions of the finite element tire model. Figure 2.2 shows a comparison between the actual tire and the FEA tire model. Technical data for the RHD 315/80R22.5 tire is shown in Table 2.1.

The model was created by first making half of the 3-dimensional tire cross-section in PATRAN. This half model was mirrored about the tire's longitudinal axis to create a full cross-section. The cross-section was then rotated about the tire axle axis in 6 degree increments to create the full tire with 60 equal pieces.

Figure 2.3 shows in detail the tire construction and the element types for each of the tire parts. These tire parts and materials include layered membrane elements for the tire carcass and Mooney-Rivlin elements for the bead fillers, shoulders, tread, and the undertread. The layered membrane elements allow for different material properties and orientations for three different layers in the same part. In this case the tire carcass includes the rubber tire carcass and the steel belts and cords. The steel cords run radially within the carcass from bead to bead. A circular beam element with a defined cross-sectional area and steel-like properties is chosen to represent the tire bead. The bead elements are attached directly to the bottom of the bead fillers. Figure 2.4 shows the half cross-section of the tire as well as the type of elements in each part.

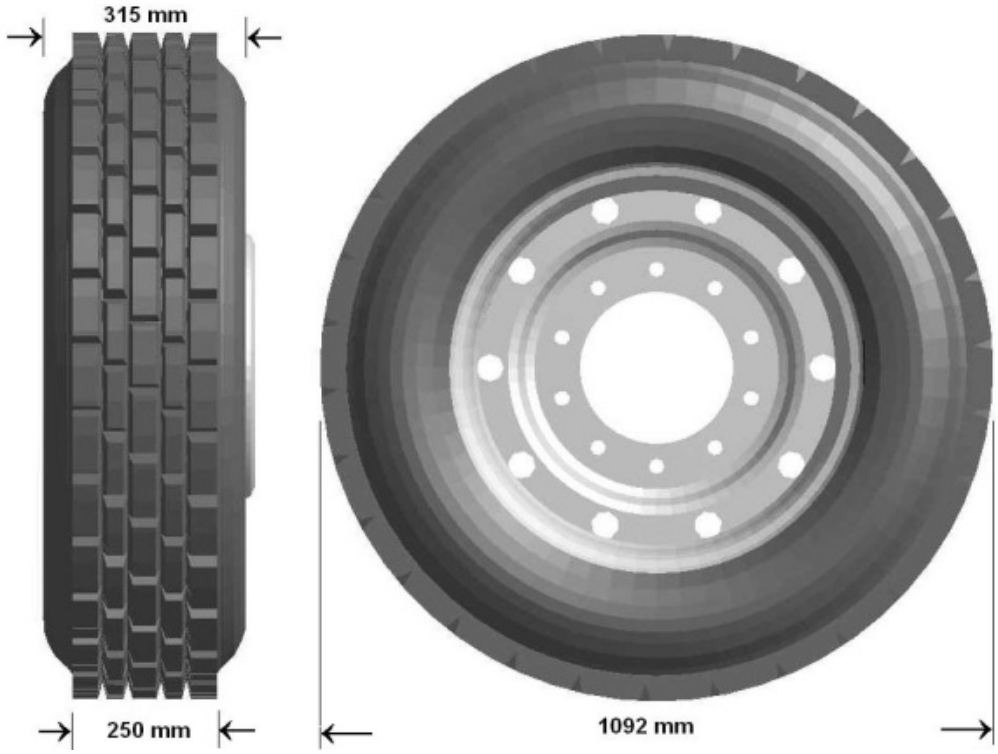

Figure 2.1: Tire basic dimensions.

(A) (B)

Figure 2.2: Comparison of actual (a) and detailed FEA (b) truck tires.

Table 2.1: Technical data for Goodyear RHD 315/80R22.5 tire (Truck Tires Technical Data Book, www.goodyear.com).

Tread depth	27 mm	1.063 in
Rim Width	229 mm	9.0 in
Rim Weight	34.8 kg	76.7 lbs
Tire Weight	72 kg	158 lbs
Total Tire Weight	106.8 kg	235.5 lbs
Overall Width	315 mm	12.4 in
Overall Diameter	1092 mm	43.0 in
Static Loaded Radius	505 mm	19.9 in
Speed Rating	120 km/hr	75 mph
Single Inflation	8.5 bar	123 psi
Dual Max Load	3350 kg	7390 lbs
Max Dual Inflation Pressure	8.5 bar	125 psi

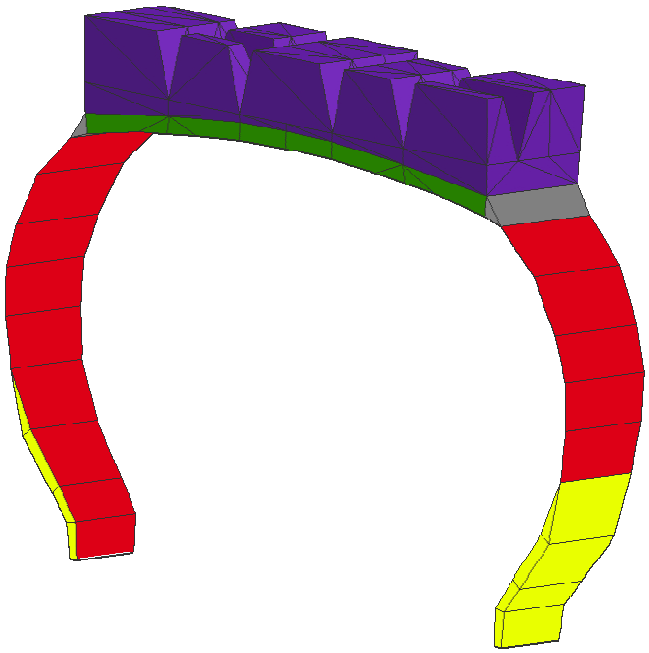

Figure 2.3: A single section of the FEA RHD 315/80R22.5 tire model. The complete tire is formed by copying and rotating this section 60 times. Layered membrane elements make up the tire carcass (red), while solid Mooney-Rivlin elements are used for the bead fillers (yellow), shoulders (grey), tread (purple), and undertread (green).

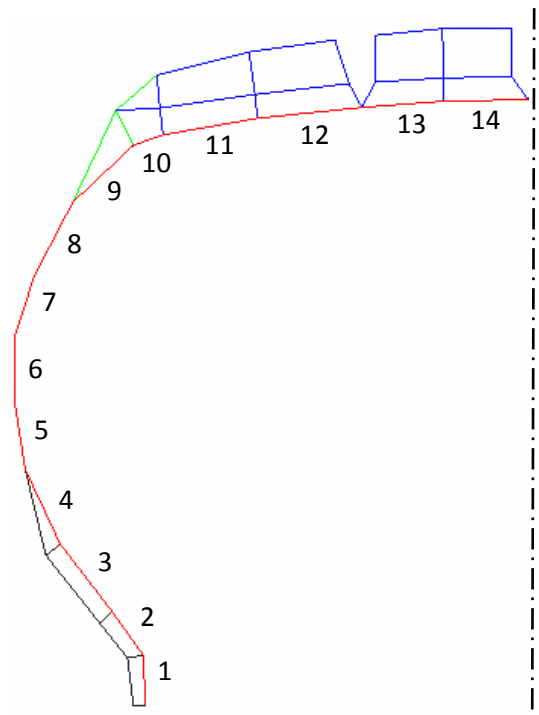

Figure 2.4: Location of the layered membrane elements (shown in red) and their corresponding part ID numbers in RHD truck tire model (Chae, 2006).

2.1.1 TREAD DESIGN

The tread patterns of the 4-groove truck tire (Chae, 2006) have been modified to more accurately represent the Goodyear RHD 315/80R22.5 tire tread. The RHD 315/80/R22.5 tire has an asymmetric tread pattern to help prevent the tire from trapping and holding stones in the tread. The complicated tread design was simplified to contain the fundamental elements while minimizing modeling and simulation processing time. Straight edges were used wherever possible to replace curves for the shape of the lugs and the grooves between the lugs. Each lug was simplified as rectangular with angled sides, and the grooves between lugs are simple V's. The tread depth is accurately modeled as 27 mm as specified by Goodyear's technical data. Solid tetrahedron (TET4) elements with Mooney-Rivlin material properties were chosen for the tread. Figure 2.5 shows the final FEA model tread design. The Mooney-Rivlin properties for the solid elements are shown in Table 2.2. Table 2.3 shows the material properties for the layered membrane elements in the tire carcass.

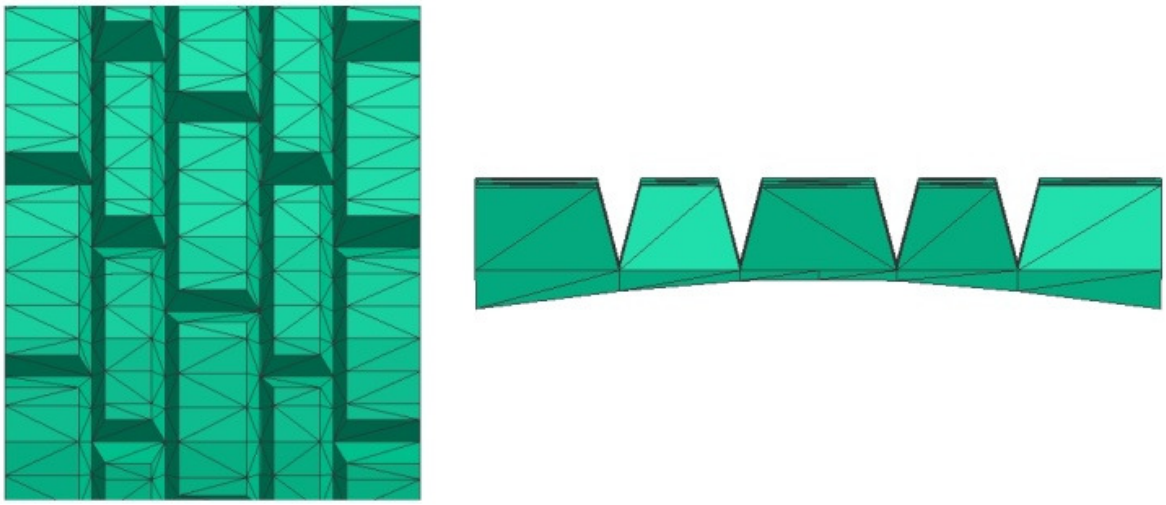

Figure 2.5: Tread design as viewed from above (left), and a cross-section of the tread showing the v-shaped grooves (right).

Table 2.2: Mooney-Rivlin material properties for solid rubber elements in tread, undertread, bead fillers, and tread shoulders.

Tire Component	Bead fillers	Tread shoulders	Under-tread	Tread
Density (kg/m^3)	882.0	693.3	596.2	693.3
1st Mooney-Rivlin coeff. (C_{10})	0.0392	0.670	0.0510	0.670
2nd Mooney-Rivlin coeff. (C_{01})	0.1268	2.460	0.1860	2.460
Poisson's ratio	0.499	0.499	0.490	0.490

Table 2.3: Material properties for layered membrane elements, which are shown as labeled 1-14 in Figure 2.4.

Tire Component					
Material I.D.	1	2	3	4	5
Density (kg/m^3)	763	764	763	733	721
Thickness (mm)	27	18	15	15	15
Isotopic parent sheet Young's modulus (MPa)	28	25	22	12	7
Isotopic parent sheet Poisson's ratio	0.3	0.3	0.3	0.3	0.3
Layer 1 Young's modulus (MPa)	36.5	31.5	49.8	42.9	40.6
Layer 1 Shear modulus (MPa)	0.0001	0.0001	0.0001	0.0001	0.0001
Layer 1 Angle of fibers with R-axis (deg)	0	0	0	0	0
Layer 2 Young's modulus (MPa)	0.0003	0.0003	0.0003	0.0003	0.0003
Layer 2 Shear modulus (MPa)	0.0001	0.0001	0.0001	0.0001	0.0001
Layer 2 Angle of fibers with R-axis (deg)	90	90	90	90	90

Tire Component					
Material I.D.	6	7	8	9	10
Density (kg/m^3)	723	719	725	744	8730
Thickness (mm)	15	15	15	12	7
Isotopic parent sheet Young's modulus (MPa)	7	7	7	9	14
Isotopic parent sheet Poisson's ratio	0.3	0.3	0.3	0.3	0.3
Layer 1 Young's modulus (MPa)	39.2	18	19.3	20.7	15.5
Layer 1 Shear modulus (MPa)	0.0001	0.0001	0.0001	0.0001	0.0001
Layer 1 Angle of fibers with R-axis (deg)	0	0	0	0	0
Layer 2 Young's modulus (MPa)	0.0003	0.0003	0.0003	0.0003	0.0003
Layer 2 Shear modulus (MPa)	0.0001	0.0001	0.0001	0.0001	0.0001
Layer 2 Angle of fibers with R-axis (deg)	90	90	90	90	90

Table 2.3 Cont.: Material properties for layered membrane elements labeled 1-14 as shown in Figure 2.4.

Tire Component				
Material I.D.	11	12	13	14
Density (kg/m^3)	1067	1065	1063	1063
Thickness (mm)	15	15	15	15
Isotopic parent sheet Young's modulus (MPa)	14	14	14	14
Isotopic parent sheet Poisson's ratio	0.3	0.3	0.3	0.3
Layer 1 Young's modulus (MPa)	20.2	15.5	15.5	19.8
Layer 1 Shear modulus (MPa)	0.0001	0.0001	0.0001	0.0001
Layer 1 Angle of fibers with R-axis (deg)	0	0	0	0
Layer 2 Young's modulus (MPa)	10700	10550	10550	10530
Layer 2 Shear modulus (MPa)	0.0001	0.0001	0.0001	0.0001
Layer 2 Angle of fibers with R-axis (deg)	90	90	90	90

2.2 TIRE CALIBRATION

There are many important characteristics for tires that must be matched closely in order to achieve the appropriate tire response. The static characteristics used for calibration and validation here include the vertical stiffness and trend comparison for the contact patch area.

2.2.1 VERTICAL STIFFNESS

The FEA RHD tire model was subjected to extensive testing to tune up the mechanical properties of the various parts in order to achieve reasonable load-deflection characteristics. Goodyear provided the Pennsylvania State University with load-deflection curves of generic 315/80R22.5 off-road tires at various inflation pressures, and this data was used for comparison with the FEA tire. In order to obtain the correct model characteristics, it is necessary to adjust the thickness (h), the Mooney-Rivlin coefficients for the rubber compounds of the tread and under-tread (C_{10} and C_{01}), and the modulus of elasticity (E) of the sidewall and of the under-tread of the tire model. A sensitivity analysis was performed

on the FEA tire model to determine the effect of changing each of these material properties on the tire's static deflection. The final tire model with the adjusted material parameters is shown under a 40 kN (9000 lb) static load with an inflation pressure of 85 psi in Figure 2.6.

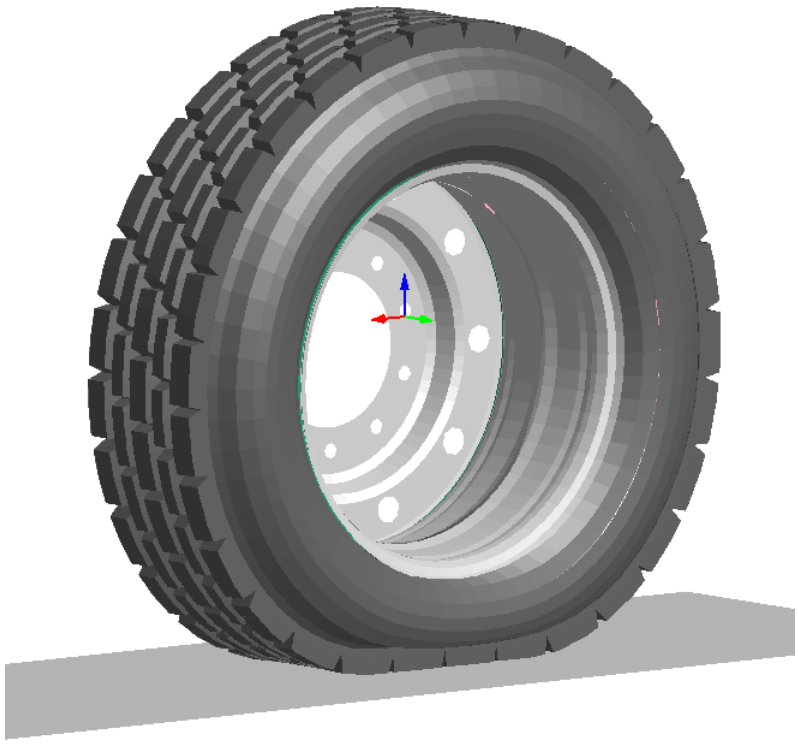

Figure 2.6: FEA RHD tire model under 40 kN load and 85 psi inflation pressure.

Figure 2.7 shows the static deflection curves from actual tire data provided by Goodyear and the simulation results using the FEA tire model over a wide range of loads and inflation pressures. Reasonable agreement can be observed and this data is presented as validation of the model. Figure 2.8 shows the relationship between the tire/road contact patch area and the applied load.

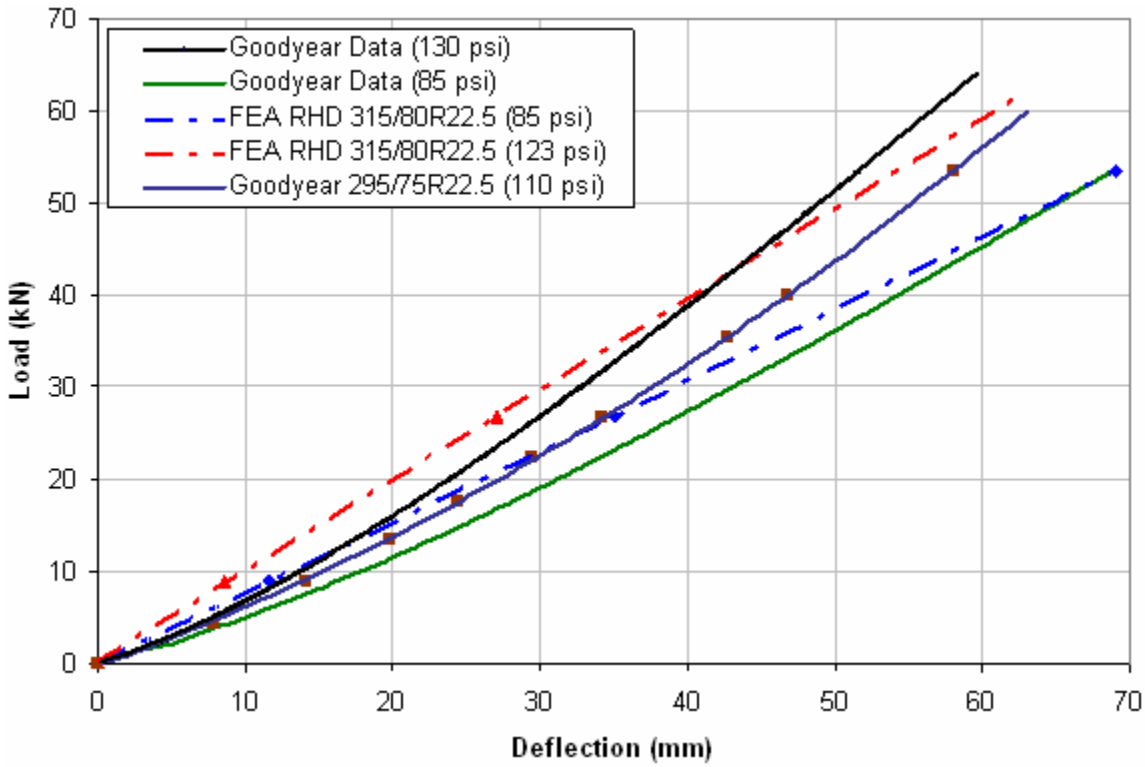

Figure 2.7: Load vs. deflection curve for FEA RHD 315/80R22.5 model and other similar tire measurements from Goodyear.

2.2.2 CONTACT PATCH AREA

The contact patch area of a tire at a given load is affected by the inflation pressure and the construction of the tire. Figure 2.8 shows the relationship between contact area and vertical load for measured data provided by Goodyear, previous tire model's developed by Chae in 2006, and the FEA RHD tire. The blue curve represents Chae's tire model, which is based on the data provided by Goodyear (yellow curve), and the red curve represents the FEA RHD tire. It can be seen that the trend of the curves are very similar for all of the tires, and the RHD tire appears to have a larger contact area than the other two tires for an equal load.

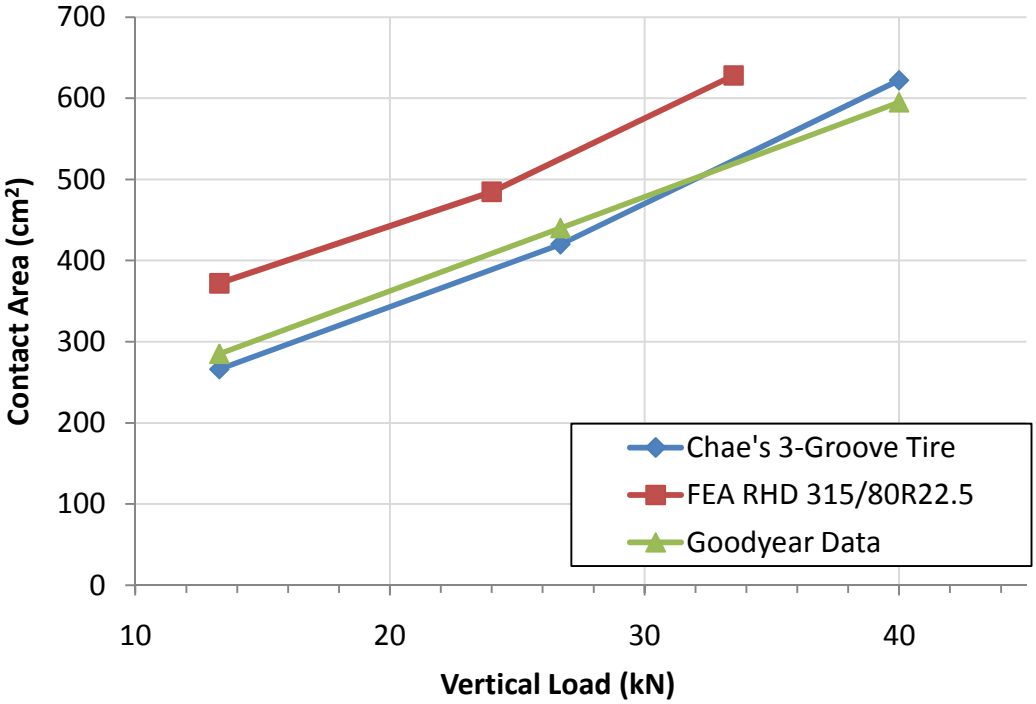

Figure 2.8: Relationship between tire to road contact area and vertical load for three truck tires with an inflation pressure of 110 psi.

2.2.3 DYNAMIC CLEAT DRUM TEST

Further important tire characteristics are the dynamic properties, such as the vertical and horizontal modes of free vibration. A rim-mounted tire can be modeled as a mass-spring-damper system. The mass is distributed throughout the system, however, the majority of the mass is located in the steel plies and tread near the outer edge of the tire (Allen II, 2007). The stiffness of the system is controlled by the inflation pressure and the material properties in the sidewalls of the tire. This setup allows for the tread and belts to resonate vertically and horizontally. Internal damping within the rubber carcass, the tread, and the steel belts has the effect of shifting the natural frequencies at which these modes of vibration occur.

A cleat drum test was conducted to determine the first mode of longitudinal and vertical free vibration. A cleat drum is simply a drum with a bump, or cleat, attached to the surface. A tire running on the cleat drum must roll over the cleat, which acts as an impact to excite the tread and carcass of the tire. This impact causes the tire to vibrate, and these vibrations can be measured and investigated using frequency analysis to determine the modes of vibration. Figure 2.9 shows the FEA tire running on the virtual cleat drum test rig. The test was run with a tire load of 18.9 kN (4250 lbs) and an inflation pressure of 85 psi.

Figure 2.9: FEA tire model on cleat drum.

A fast fourier transform (FFT) algorithm was applied to the vertical reaction force at the tire spindle to obtain the frequency analysis shown in Figure 2.10. The peaks in the figure represent free vibration modes. The cleat drum rotates at an angular velocity of 15 rad/sec which results in approximately a 2.5 Hz excitation due to the cleat impact. This impact is shown by the first peak from around 1 to 4 Hz in the FFT. The second peak, at approximately 45 Hz, corresponds to the first longitudinal free vibration mode and the third

peak around 53 Hz represents the first vertical free vibration mode. The third peak, at approximately 67 Hz represents the second longitudinal mode of free vibration.

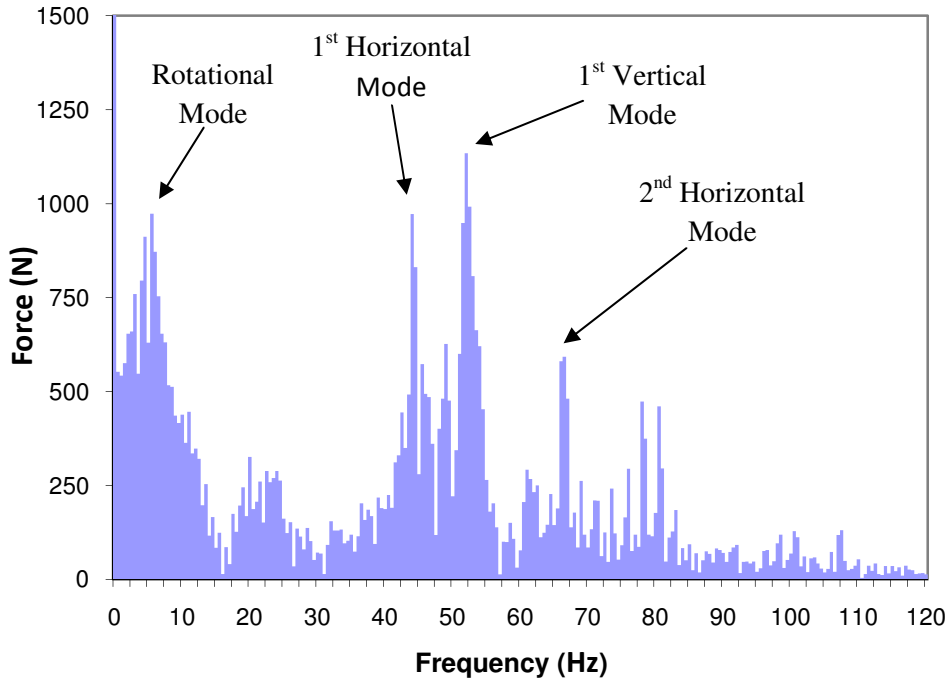

Figure 2.10: Vertical free vibration frequency response analysis for the RHD tire under an 18.9 kN (4250 lb) vertical load and 85 psi inflation pressure.

CHAPTER 3

SOIL MODELING AND VALIDATION USING PAM-CRASH

3.1 NEWLY DEVELOPED FEA SOIL MODELS

Four new types of soil were created using an elastic-plastic solid material (PAM-CRASH Material 1). The soils being modeled are a dense sand, loose sand, silty sand, and sand with gravel. Figure 3.1 shows the particle composition of various soil types (Idaho OnePlan, 2009). In this thesis, only the dense sand is fully validated and used for the calculations of the rigid ring model parameters. It should be noted that although dense sand does not appear on the composition triangle in Figure 3.1, dense sand can be considered very similar to the sandy loam. This simplified linear soil model takes into account the stiffness, yield stress, and density of the soil, however it does not include parameters for moisture and the cohesion of soil particles. The material properties for these new soils are listed in Table 3.1. It should be noted that the material properties have been chosen as the mean value of the ranges given in publications by the U.S. Department of Transportation, Federal Highway Administration.

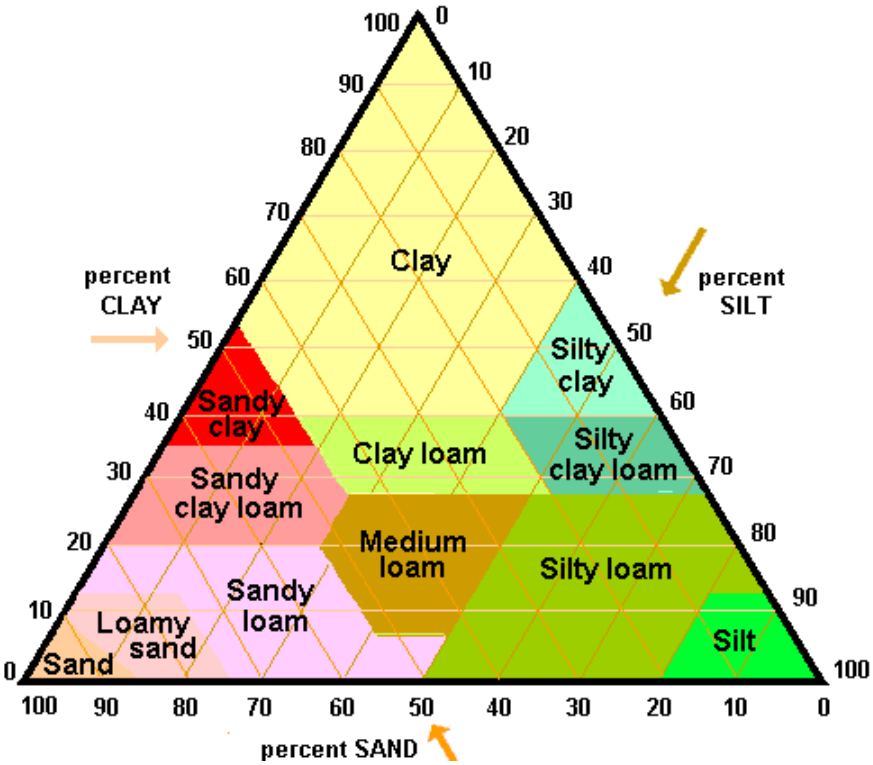

Figure 3.1: Composition of various soil types (Idaho OnePlan, 2009).

Table 3.1: Material properties for new types of soils.

Soil Type	Elastic Modulus, E (MPa)	Bulk Modulus, K (MPa)	Shear Modulus, G (MPa)	Yield Stress, Y (MPa)	Density, ρ (ton/mm^3)
Dense sand/sandy loam	22	15	9	0.016	1.60E-09
Loose sand	17	11	7	0.004	1.44E-09
Silty sand	45	30	18	0.02	1.68E-09
Sand and gravel	121	80	48	0.024	1.92E-09

3.2 VALIDATION METHODS

In order to validate the new soil models, a comparison has been made between published data and various quantifiable characteristics of the tire-soil interaction. These include trend comparisons of the longitudinal and lateral forces which occur between the tire and soil for a

range of slip angles and % longitudinal slip. In addition, pressure-sinkage curves and soil flow have also been compared.

3.2.1 PRESSURE-SINKAGE RELATIONSHIP

Soil characteristics can be compared and validated by looking at the relationship between applied pressure and soil sinkage. This type of testing is discussed in detail in Wong (2001). The pressure-sinkage test is performed by applying a known pressure over a circular plate placed on the soil and observing how far the plate sinks into the soil. The four new soils types can be compared using the Bekker formula (Equation 3.1) and the terrain values given in Table 3.2 (Wong, 2001) which are obtained from applying the Bekker formula to experimental data.

$$p = \left(\frac{k_c}{b} + k_\varphi\right) z^n \tag{3.1}$$

Where: z = sinkage of disk in meters.

b = radius of circular pressure plate in meters.

Table 3.2: Excerpt from table of terrain values, Table 2.3, in Wong (2001).

			k_c		k_φ		c		φ
Terrain	Moisture content (%)	n	lb/in.$^{n+1}$	kN/m^{n+1}	lb/in.$^{n+2}$	kN/m^{n+2}	lb/in.^{2}	kPa	deg
Dry sand (Land Locomotion Lab., LLL)	0	1.1	0.1	0.99	3.9	1528.43	0.15	1.04	28°
Sandy loam	15	0.7	2.3	5.27	16.8	1515.04	0.25	1.72	29°
Heavy clay	25	0.13	45	12.7	140	1555.95	10	68.95	28°

Figure 3.2 shows an example of a pressure-sinkage simulation of the soil with a rigid 15 cm circular plate. The results of the pressure-sinkage simulations for the four soil types are shown in Figure 3.3. As validation, the pressure-sinkage relationship for the similar sandy loam using the Bekker equation (Equation 3.1) and the parameters from Table 3.2 (Table 2.3

in Wong, 2001) is compared and found to closely approximate the simulation results for the dense sand.

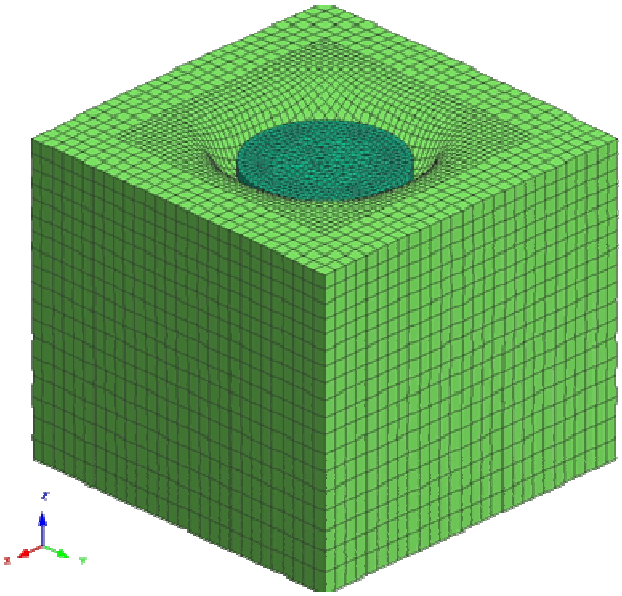

Figure 3.2: Virtual measurements of pressure-sinkage using a 15 cm circular plate on sand and gravel soil with an applied pressure of 0.3 MPa.

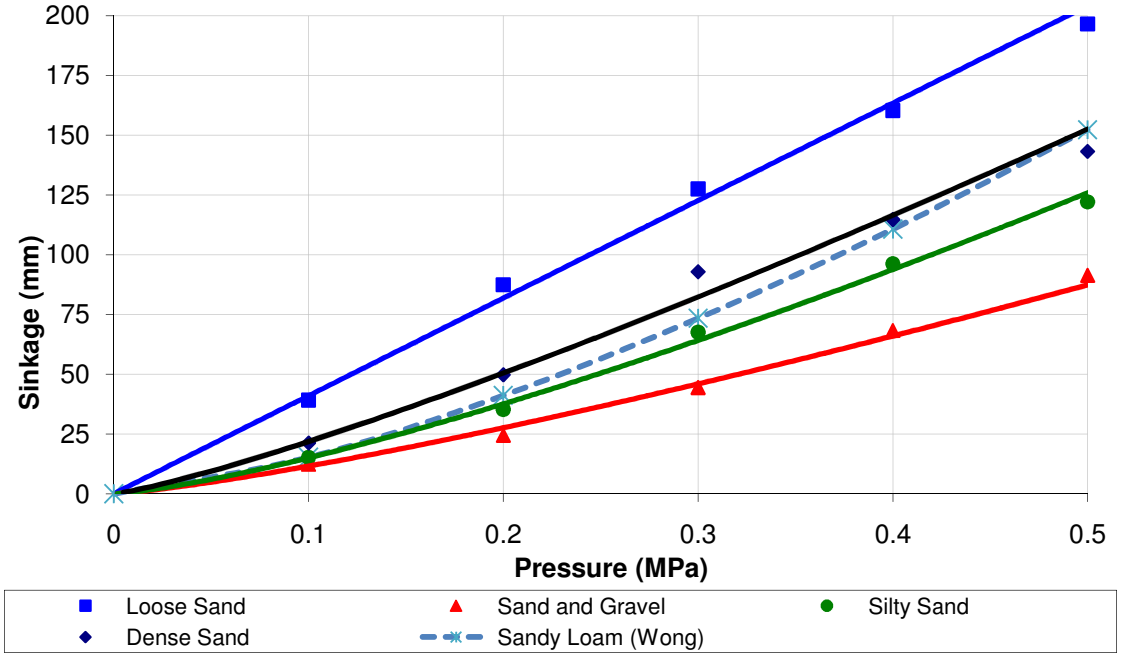

Figure 3.3: Pressure-sinkage relationship for the four new types of soil determined by FEA simulations plotted along with the theoretical pressure-sinkage relationship from the Bekker equation for sandy loam (shown as the dotted light blue line) (Wong 2001).

3.2.2 SOIL FLOW AND PRESSURE DISTRIBUTIONS WITH RIGID WHEEL

Another method used to validate the soil models was to qualitatively compare the pressure distributions and soil flows in the soil for four standard test cases defined in Wong (2001). These cases are a driven rigid wheel, a towed-rolling rigid wheel, a towed-locked rigid wheel, and a spinning rigid wheel. The towed-locked rigid wheel does not rotate, so it is considered to have 100% slip. The spinning rigid wheel rotates but is not allowed to translate in any direction and therefore it is also considered to have 100% slip. The pressure distributions and flows were simulated for speeds of 25 km/hr and a friction coefficient of 0.8. The results are shown in Figure 3.4, Figure 3.5, Figure 3.6 and Figure 3.7 with white arrows in the soil representing velocity of soil elements and the black lines representing the rigid wheel and the approximate shape of soil flow. The black lines and arrows on the figures are superimposed diagrams of soil flow under the four cases described above and in section 2.2 of *"The Theory of Ground Vehicles"* by Wong (2001). The colors in the soil indicate the pressure at that location, with the cooler colors representing lower pressures and the warmer colors representing higher pressures. It can be seen from the figures that the simulation results show approximately the same flow, pressure distributions, and outlines as in Wong (2001).

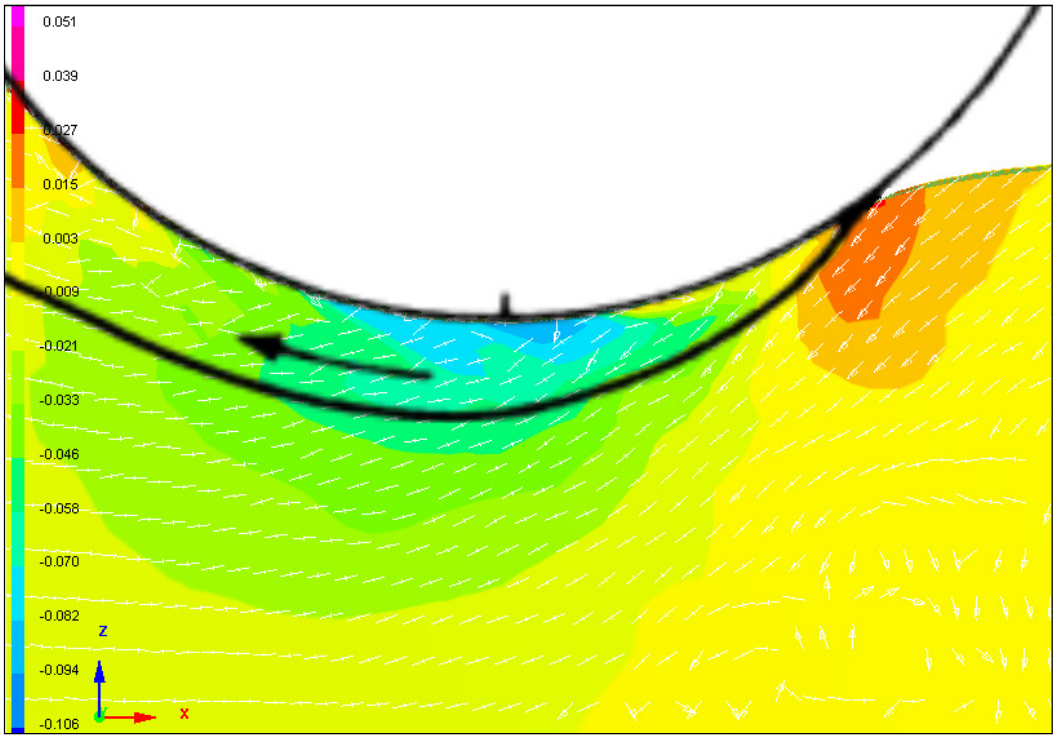

Figure 3.4: Pressure distribution and soil flow for spinning rigid wheel.

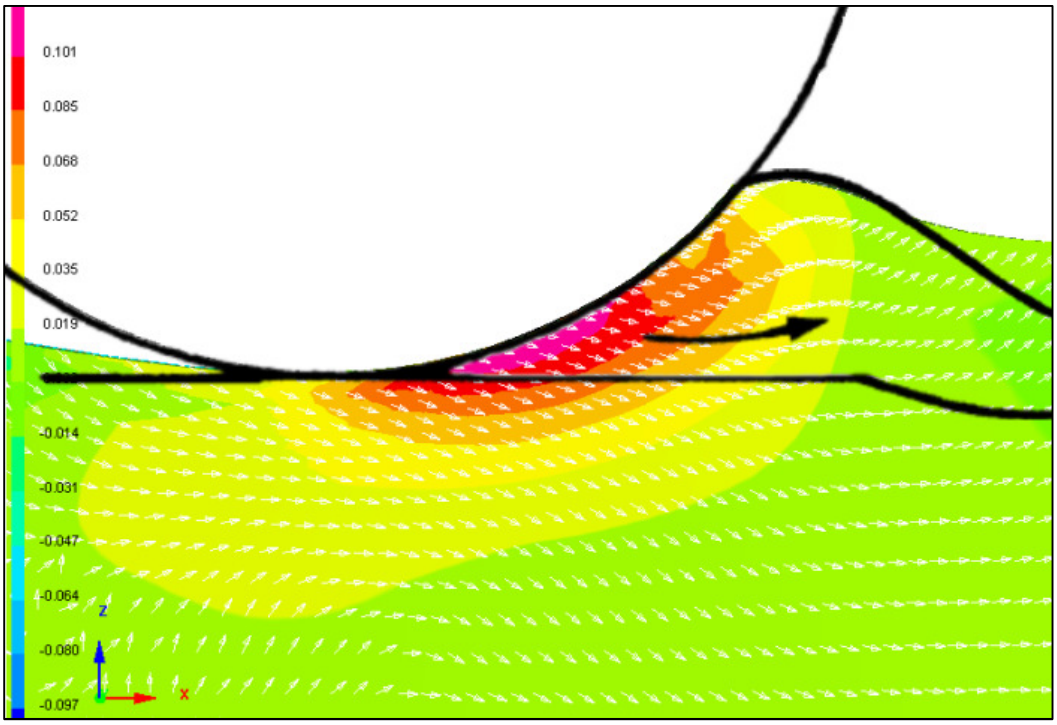

Figure 3.5: Pressure distribution and soil flow for towed-locked rigid wheel.

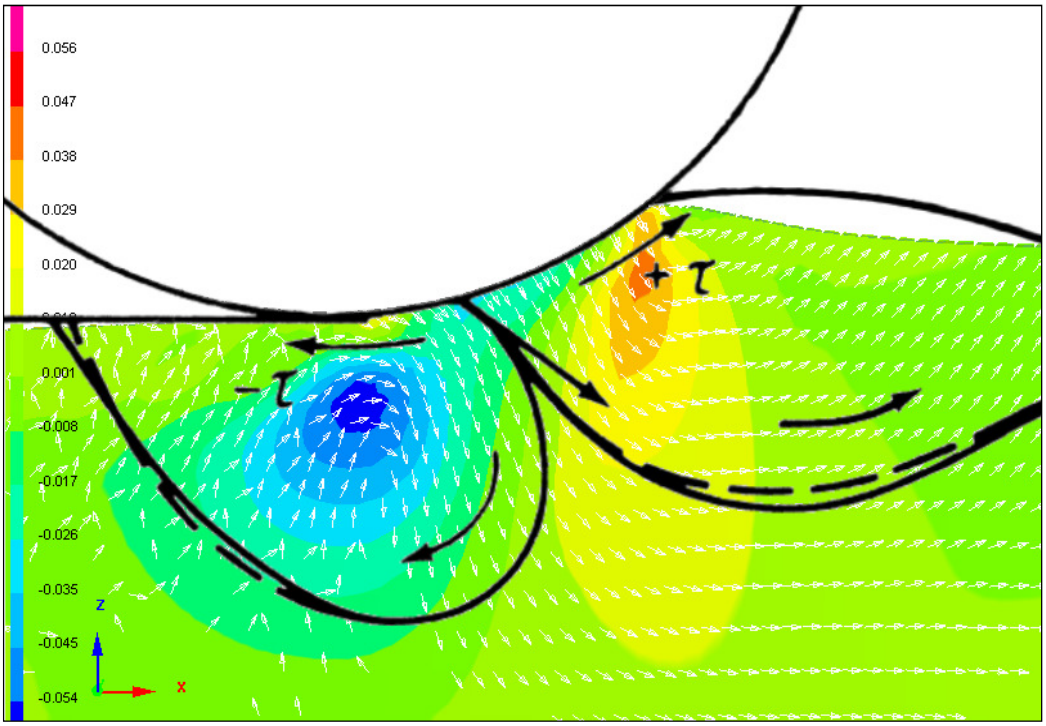

Figure 3.6: Pressure distribution and soil flow for towed-rolling rigid wheel.

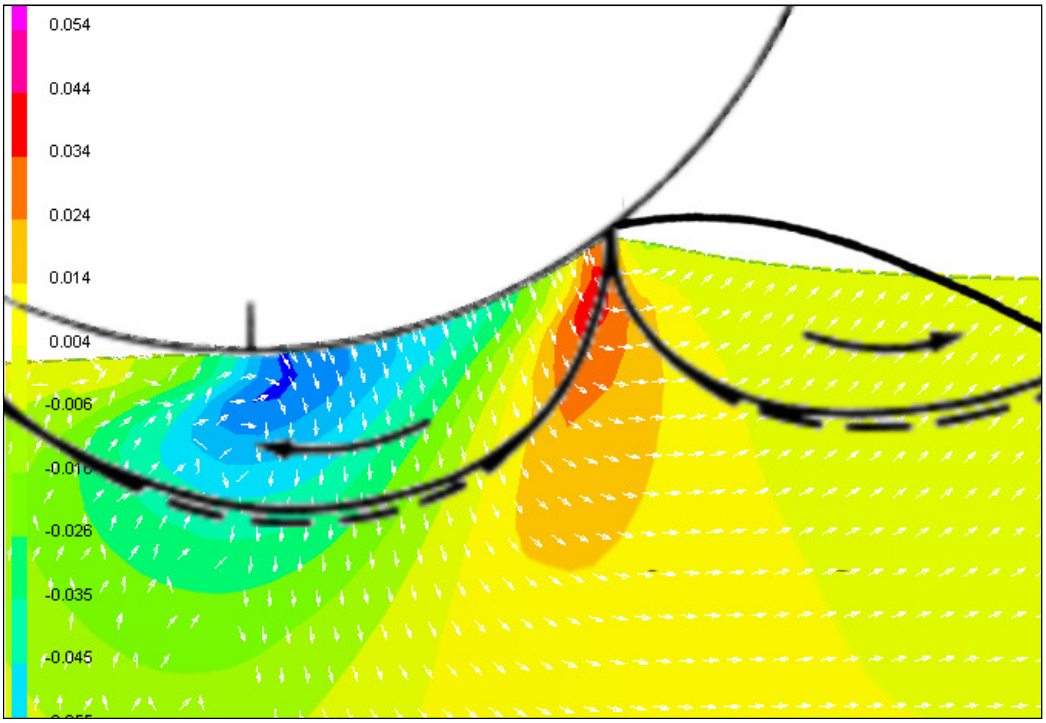

Figure 3.7: Pressure distribution and soil flow for driven rigid wheel.

3.2.3 FRICTION COEFFICIENT

Since it is very difficult to estimate the friction coefficient for a tire on soft soil without extensive physical testing, an arbitrary friction coefficient of 0.8 has been used in the tests within this thesis. Sensitivity analyses have been used to determine the effect of the loading and also the friction coefficient on the lateral tire forces. Figure 3.8 and Figure 3.9 show the results from the sensitivity analysis. It can be seen that the relationship between the lateral force and vertical load is essentially linear. The relationship between lateral force and the friction coefficient, μ, is more closely quadratic. These results confirm the importance of an accurate friction coefficient and necessitate further research to determine an appropriate value for each soil.

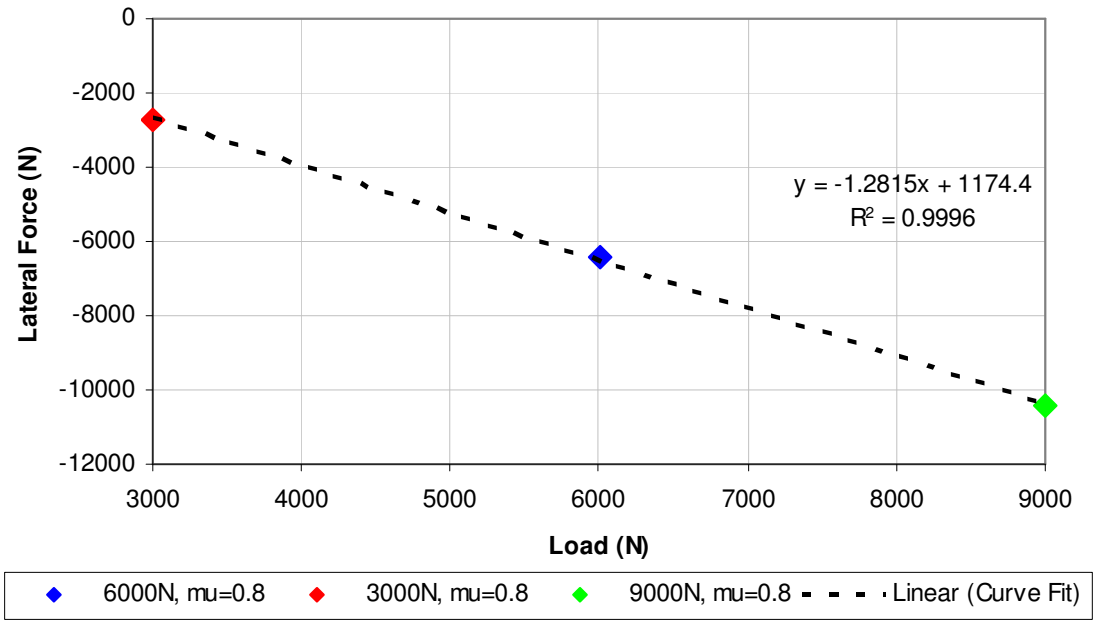

Figure 3.8: Effect of load on the lateral forces of a tire on soil.

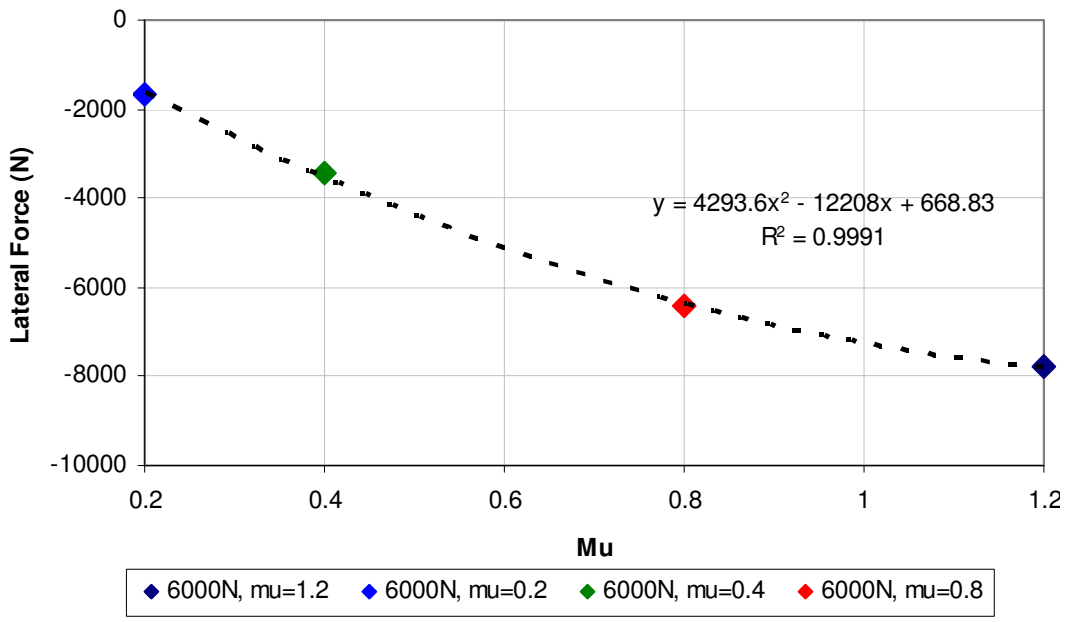

Figure 3.9: Effect of friction coefficient on the lateral forces of a tire on soil.

3.2.4 MOTION RESISTANCE

The motion resistance coefficient (F_x/F_z) of the tire on the soil is determined using an inflation pressure of 1.5 bar (22 psi), a load of 6 kN, and a speed of 25 km/hr. Table 3.3 shows the preliminary results which clearly indicate that the motion resistance coefficients increase as the soil becomes softer. Further tests will be performed to study the effect of speed, load, and inflation pressure.

Table 3.3: Effect of soil type on motion resistance coefficient.

Soil Type	Relative Hardness	Motion Resistance Coefficient
Loose sand	Softest	0.422
Dense sand/sandy loam	Soft	0.311
Silty sand	Medium	0.284
Sand and gravel	Hard	0.267
Rigid road	Hardest	0.100

CHAPTER 4

NEW OFF-ROAD RIGID RING MODEL

4.1 ORIGINAL RIGID RING MODEL ON RIGID ROAD

The rigid ring tire model originally developed by Zegelaar and Pacejka has been validated for most driving situations and can be used to describe the behavior of a pneumatic tire running on a rigid surface. This chapter will explain the parameters used in the rigid ring model and the methods used to determine their values. This chapter will also describe a newly developed off-road rigid ring model for use with off-road tires running on soils.

4.1.1 IN-PLANE PARAMETERS FOR ORIGINAL RIGID RING MODEL

The in-plane rigid ring model, shown in Figure 4.1, represents a pneumatic tire in contact with a rigid road surface. For in-plane tire motion, the elastic sidewall of the pneumatic tire is modeled by using translational and rotational springs and dampers. A rigid band is used to represent the tread and a spring (k_{vr}) and damper (C_{vr}) between the rigid tread band and the road incorporates the stiffness and damping of the tread. In this model the wheel rim and the tread are also modeled as rigid parts. Since the vertical/translational stiffness of the sidewall alone cannot predict the large deformation of the tire when it is in contact with the road surface, the residual vertical stiffness is introduced. Both the vertical sidewall stiffness (k_{bz}) and the residual vertical stiffness (k_{vr}) contribute to the vertical motion of the wheel rim. In the rigid ring model the mass of the whole tire without the rim is defined as the tire belt mass, m_b. The mass of the rim is defined as m_a. The vertical stiffness, (k_{bz}), is regarded as the same as the longitudinal stiffness, (k_{bx}), due to symmetry about the tire's spindle. The index 'b' in the subscripts of the parameters indicates that they are associated only with the behavior of the sidewall. The parameters with index 'v' are associated only with the behavior of the tread.

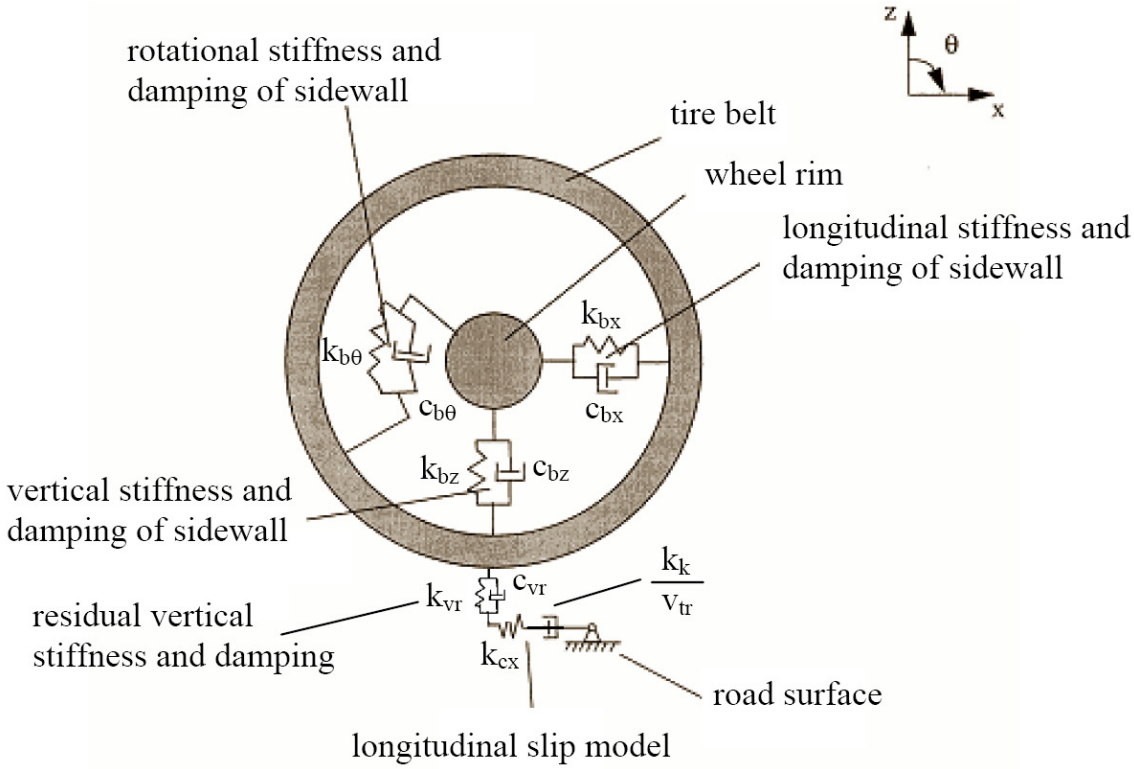

Figure 4.1: In-plane rigid ring model and parameters for rigid road.

The rotational motion of the rigid tread band can be modeled by using a rotational spring ($k_{b\theta}$) and damper ($C_{b\theta}$) between the wheel rim and the rigid tread band, as can be seen in Figure 4.1. The longitudinal slip between the tire and the road surface during braking and accelerating is also modeled by using a longitudinal spring (k_{cx}) and damper (k_k/v_{tr}).

As stated above, many parameters need to be calculated to represent the full rigid ring tire model. In this study, the parameters for the rigid ring model are calculated based on the FE truck tire simulation results. The vertical static load is chosen as 18.9 kN (4250 lbs), which is half of the total maximum load limit for dual tires on a tandem drive axle. All following calculations are the values for the static vertical load of 18.9 kN (4250 lbs) and an inflation pressure of 85 psi.

4.1.2 OUT-OF-PLANE PARAMETERS FOR ORIGINAL RIGID RING MODEL

The out-of-plane rigid ring model is shown in Figure 4.2. For out-of-plane tire motion, the elastic sidewall of the pneumatic tire is modeled by using translational and rotational springs and dampers. In this model the wheel rim and the tread are also modeled as rigid parts. The mass of the whole tire without the rim is defined as the tire belt mass, m_b. The mass of the rim is defined as m_a. The lateral stiffness and damping of the sidewall is represented by k_{by} and C_{by}, respectively. The rotational sidewall stiffness, ($k_{b\gamma}$), and the rotational sidewall damping, ($C_{b\gamma}$) are represented by a torsional spring and damper. The residual vertical stiffness of the tread, (k_{vr}), is modeled the same as in the in-plane model. The lateral slip model is very similar to the longitudinal slip model found in the in-plane rigid ring model. The index 'b' in the subscripts of the parameters indicates that they are associated only with the behavior of the sidewall. The parameters with index 'v' are associated only with the behavior of the tread.

The schematic drawing to represent out-of-plane tire parameters on rigid road are shown in Figure 4.2. The out-of-plane parameters for the rigid ring model are calculated based on the FEA RHD truck tire simulations for a vertical load of 18.9 kN.

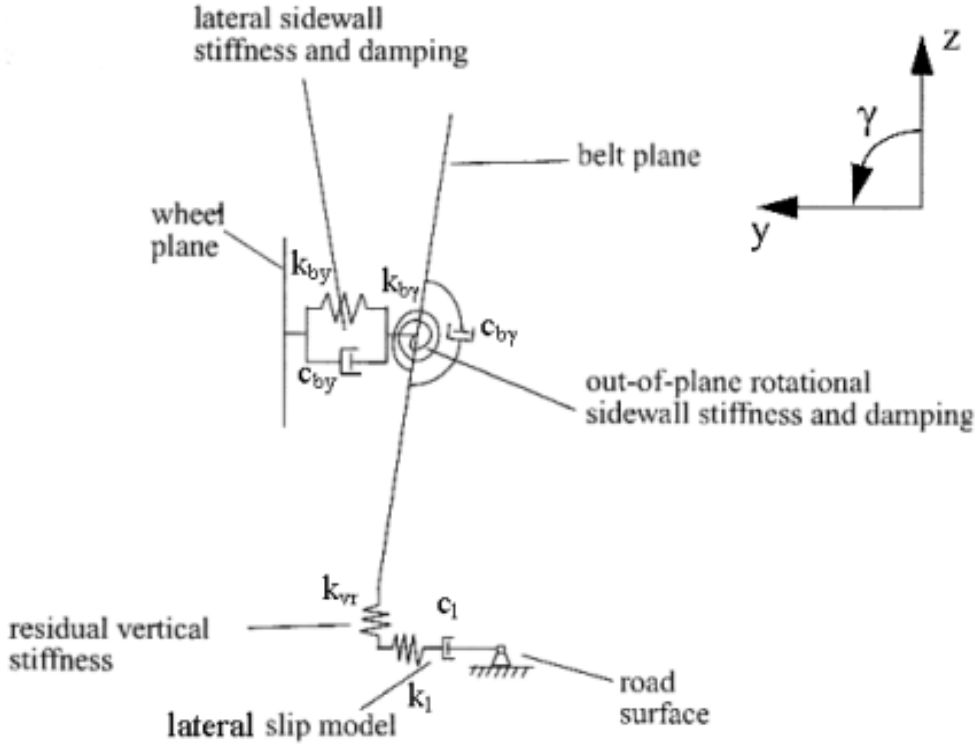

Figure 4.2: Out-of-plane rigid ring model and parameters for rigid road.

4.2 NEW OFF-ROAD RIGID RING MODEL

The rigid ring tire model originally developed by Zegelaar and Pacejka can only be used in situations where the road surface is considered to be rigid. While this assumption may be very good when driving on paved roads, it presents a problem when trying to predict vehicle behavior when driving off-road. In order to fully describe an off-road tire running on soil, modifications must be made to the original rigid ring model. A new off-road rigid ring model is presented in this section which includes additional parameters for the vertical and longitudinal stiffness of the soil of interest.

4.2.1 IN-PLANE PARAMETERS FOR THE NEW OFF-ROAD RIGID RING MODEL

In order to use the rigid ring model for tire and soft soil interaction it is necessary to consider the addition of new parameters to describe the soil. It is recommended to use the following model, as shown in Figure 4.3, which includes the additional parameter k_{soil}. This model

assumes that the soil acts as a linear spring in series with the vertical and residual stiffness of the tire over a specific load range. Simulating the Goodyear® RHD tire running on soft soil requires extensive simulation time and many simulations over a wide range of loads, tire velocities, and slip angles in order to capture the soil stiffness under various conditions. The soil model has already been validated in Chapter 3 by analyzing the motion of the soil, pressure-sinkage curves, and pressure distributions throughout the soil during loading. Chapter 5 explains in detail the simulations and methods used to determine each of these parameters.

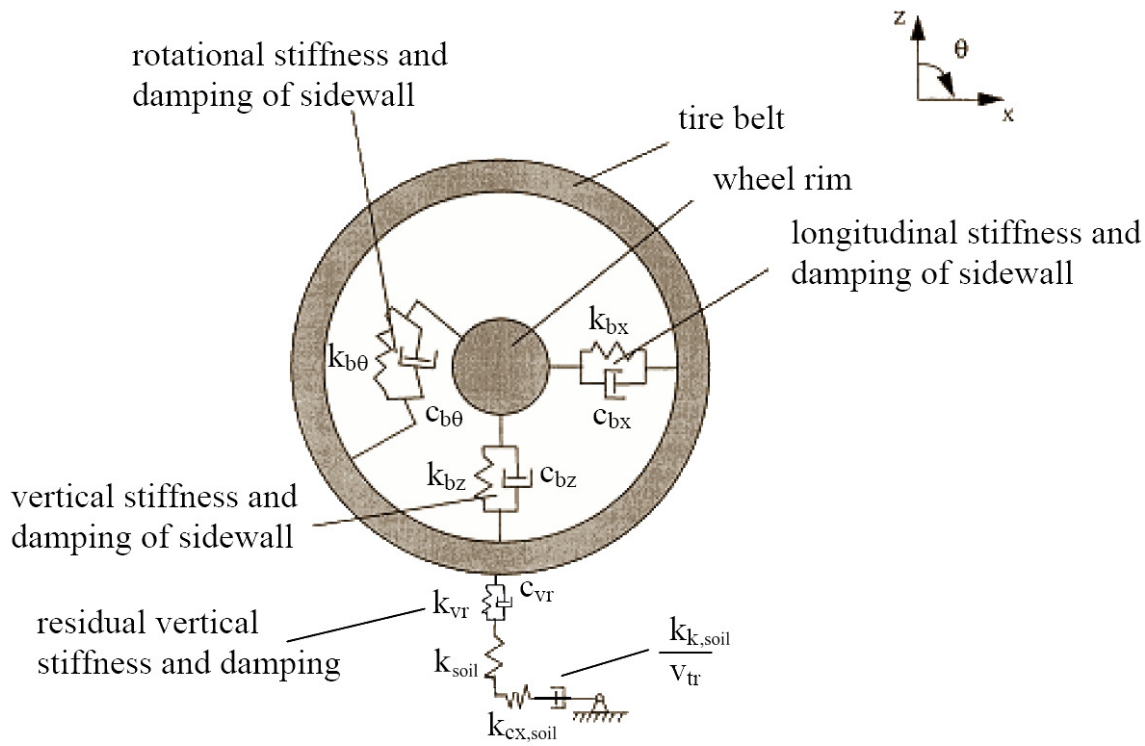

Figure 4.3: Recommended in-plane rigid ring model and parameters for soft soil.

4.2.2 OUT-OF-PLANE PARAMETERS FOR THE NEW OFF-ROAD RIGID RING MODEL

Figure 4.4 shows the recommended out-of-plane rigid ring tire model parameters for soft soil. The parameters k_{soil} and $k_{l,soil}$ have been introduced to the model in order to represent the vertical and longitudinal flexibility of the soil, respectively. These parameters will be determined using the FEA RHD tire model running on the FEA dense sand model. The equations for these parameters and further explanation on the methods used to determine them are explained in Chapter 6.

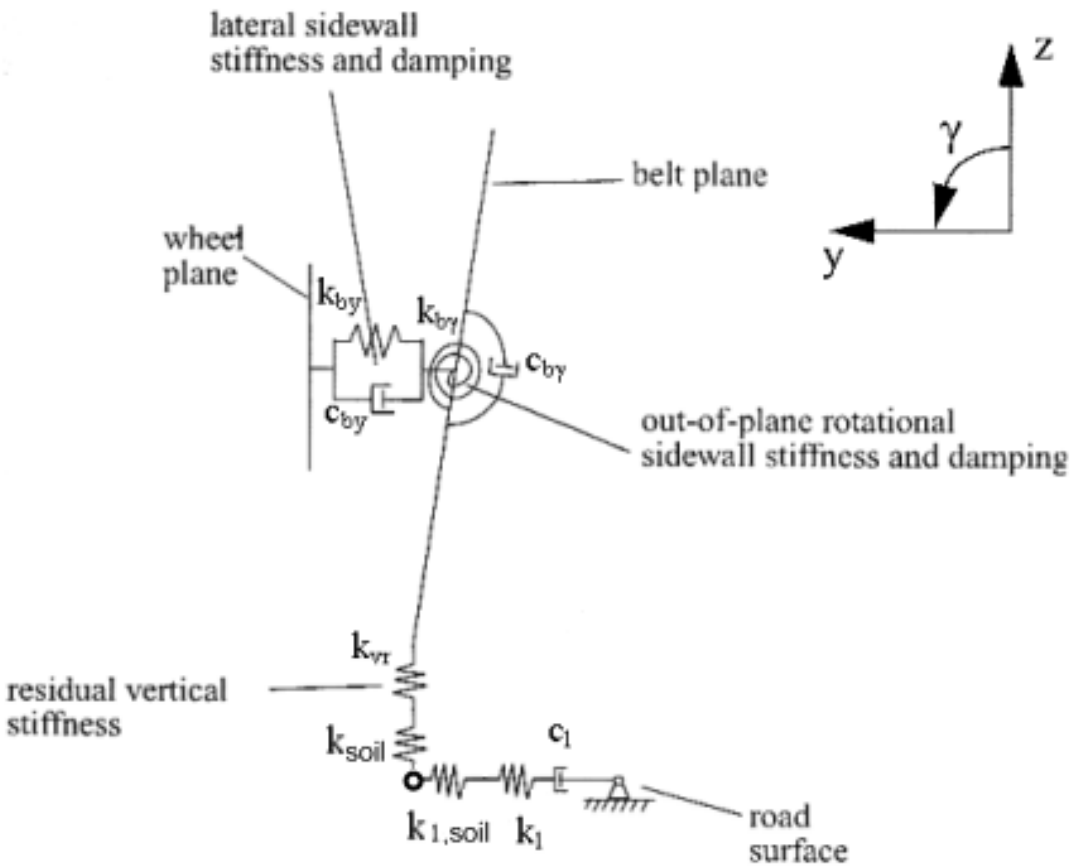

Figure 4.4: Recommended out-of-plane rigid ring model and parameters for soft soil.

CHAPTER 5

DETERMINATION OF IN-PLANE RIGID RING PARAMETERS

5.1 IN-PLANE RIGID RING PARAMETERS FOR TIRE ON RIGID SURFACE

This chapter will focus on the equations and specific tests performed to obtain each of the in-plane rigid ring model parameters for a tire running on both a rigid surface and on soft soil.

5.1.1 IN-PLANE TRANSLATIONAL/VERTICAL STIFFNESS, (k_{bx}, k_{bz}), AND RESIDUAL VERTICAL STIFFNESS, k_{vr}

The in-plane rigid ring model for a tire on a rigid surface (shown in Figure 4.1) has already been explained and presented in Chapter 4. The vertical stiffness, (k_{bz}), is regarded as the same as the longitudinal stiffness, (k_{bx}), due to symmetry about the tire's spindle. The rigid ring model explained in Chapter 4 describes that there are two springs arranged in series that determine the vertical stiffness of the tire. The values for both of these springs must be determined via simulations and equations relating the total stiffness to the stiffness of each individual component. The in-plane vertical and longitudinal stiffness can be determined from two simple simulations.

The first simulation to determine the tire's translational/vertical stiffness involves inflating the tire to 85 psi and then loading the tire in a ramped fashion from 0 to 37.8 kN (0 to 8500 lbs), which is twice the maximum load for a dual axle truck tire, in order to obtain a vertical stiffness curve shown in Figure 5.1. From this simulation it is possible to obtain the overall vertical stiffness (k_{tot}) of the tire, which is simply the slope of the load-deflection curve at the specific load of interest.

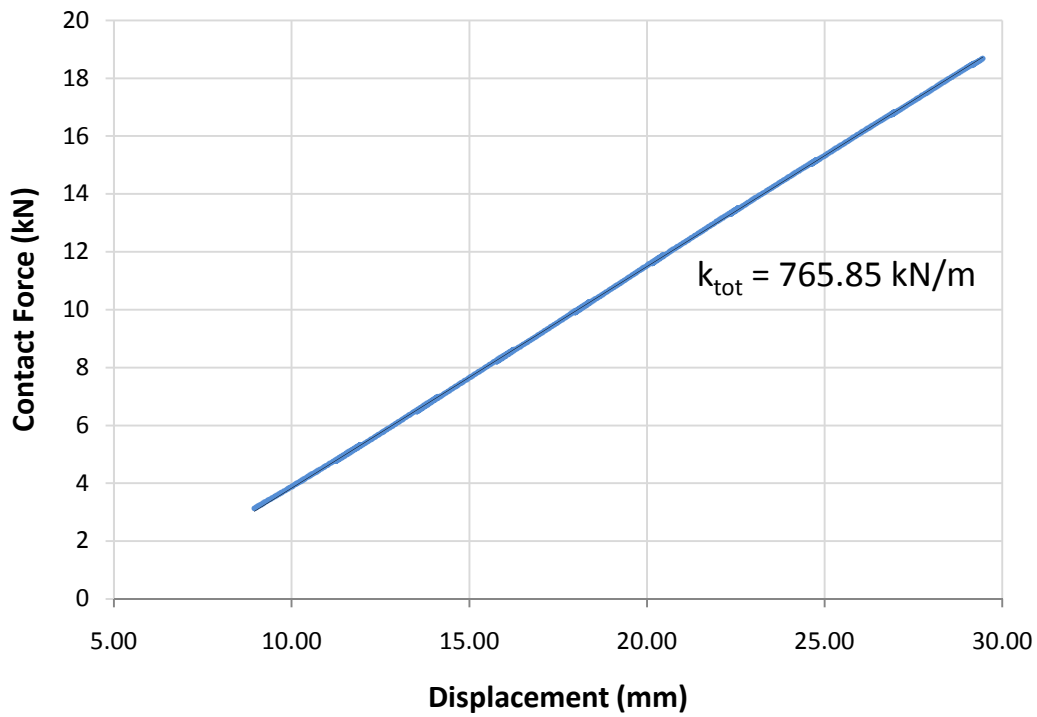

Figure 5.1: Load-deflection relationship for the RHD tire.

The second simulation to determine the residual tread stiffness involves testing the stiffness of the tread alone to determine the residual tread stiffness (k_{vr}). This is done by removing the rest of the tire and placing a rigid backing on the inside of the tread before loading the tread on the road. Figure 5.2 shows the stiffness of the tread alone and can be used in combination with the previously calculated total stiffness (k_{tot}) to calculate the translational/vertical stiffness (k_{bz}). The tread stiffness is defined here as the slope of the load-deflection curve, which is taken at the 10-40 kN load range where the curve becomes linear as this is a typical operating range. Equation 5.1 is the relationship for springs in series, and by substituting the known values for k_{vr} and k_{tot} we can calculate the translations/vertical stiffness (k_{bz}).

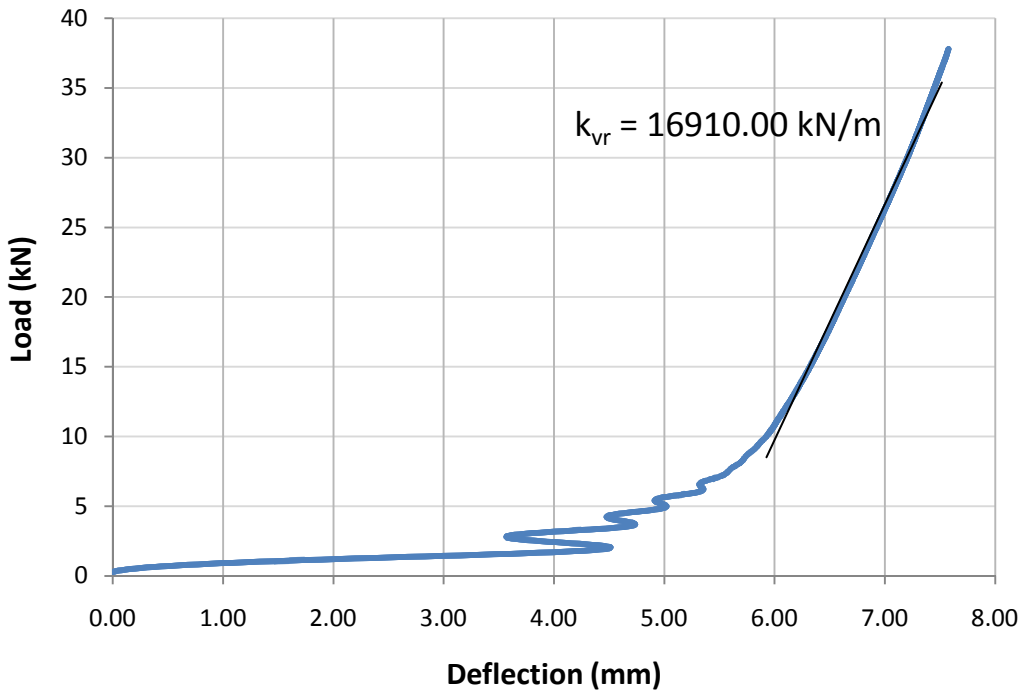

Figure 5.2: Load-deflection relationship for only the tread of the tire.

$$\frac{1}{k_{tot}} = \frac{1}{k_{vr}} + \frac{1}{k_{bz}} \tag{5.1}$$

Table 5.1: In-plane sidewall translational stiffness and residual vertical stiffness for the rigid ring tire model.

Static Vertical Load (kN)	k_{tot} (kN/m)	k_{bz} (kN/m)	k_{vr} (kN/m)
18.911	765.85	732.67	16910

5.1.2 IN-PLANE TRANSLATIONAL/VERTICAL DAMPING CONSTANTS (C_{bx}, C_{bz}) OF THE SIDEWALL AND RESIDUAL DAMPING CONSTANT (C_{vr})

The vertical damping, (C_{bz}), is regarded as the same as the longitudinal damping, (C_{bx}), due to symmetry about the tire's spindle. The rigid ring model explained in Chapter 4 describes that there are two dampers arranged in series that determine the translational/vertical damping of the tire. The values for both of these dampers must be determined via simulations and equations relating the total damping to the damping of each individual

component. The in-plane vertical and longitudinal damping can be determined from two simple simulations known as "drop tests."

The first drop test simulation involves holding the RHD tire 20 mm above the rigid road, inflating the RHD tire to 85 psi, and then applying am 18.9 kN (4250 lbs) vertical load to the tire such that it will bounce vertically on the road several times. Figure 5.3 describes the setup for this simulation. It is known that tires are underdamped and therefore have a damping ratio, ξ, of far less than 1, therefore Equation 5.2 can be used to calculate the logarithmic decrement from the values for two consecutive peaks in the displacement curve (Figure 5.4). Equation 5.3 is used to calculate the damping ratio, ξ_{tot}, from the logarithmic decrement. Once ξ_{tot} is determined ξ_{tot}, m_{tot}, and k_{tot} can be substituted into Equation 5.5 to determine C_{tot}.

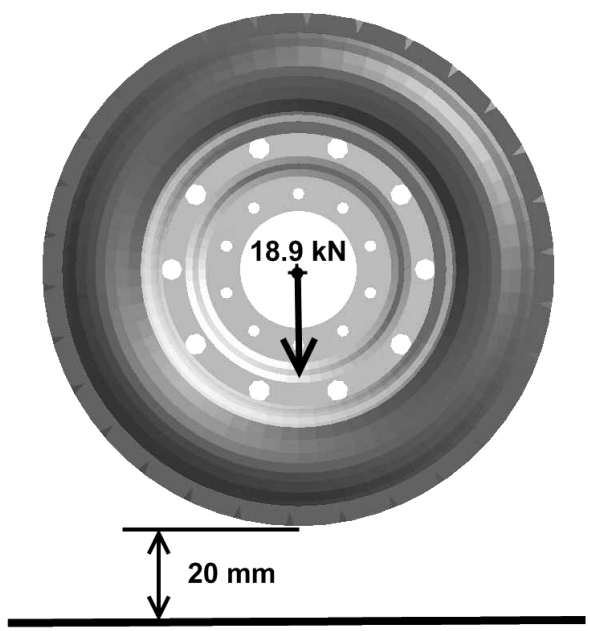

Figure 5.3: Simulation setup for drop test of whole tire, which is used to determine the total damping, C_{tot}.

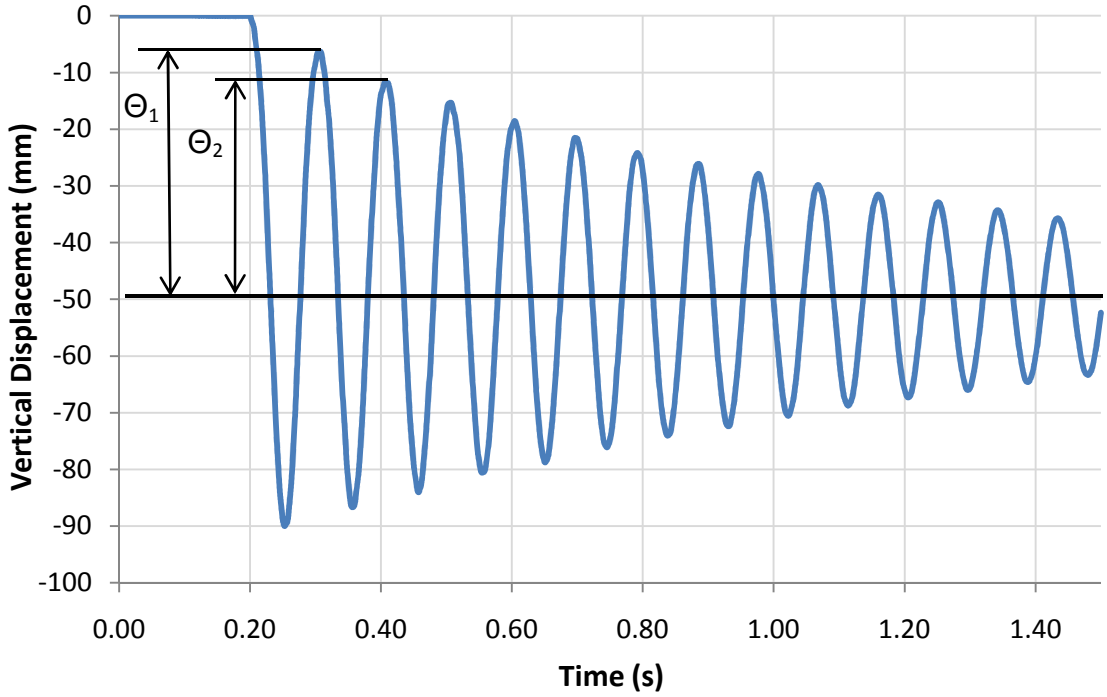

Figure 5.4: Displacement of the center of the tire during a drop test. It can be seen that the total damping in the tire is quite low and results in the tire bouncing and oscillating many times.

Since the dampers used to represent the tire, tread, and soil damping in this model are also in series, Equation 5.4 can be used to describe the relationship between each of the damping constants. It can be seen from the equation that if we have the total damping constant, C_{tot}, and either C_{bz}/C_{bx} or C_{vr} it is possible to calculate the remaining unknown constant.

$$\delta = \ln\left(\frac{\theta_1}{\theta_2}\right) \tag{5.2}$$

Where: θ_1 = First peak from Figure 5.4,

θ_2 = Second peak from Figure 5.4.

$$\xi = \frac{\delta}{\sqrt{4\pi^2 + \delta^2}} \tag{5.3}$$

$$\frac{1}{C_{tot}} = \frac{1}{C_{vr}} + \frac{1}{C_{bz}} \tag{5.4}$$

$$C_{tot} = 2\xi_{tot}\sqrt{m_{tot}k_{tot}} \tag{5.5}$$

$$C_{vr} = 2\xi_{tread}\sqrt{m_{tread}k_{vr}} \tag{5.6}$$

A second drop test on just the tread from the tire, pictured in Figure 5.5, is used to determine C_{vr}. In this simulation a tire model with the tire's sidewall and rim removed is held 20 mm above the rigid road and then loaded with an 18.9 kN (4250 lbs) vertical load so that it bounces vertically. The logarithmic decrement, Equation 5.2, can again be found by using the values for two consecutive peaks from the displacement curve (Figure 5.6), and Equation 5.3 can be used to calculate the damping ratio, ξ_{tread}. Once ξ_{tread} is determined, C_{vr} is found by substitute ξ_{tread}, m_{tread}, and k_{tread} into Equation 5.5. The values for the parameters used in the calculations of the damping constants are shown in Table 5.2. Table 5.3 shows the values for the in-plane translation damping constants of the sidewall, C_{bz}, and the residual damping constant of the tread, C_{vr}, for a load of 18.911 kN.

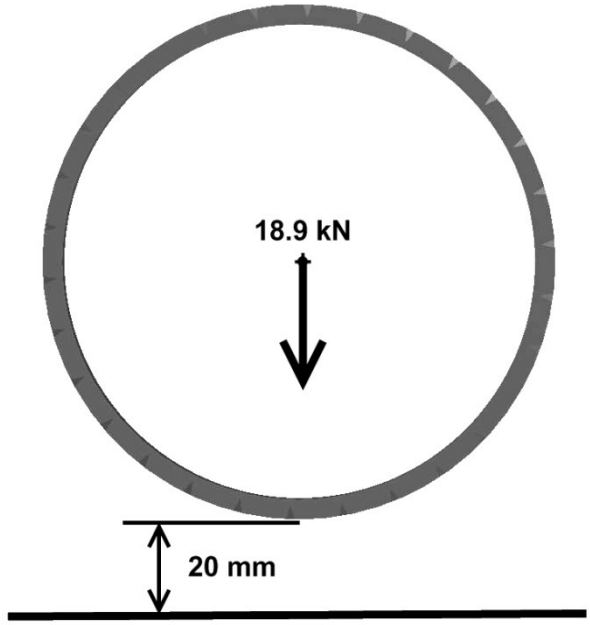

Figure 5.5: Simulation setup for drop test of tread only, which is used to determine the residual damping, C_{vr}.

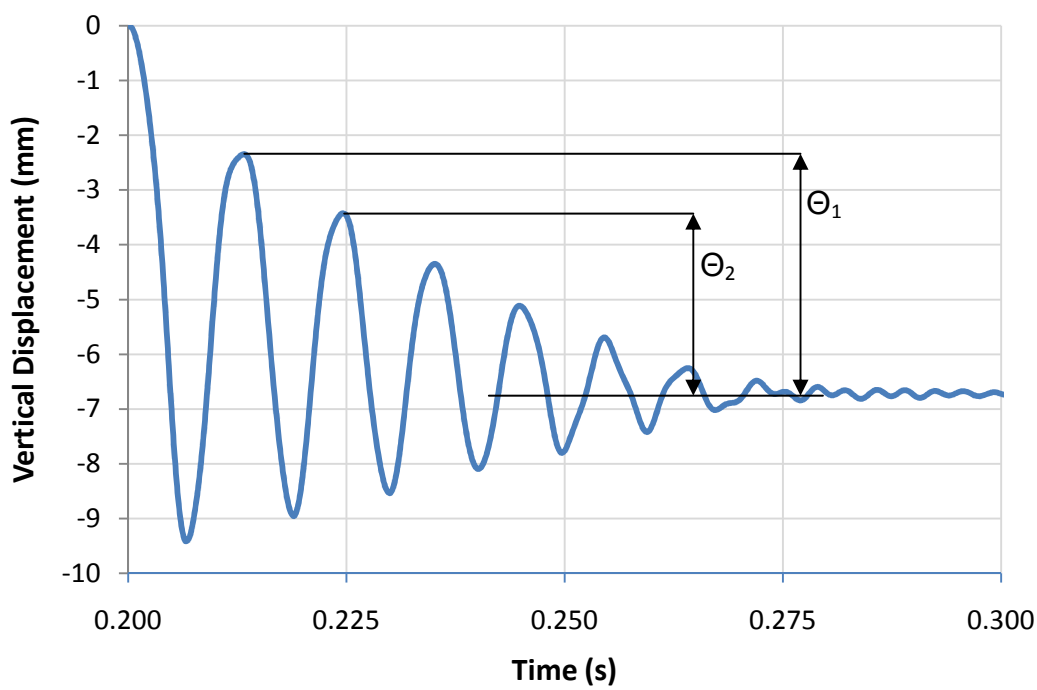

Figure 5.6: Displacement of the center of the tread during a drop test. It can be seen that the material damping within the tread quickly damps out oscillations.

Table 5.2: Table of parameters used in the calculations for the damping constants.

Parameter	Value	Units
k_{tot}	765.85	kN/m
k_{vr}	16910	kN/m
k_{bz}	732.67	kN/m
m_{tot}	106.80	Kg
m_{tread}	31.18	Kg
δ_{tot}	0.137706	-
δ_{tread}	0.281280529	-
ξ_{tot}	0.021911	-
ξ_{tread}	0.044722395	-

Table 5.3: In-plane translational damping constants of the sidewall and the residual damping constant in the tread.

Static Vertical Load (kN)	C_{bz} (N s/m)	C_{vr} (N s/m)
18.911	470.089	2053.832

5.2 DETERMINATION OF THE ROTATIONAL STIFFNESS, $k_{b\theta}$, AND THE ROTATIONAL DAMPING CONSTANT OF THE SIDEWALL, $C_{b\theta}$

In order to calculate the in-plane sidewall rotational stiffness and damping constants, the rim of the tire model is locked in place (constrained not to be translated or rotated). The tread is constrained to be rigid and is allowed to move only in rotation within the plane of the tire. After the tire is inflated, a tangential force of 18.9 kN (4250 lbs) is applied to a node at the bottom edge of the tread band as seen in Figure 5.7. The force on the tread band causes it to rotate with respect to the rim of the tire model, and due to the tire's sidewall rotational stiffness it reaches a steady state condition at a certain angular displacement to the rim. At this point the tangential load is quickly removed, allowing the tread band to oscillate rotationally.

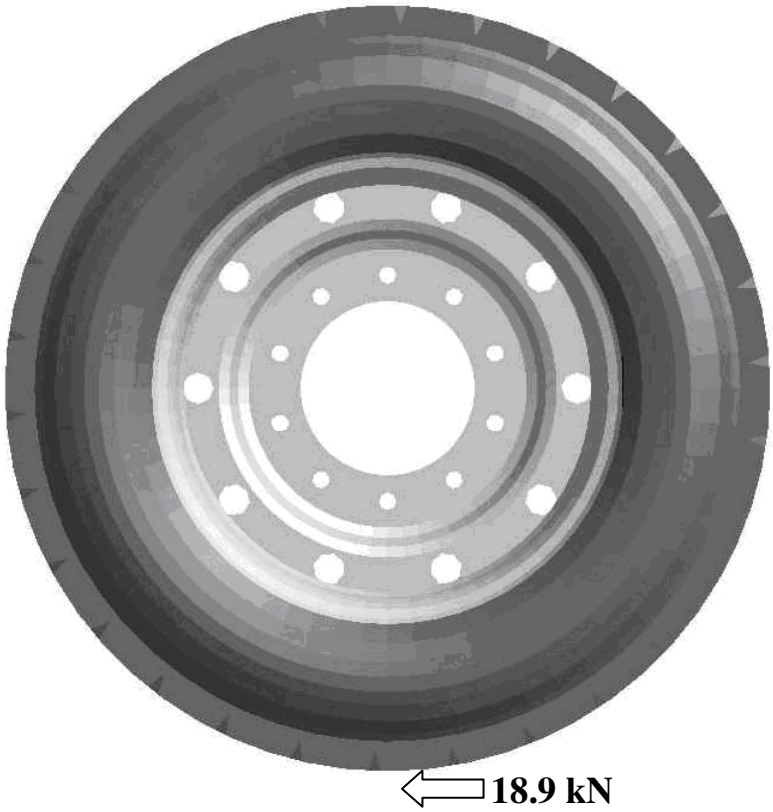

Figure 5.7: Rotational excitation of the RHD truck tire.

5.2.1 IN-PLANE ROTATIONAL STIFFNESS, $k_{b\theta}$

Figure 5.8 shows the tread band's angular displacement as a function of time. It can easily be seen that the tread band reaches a steady state angular displacement, θ_{ss}, of about 0.0268 radians very quickly. The in-plane rotational stiffness of the sidewall ($k_{b\theta}$) can be calculated from Equation 5.7 using this angular displacement and the moment applied to the tread band.

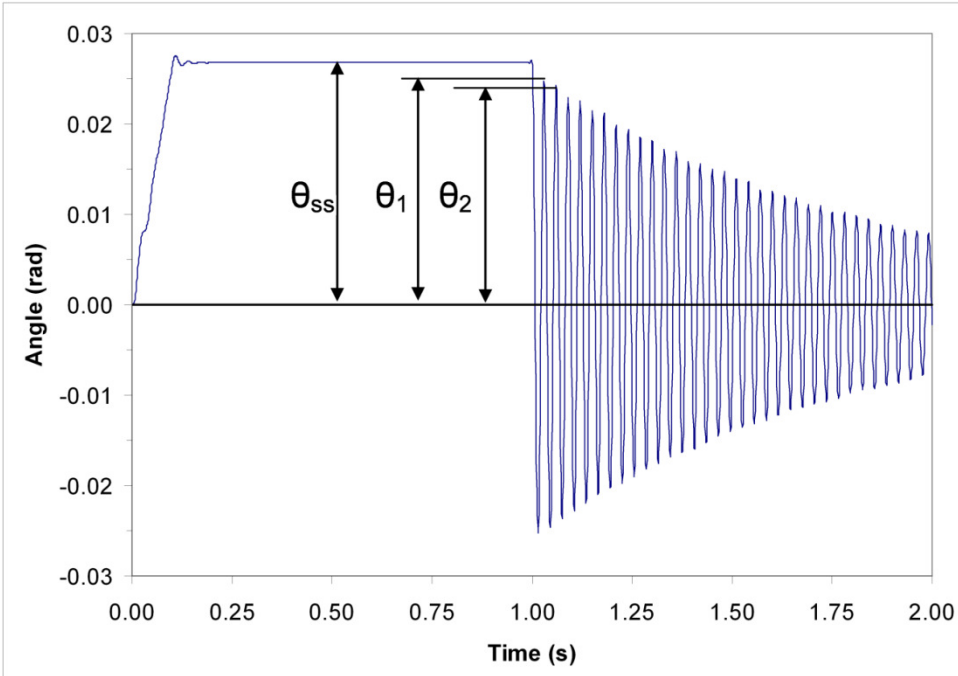

Figure 5.8: Angular displacement of the tread with respect to the rim vs. time. The damping in the sidewall is visible as a decay of the oscillations once the load is released after 1 second.

$$k_{b\theta} = \frac{Applied\ Moment}{Angular\ Displacement} = \frac{18.911\ kN*0.546m}{0.0268\ rad} = 385.276\ \text{kN m/rad} \qquad (5.7)$$

5.2.2 IN-PLANE ROTATIONAL DAMPING CONSTANT, $C_{b\theta}$

It can also be observed from Figure 5.8 that once the force applied to the tread band is released, the magnitude of the tread band's angular displacement decays over time. The logarithmic decrement can therefore be applied in order to calculate the damping constant. From Figure 5.8 two neighboring peak points are selected to calculate damping constant.

Angular displacement θ_1=0.024786 rad at time t_1=1.031.

Angular displacement θ_2=0.024224 rad at time t_2=1.061.

Angular displacement θ_{ss}=0.026800 rad at steady state load.

$$\delta = \ln\left(\frac{\theta_1}{\theta_2}\right) \tag{5.8}$$

Where: θ_1 = First peak from Figure 5.8,

θ_2 = Second peak from Figure 5.8.

$$\xi = \frac{\delta}{\sqrt{4\pi^2 + \delta^2}} \tag{5.9}$$

The damped period of vibration ($\tau_d = t_2 - t_1$) is 0.03 sec. From the Equation 5.10 the undamped natural frequency, ω_n, can be calculated as 462 rad/sec.

$$\tau_d = \frac{2\pi}{\omega_{dr}} = \frac{2\pi}{\omega_{nr}\sqrt{1-\xi^2}} \tag{5.10}$$

Where: ω_{dr} = Damped rotational natural frequency = 209.439 (rad/s),

ω_{nr} = Undamped rotational natural frequency = 209.44 (rad/s).

Therefore, the critical damping constant (C_c) can be obtained using Equation 5.11 with the moment of inertia of the tire belt (I_{by}, 12.073 kg m^2).

$$C_c = 2 * I_{by} * \omega_{nr} = 5.057\ kN\ m\ s/rad \tag{5.11}$$

Finally, the in-plane rotational damping constant ($C_{b\theta}$) is calculated by Equation 5.12.

$$C_{b\theta} = \xi * C_c = 0.0142\ kN\ m\ s/rad \tag{5.12}$$

5.3 DETERMINATION OF LONGITUDINAL TREAD STIFFNESS, k_{cx}, AND LONGITUDINAL SLIP STIFFNESS, k_k, ON A RIGID SURFACE

In order to determine the longitudinal tread stiffness and slip stiffness, the RHD tire model was placed on a 3.4 m diameter smooth drum. The tire was loaded with 18.9 kN (4250 lbs) and was inflated to 85 psi. The tire was quickly accelerated to an angular speed equivalent to a linear velocity of 10 km/hr. Due to inertia the drum model was unable to accelerate as quickly as the tire, causing slip between the tire and the drum surface. The longitudinal or tractive force at the contact area is plotted as a function of slip in Figure 5.9, and the longitudinal slip stiffness, (k_k), can be calculated as the slope of the curve as slip approaches zero. The longitudinal slip stiffness is assumed to equivalent for both braking and acceleration.

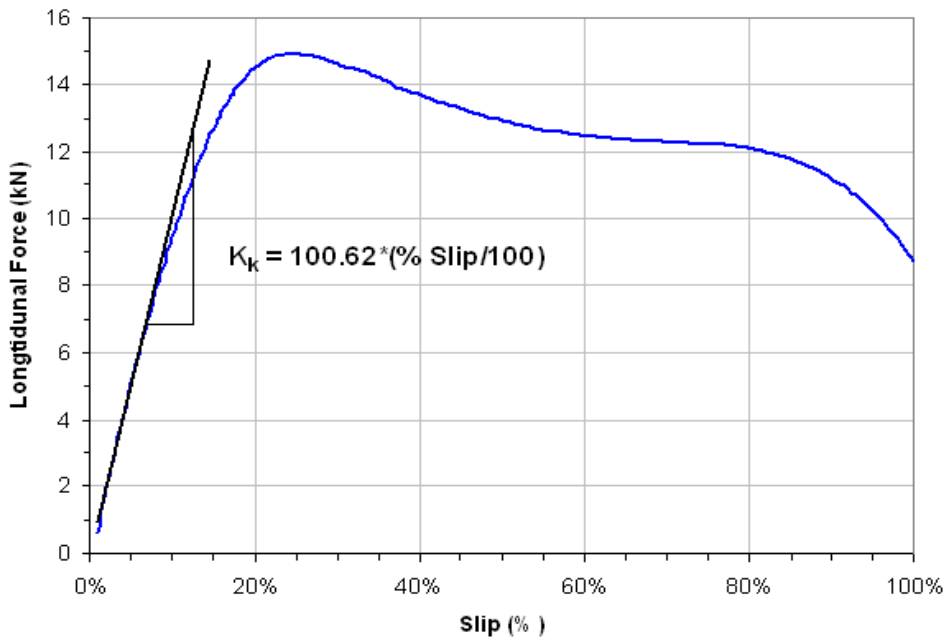

Figure 5.9: Relationship between longitudinal force and slip for the RHD tire running on a smooth drum. 0% slip corresponds to the tire and the drum speed having completely synchronized while 100% slip corresponds to the tire spinning while the drum remains at rest.

5.3.1 LONGITUDINAL SLIP STIFFNESS, k_k

The slope at zero slip ratio is defined as longitudinal slip stiffness (k_k) and can be found applying a linear curve fit to Figure 5.9.

$$k_k = 100.6 \frac{kN}{slip\ unit} \tag{5.13}$$

5.3.2 LONGITUDINAL TREAD STIFFNESS, k_{cx}

The longitudinal tread stiffness, k_{cx}, can be expressed by Equation 5.14 which comes from the work by Zegelaar and Pacejka in 1997.

$$k_{cx} = \frac{k_k}{a} \tag{5.14}$$

Where: a = the half the contact length (m). Figure 5.14 describes the concept of contact length for the RHD tire on soft soil.

From Equation 5.14 with half contact length on the drum (0.114m) at 18.9 kN (4250 lbs) vertical load, the longitudinal tread stiffness is calculated as 1765.263 kN/m. Table 5.4 summarizes the in-plane rigid ring tire model parameters on rigid road as determined by the FEA RHD truck tire simulations described here under a vertical load of 18.9 kN.

Table 5.4: Rigid ring model parameters for rigid road.

Rigid Ring Parameter	18.911 kN Vertical Load (4250 lbs)
a (m)	0.114
C_{bx}, C_{bz} (kN s/m)	0.470
$C_{b\theta}$ (kN ms/rad)	0.0142
k_{cx} (kN/m)	1765.263
k_k (kN/unit slip)	100.624
k_{tot} (kN/m)	765.85
C_{vr} (kN s/m)	2.054
f_r	0.070
I_{ay} (kg m^2)	3.034
I_{ax}, I_{az} (kg m^2)	1.786
I_{by} (kg m^2)	12.073
I_{bx}, I_{bz} (kg m^2)	6.840
k_{bx}, k_{bz} (kN/m)	732.67
$k_{b\theta}$ (kN m/rad)	385.276
k_{vr} (kN/m)	16910
m_a (kg)	34.800
m_b (kg)	72.000
R_r (m)	0.502

5.4 DETERMINATION OF ADDITIONAL SOIL IN-PLANE PARAMETERS OF THE RIGID RING TIRE MODEL ON SOFT SOIL

The recommended rigid ring model for soft soil (Figure 4.3) has already been developed in Chapter 4, therefore only the calculations and tests performed to determine the in-plane parameters will be presented here.

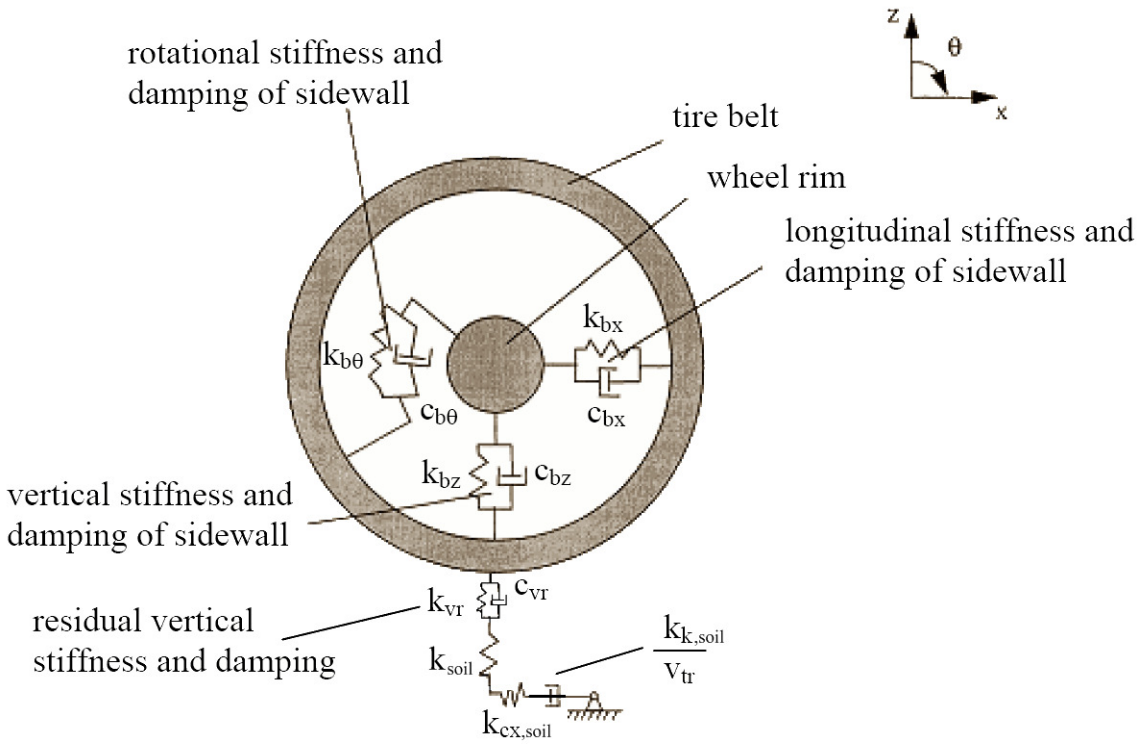

Figure 5.10: Newly developed in-plane rigid ring model and parameters for soft soil.

5.4.1 DETERMINATION OF THE LONGITUDINAL SLIP STIFFNESS ON SOFT SOIL, $k_{k,soil}$

Figure 5.11 shows the traction test of the RHD tire on soft soil to determine the longitudinal slip stiffness. The tire is quickly accelerated to a rotational velocity of 20 km/hr and is allowed to roll forward. Initially there is nearly 100% slip before the tire begins to move forward, and the slip approaches 0% as the tire asymptotically nears a linear velocity of 20 km/hr.

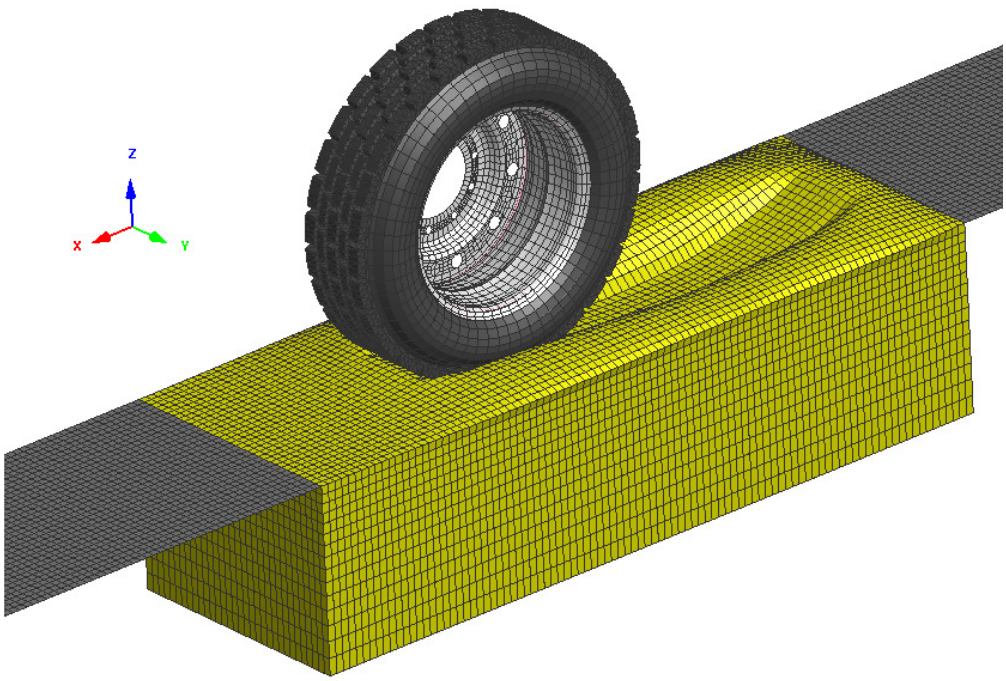

Figure 5.11: Tire traction test on soft soil.

Figure 5.12 shows the time history plot for % slip, contact force in the z direction (vertical), and contact force in the x direction (longitudinal) which is obtained from the traction test shown in Figure 5.11. The slope of the longitudinal force vs. slip curve at a slip ratio of zero is defined as the longitudinal slip stiffness ($k_{k,soil}$), and can be found by applying a linear curve fit to the data in Figure 5.13.

$$k_{k,soil} = 23.635 \frac{kN}{slip\ unit} \tag{5.15}$$

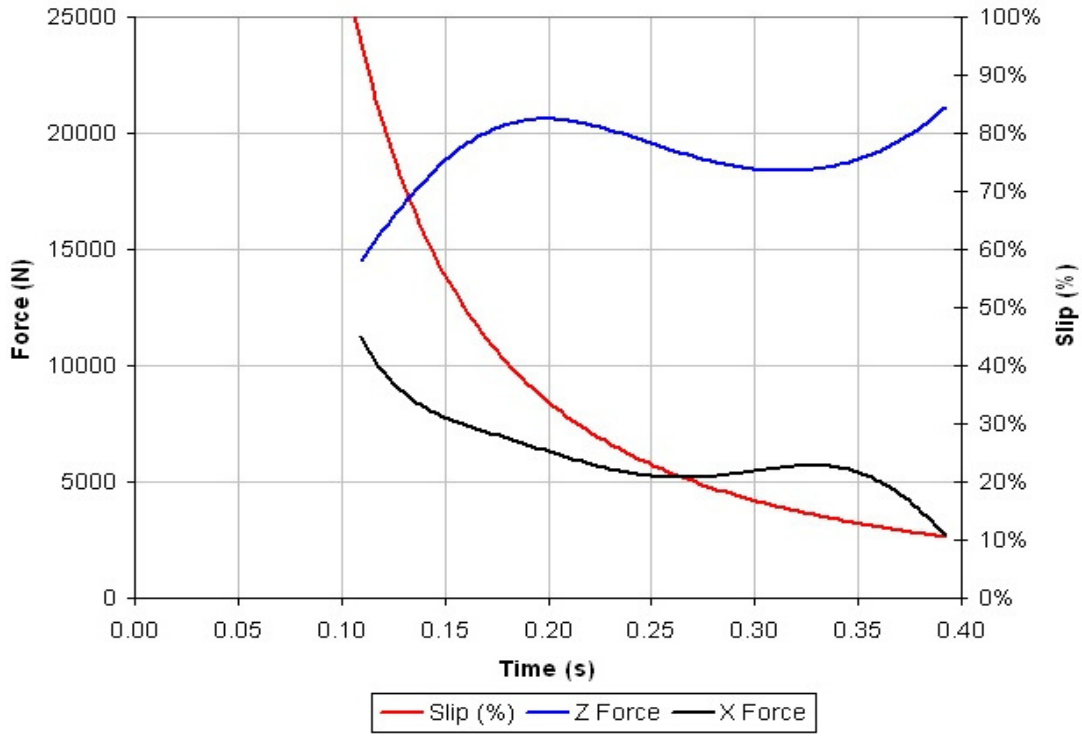

Figure 5.12: Traction characteristics on soft soil.

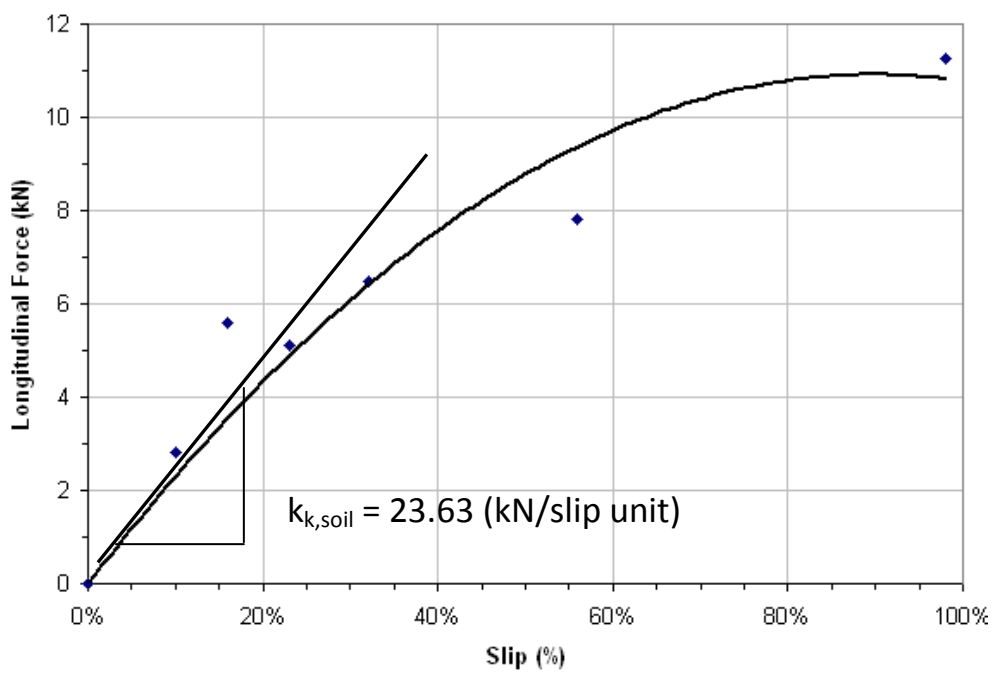

Figure 5.13: Longitudinal force as a function of slip ratio for a tire on soft soil.

5.4.2 IN-PLANE TIRE TOTAL EQUIVALENT VERTICAL STIFFNESS ON SOFT SOIL, $k_{tot,soil}$

The in-plane sidewall and residual stiffness (k_{bz} and k_{vr}, respectively) will remain the same whether the tire is running on rigid road or soft soil. An additional parameter, k_{soil}, must be introduced to account for the additional flexibility of the soil. When a tire is loaded on the soil the deflection of the soil (termed the sinkage) can be plotted against load to obtain the soil's stiffness. The vertical stiffness of the soil alone is represented by the parameter k_{soil}, which is described by Equation 5.16, and its value is found by obtaining the slope from a linear curve fit to the load vs. sinkage data in Figure 5.15. The tire sidewall, tread residual, and soil stiffnesses are physically represented as springs in series, therefore they can be combined using Equation 5.17 to find an equivalent total tire stiffness ($k_{tot,soil}$). This parameter incorporates the stiffness of the soil and will therefore change depending on the type of soil in the model.

$$k_{soil} = \frac{Load}{Sinkage} = 321.62\ kN/m \tag{5.16}$$

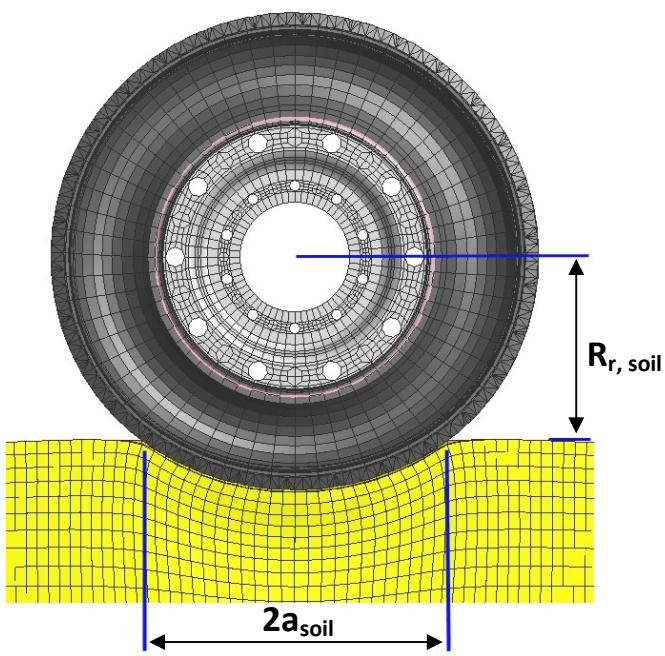

Figure 5.14: Projected contact length and rolling radius of RHD tire on soft soil.

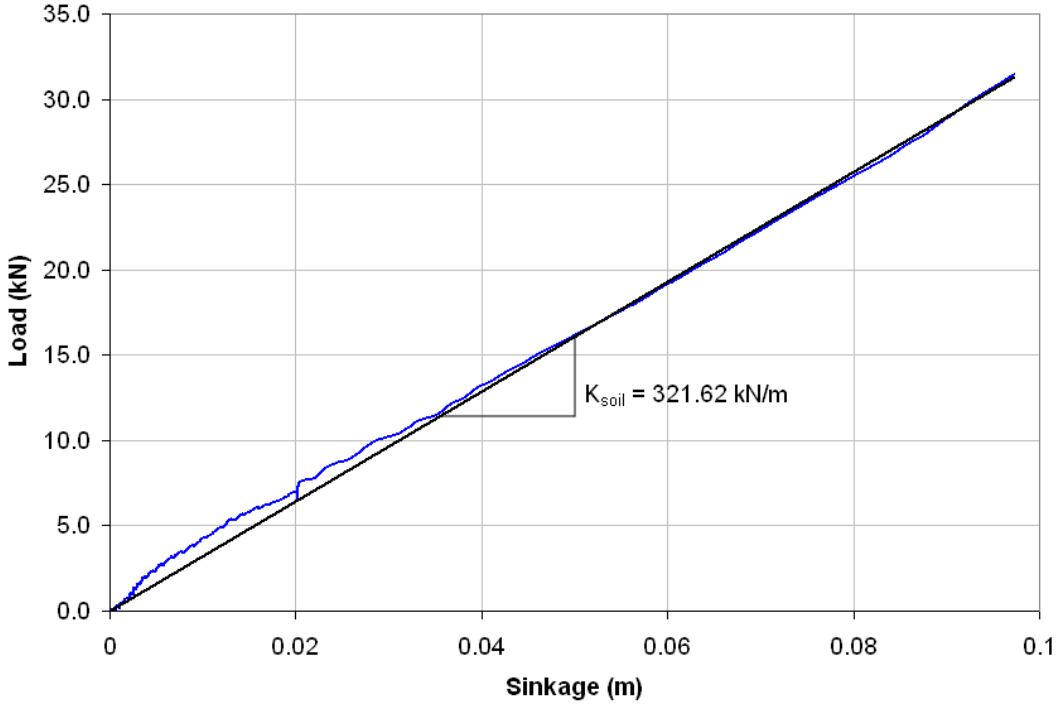

Figure 5.15: Relationship between load and soil sinkage.

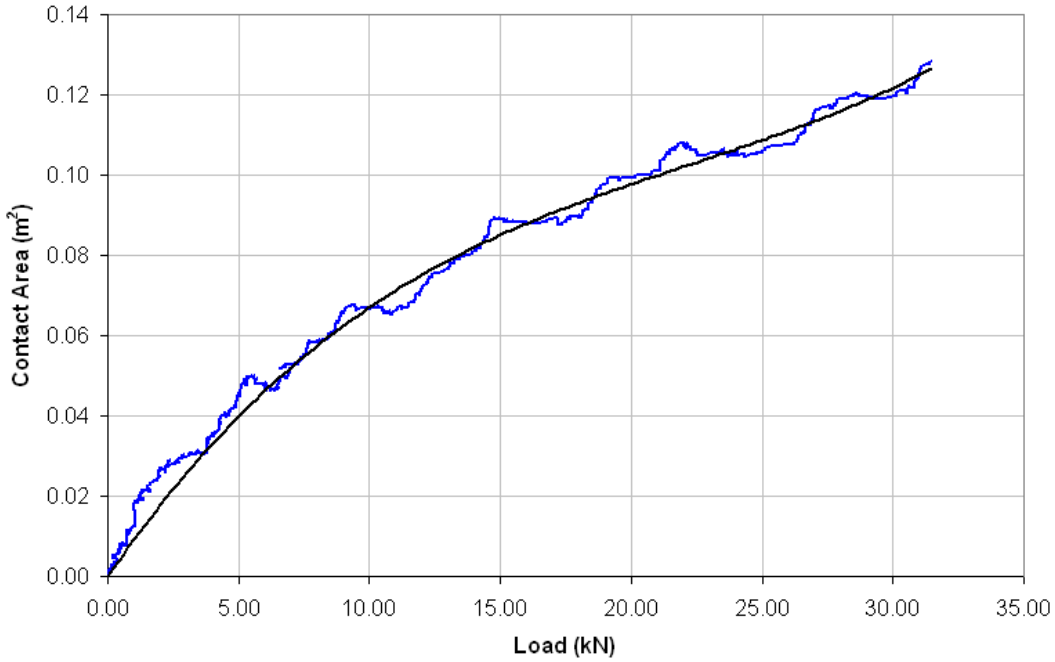

Figure 5.16: Contact area vs. load of RHD tire on soft soil. The blue line represents the actual simulation results, while the black line represents a polynomial curve fit.

$$\frac{1}{k_{tot,soil}} = \frac{1}{k_{soil}} + \frac{1}{k_{bx}} + \frac{1}{k_{vr}} \tag{5.17}$$

Where: k_{soil} = 321.624 kN/m, k_{bz} = 732.67 kN/m, k_{vr} = 16910.00 kN/m.

The equivalent tire stiffness on soft soil, $k_{tot,soil}$ = 226.985 kN/m. For comparison, the total stiffness on soft soil is about one third as much as the tire stiffness on rigid road, k_{tot} = 765.850 kN/m.

The equivalent longitudinal tread stiffness on soft soil, $k_{cx,\ soil}$, using the projected half-contact length (a_{soil}) can be expressed by the same method used on hard surface in Zegelaar and Pacejka (1997).

$$k_{cx,soil} = \frac{k_{k,soil}}{a_{soil}} = 91.216\frac{kN}{m} \tag{5.18}$$

Table 5.5 shows the summary of the in-plane-parameters for the rigid ring model if moving on same soft soil.

Table 5.5: Rigid ring model parameters for soft soil

Rigid Ring Parameter	18.911 kN Vertical Load (4250 lbs)
a_{soil} (m)	0.255
$a_{soil,\ actual}$ (m)	0.259
C_{bx}, C_{bz} (kN s/m)	0.470
$C_{b\theta}$ (kN ms/rad)	0.0142
$k_{cx,soil}$ (kN/m)	91.216
$k_{k,soil}$ (kN/unit slip)	23.625
$k_{tot,soil}$ (kN/m)	226.99
C_{vr} (kN s/m)	2.054
$f_{r,soil}$ with 18.9 kN (4250 lbs) load and a velocity of 20 km/hr	0.340
I_{ay} (kg m^2)	3.034
I_{ax}, I_{az} (kg m^2)	1.786
I_{by} (kg m^2)	12.073
I_{bx}, I_{bz} (kg m^2)	6.840
k_{bx}, k_{bz} (kN/m)	732.67
$k_{b\theta}$ (kN m/rad)	385.276
k_{vr} (kN/m)	16910
$k_{tot,soil}$ (kN/m)	226.985
m_a (kg)	34.800
m_b (kg)	72.000
$R_{r,\ soil}$ (m) at a vertical load of 18.9 kN (4250 lbs)	0.458

CHAPTER 6

OUT-OF-PLANE RIGID RING PARAMETERS

6.1 DETERMINATION OF OUT-OF-PLANE PARAMETERS FOR THE RIGID RING TIRE MODEL

This chapter will focus on the equations and specific tests performed to obtain each of the out-of-plane rigid ring model parameters for a tire running on both a rigid surface and on soft soil.

6.1.1 DETERMINATION OF THE OUT-OF-PLANE TRANSLATIONAL STIFFNESS, k_{by}, AND DAMPING CONSTANT, C_{by}

The out-of-plane rigid ring model for a tire on a rigid surface (shown in Figure 4.2) has already been explained and presented in Chapter 4. In order to calculate the out-of-plane sidewall translational stiffness and damping constant, the rim of the tire model is set to a rigid body and constrained not to be translated and rotated. The tread base and tread parts are also set to a rigid body but are free to move only in lateral direction. Then, lateral forces on selected two nodes of the rigid tread are applied to excite the rigid tread part laterally as shown in Figure 6.1. Due to the sidewall out-of-plane translational stiffness, the tread is translated a certain lateral distance. Then, the lateral load is quickly removed to excite the translational vibration and predict a translational damping constant. A lateral force of 15 kN (3372 lbs) was applied on the top and bottom of the tire in same directions after inflation as can be seen in Figure 6.1.

Figure 6.1: Out-of-plane translational excitation of the sidewall.

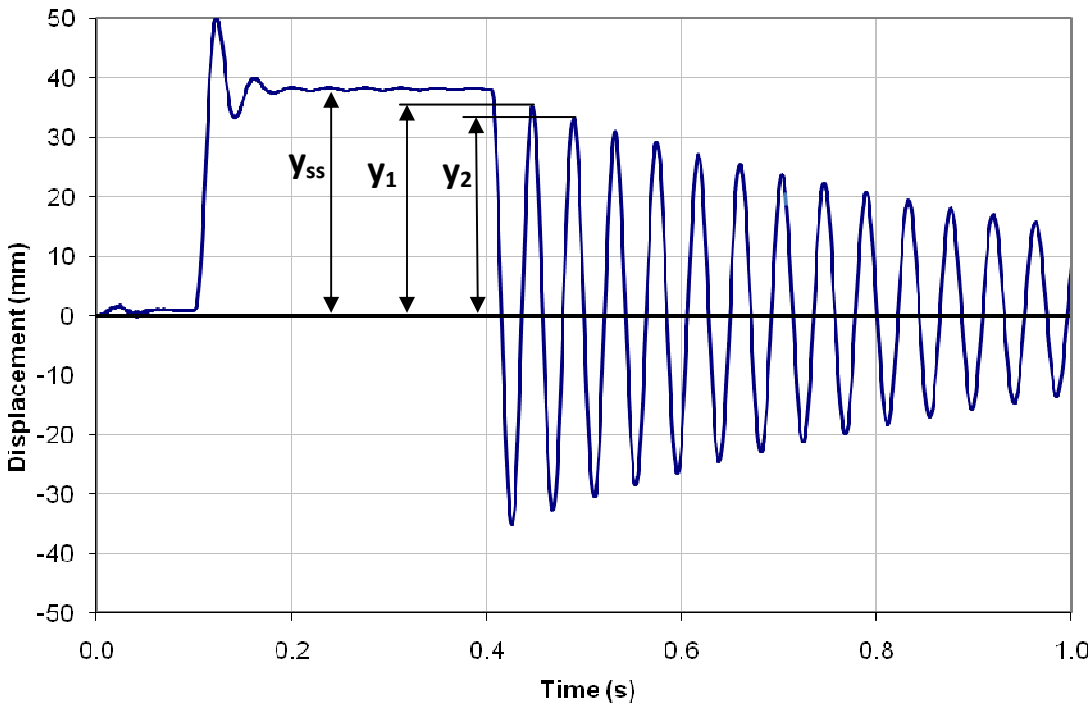

Figure 6.2: Out-of-plane sidewall translation displacement and damping response.

Figure 6.2 shows the simulation result. The figure shows the steady state lateral displacement and transient state of damping response of the sidewall. Figure 6.2 shows the lateral displacement of 38.1 mm due to the applied lateral force of 30 kN on the rigid tread band. Using Equation 6.1 and the applied force and lateral displacement, the out-of-plane translational stiffness, k_{by}, can be calculated.

$$k_{by} = \frac{Lateral\ Force}{Lateral\ Displacement} = \frac{30\ kN}{0.0381\ m} = 787.4\ kN/m \tag{6.1}$$

When the applied lateral forces are quickly removed, the rigid tread band undergoes out-of-plane translational vibrations whose magnitudes are decreasing with time as can be seen in Figure 6.2. This logarithmic decrement of the angular displacements is adopted to calculate the out-of-plane translational damping constant of the sidewall. Two neighboring peak points are selected from Figure 6.2 to calculate damping constant.

Lateral displacement y_1=34.978 mm at time t_1=0.448.
Lateral displacement y_2=32.932 mm at time t_2=0.490.

Then, the logarithmic decrement (δ) becomes:

$$\delta = \ln\left(\frac{y_1}{y_2}\right) = \ln\left(\frac{34.978\ mm}{32.932\ mm}\right) = 0.06027 \tag{6.2}$$

From Equations 6.3 and 6.4 the dimensionless damping ratio, ξ, and damped period of vibration, τ_d, are found to be 0.009547 and 0.0420, respectively.

$$\xi = \frac{\delta}{\sqrt{4\pi^2 + \delta^2}} = \frac{0.060274463}{\sqrt{4\pi^2 + (0.060274463)^2}} = 0.009547 \tag{6.3}$$

$$\tau_d = t_2 - t_1 = (0.490 - 0.448) = 0.0420 \tag{6.4}$$

Now that ξ and the damped period of vibration have been determined, the next step is to find the translational damped and undamped natural frequencies, ω_d and ω_n, respectively. Table 6.1 shows the values of the parameters used in the calculation steps for the out-of-plane translational damping constant.

$$\tau_d = \frac{2\pi}{\omega_d} = \frac{2\pi}{\omega_n\sqrt{1-\xi^2}} \tag{6.5}$$

Therefore,

$$\omega_d = \frac{2\pi}{\tau_d} = 149.6\ Hz \tag{6.6}$$

$$\omega_n = \frac{2\pi}{\tau_d\sqrt{1-\xi^2}} = 149.9\ Hz \tag{6.7}$$

Where: ω_d = Damped natural frequency,

ω_n = Undamped natural frequency.

Therefore, the critical damping constant (C_c) can be obtained by using Equation 6.8 with the known mass of the tire belt (m_b, 72 kg).

$$C_c = 2 * m_b * \omega_n = 21.586\ kN\ s/m \tag{6.8}$$

Finally, the out-of-plane translational damping constant (C_{by}) is calculated by Equation 6.9.

$$C_{by} = \xi * C_c = 1.301\ kN\ s/m \tag{6.9}$$

Table 6.1: Parameters used in the calculation of the out-of-plane translational damping constant.

Parameter	Symbol	Value	Unit
Translational stiffness	k_{by}	787.402	kN/m
Logarithmic decrement	δ	0.06027	-
Dimensionless damping ratio	ξ	0.009547	-
Damped period of vibration	τ_d	0.0420	s
Critical damping constant	C_c	21.586	kN s/m
Translational damping constant	C_{by}	1.301	kN s/m

6.1.2 DETERMINATION OF THE OUT-OF-PLANE ROTATIONAL STIFFNESS, $k_{b\gamma}$, AND DAMPING CONSTANT, $C_{b\gamma}$

In order to calculate the out-of-plane sidewall rotational stiffness and damping constant, the rim of the tire model is set to a rigid body and constrained not to be translated and rotated. The tread base and tread parts are also set to a rigid body and free only in out-of-plane rotational direction. Then, lateral forces on selected two nodes of the rigid tread are applied to rotate the rigid tread part about the spindle of the tire. Due to the sidewall out-of-plane rotational stiffness, the belt is rotated a certain angle. Then, the lateral load is quickly removed to excite the rotational vibration. The rotational stiffness and damping constant can then be calculated using the same logarithmic decrement procedures used to determine the lateral parameters. The equation for the critical damping must be changed by replacing the mass of the tire belt with the moment of inertia of the tire belt due to the rotational nature of the simulation. A lateral force of 15 kN (3372 lbs) was applied on the top and bottom of the tire in opposite directions after inflation as can be seen in Figure 6.3.

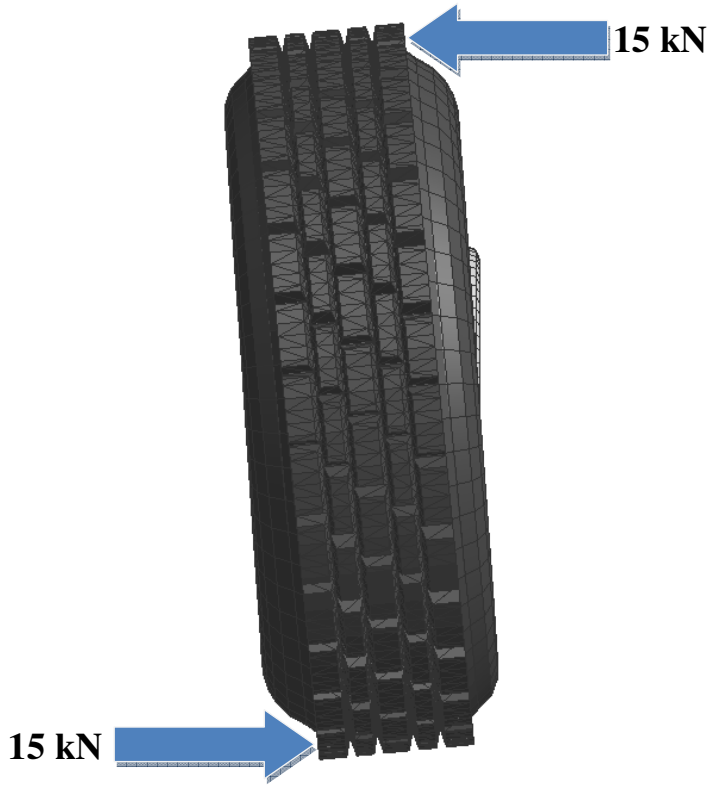

Figure 6.3: Out-of-plane rotational excitation of the sidewall.

Figure 6.3 shows the simulation result. The figure shows mainly the steady state rotational displacement and transient state of damping response of the sidewall. Using this applied moment and angular displacement, the out-of-plane translational stiffness, $k_{b\gamma}$, can be calculated as follows.

$$k_{b\gamma} = \frac{Moment}{Angular\ Displacement} = \frac{2 * 15\ kN * (1.092\ m/2)}{0.09920\ rad} = 276.8\ \frac{kN\ m}{rad} \qquad (6.10)$$

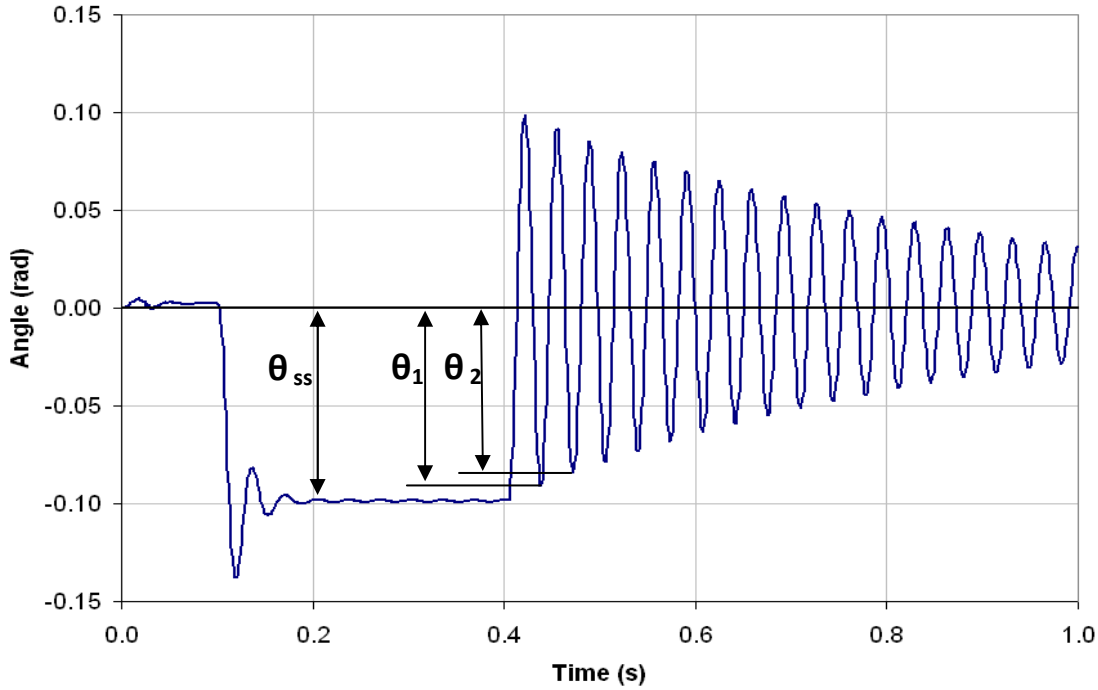

Figure 6.4: Out-of-plane sidewall rotational displacement and damping response.

When the applied lateral forces are quickly removed, the rigid tread band undergoes out-of-plane rotational vibrations whose magnitudes are decreasing with time as can be seen in Figure 6.4. This logarithmic decrement of the angular displacements is adopted to calculate the out-of-plane rotational damping constant of the sidewall. Two neighboring peak points are selected from Figure 6.4 to calculate the damping constant as:

Angular displacement θ_1=0.09098 rad. at time t_1=0.439.

Angular displacement θ_2=0.08418 rad. at time t_2=0.473.

Angular displacement θ_{ss}=0.09920 rad.

Then, the logarithmic decrement (δ) becomes:

$$\delta = \ln\left(\frac{y_1}{y_2}\right) = \ln\left(\frac{0.09098}{0.08418}\right) = 0.07768 \qquad (6.11)$$

From Equation 6.12, the dimensionless damping ratio (ξ) is found to be 0.012287.

$$\xi = \frac{\delta}{\sqrt{4\pi^2 + \delta^2}} = \frac{0.07768}{\sqrt{4\pi^2 + (0.07768)^2}} = 0.012287 \tag{6.12}$$

The damped period of vibration ($\tau_d = t_2 - t_1$) equal to 0.034 sec is calculated using Equation 6.13.

$$\tau_d = t_2 - t_1 = (0.490 - 0.448) = 0.0420 \tag{6.13}$$

Now that ξ and the damped period of vibration have been determined, the next step is to find the rotational damped and undamped natural frequencies, ω_d and ω_n respectively. The damped and undamped natural frequencies, ω_d and ω_n, can be calculated as 184.8 rad/sec and 184.8 rad/sec using Equations 6.15 and 6.16, respectively.

$$\tau_d = \frac{2\pi}{\omega_d} = \frac{2\pi}{\omega_n\sqrt{1-\xi^2}} \tag{6.14}$$

Therefore,

$$\omega_d = \frac{2\pi}{\tau_d} = 184.8 \text{ rad/s} \tag{6.15}$$

$$\omega_n = \frac{\omega_d}{\sqrt{1-\xi^2}} = 184.8 \text{ rad/s} \tag{6.16}$$

Where: ω_d = Damped natural frequency,

ω_n = Undamped natural frequency.

Therefore, the critical damping constant (C_c) can be obtained by using Equation 6.17 with the moment of inertia of the tire belt (I_{bx}, 6.840 kg m^2).

$$C_c = 2 * I_{bx} * \omega_n = 2.528\ kN\ m\ s/rad \tag{6.17}$$

Finally, the out-of-plane rotational damping constant ($C_{b\gamma}$) is calculated by Equation 6.18.

$$C_{b\gamma} = \xi * C_c = 0.03107\ kN\ m\ s/rad \tag{6.18}$$

Table 6.2 shows the parameters used in the calculations of the out-of-plane rotational damping constants for the FEA RHD tire model.

Table 6.2: Parameters used in the calculation of the out-of-plane rotational damping constant.

Parameter	Symbol	Value	Unit
Rotational stiffness	$k_{b\gamma}$	276.85	kN/m
Logarithmic decrement	δ	0.07768	-
Dimensionless damping ratio	ξ	0.01229	-
Damped period of vibration	τ_d	0.034	s
Critical damping constant	C_c	2.528	kN s/m
Rotational damping constant	$C_{b\gamma}$	0.03107	kN s/m

6.1.3 DETERMINATION OF THE LATERAL SLIP STIFFNESS, k_l, AND DAMPING CONSTANT, C_l, ON RIGID ROAD

The lateral slip stiffness (k_l) and damping constant (C_l) of the tire at the contact area at a vertical load of 18.9 kN can be predicted by the lateral free vibration test. In this test, a lateral load of 5.0 kN is applied as shown in Figure 6.5 and suddenly released. The steady state lateral displacement and transient state of damping response of the tire are observed in Figure 6.6.

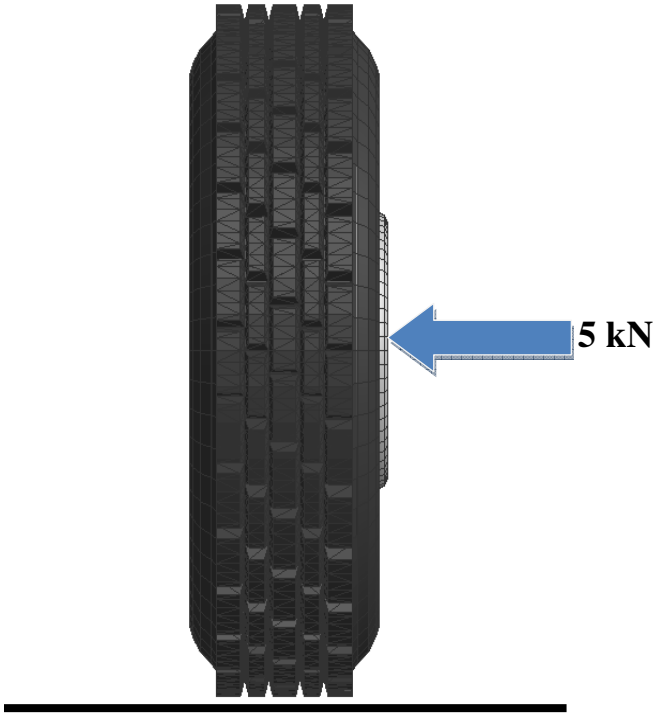

Figure 6.5: Lateral excitation at tire spindle.

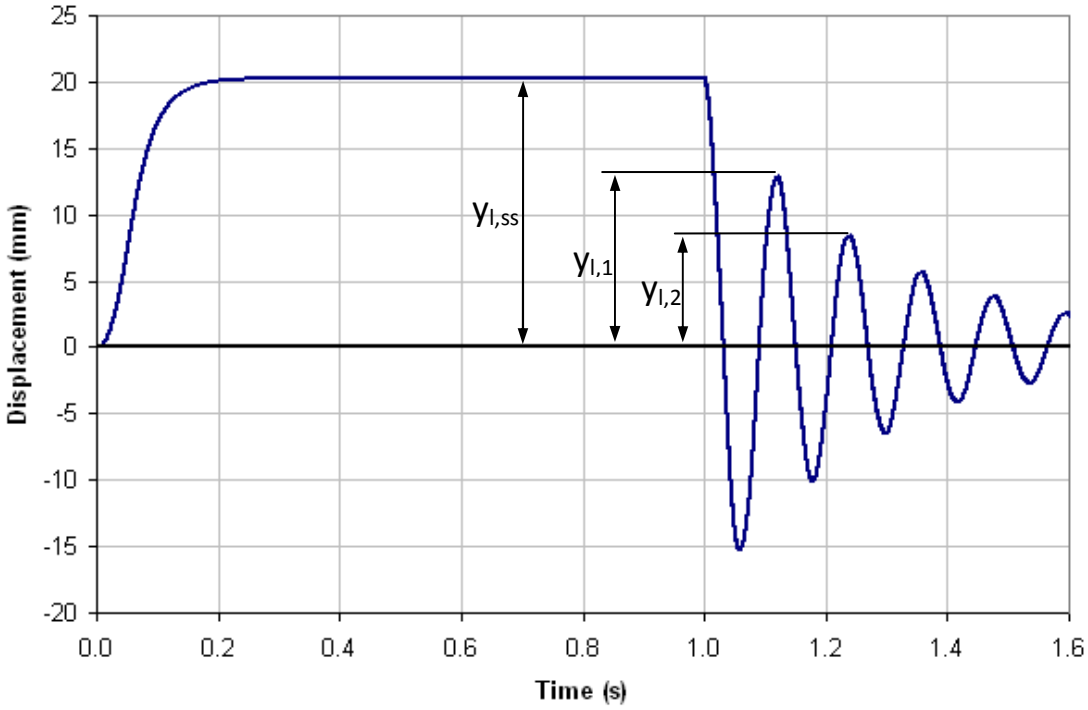

Figure 6.6: Lateral free vibration test results for a vertical tire load of 18.9 kN.

Figure 6.6 shows the lateral displacement of 20.2 mm due to the applied lateral force of 5.0 kN on the tire center. By using this applied force and the displacement, the lateral slip stiffness (k_l) of the tire at contact area can be calculated as follows.

$$k_l = \frac{Lateral\ Force}{Lateral\ Displacement} = \frac{5\ kN}{0.0202\ m} = 247.525\ kN/m \tag{6.19}$$

When the applied lateral forces are quickly removed, the tire undergoes out-of-plane translational vibration as seen in Figure 6.6. The logarithmic decrement of the angular displacements is adopted to calculate the out-of-plane slip stiffness and damping at the contact area. From Figure 6.6, two neighboring peak points are selected to calculate damping constant such as:

Lateral displacement y_1= 12.874 mm at time t_1=1.1206 second,
Lateral displacement y_2= 8.397 mm at time t_2=1.2388 second.

Then, the logarithmic decrement (δ) becomes,

$$\delta = \ln\left(\frac{y_1}{y_2}\right) = 0.4273 \tag{6.20}$$

From Equation 6.21, the dimensionless damping ratio, ξ, is found to be 0.06574.

$$\xi = \frac{\delta}{\sqrt{4\pi^2 + \delta^2}} = \frac{0.}{\sqrt{4\pi^2 + (0.)^2}} = 0.06574 \tag{6.21}$$

The damped period of vibration ($\tau_d = t_2 - t_1$) is 0.1182 sec. From Equation 6.22, damped and undamped natural frequencies, ω_d and ω_n, can be calculated as 53.16 rad/sec and 53.27 rad/sec respectively.

$$\tau_d = \frac{2\pi}{\omega_d} = \frac{2\pi}{\omega_n\sqrt{1-\xi^2}} \tag{6.22}$$

Where: ω_d = Damped natural frequency,

ω_n = Undamped natural frequency.

Therefore, the critical damping constant (C_c) can be obtained by using Equation 6.23 with the mass of the tire and rim (m_{wheel}, 106.8 kg). Finally, the out-of-plane translational damping constant (C_{by}) is calculated by Equation 6.24. Table 6.3 shows the parameters used for the calculation of the out-of-plane slip damping constant at the contact area.

$$C_c = 2 * m_{wheel} * \omega_n = 11.08\ kN\ s/m \tag{6.23}$$

The out-of-plane slip damping constant at the contact area (c_l) is calculated from Equation 6.24.

$$C_l = \xi * C_c = 0.728\ kN\ s/m \tag{6.24}$$

Table 6.3: Parameters used in the calculation for the out-of-plane slip damping constant.

Parameter	Symbol	Value	Unit
Logarithmic decrement	δ	0.4273	-
Dimensionless damping ratio	ξ	0.06574	-
Damped period of vibration	τ_d	0.1182	s
Undamped natural frequency	ω_n	53.27	rad/s
Mass of tire and rim	m_{wheel}	106.80	kg
Critical damping constant	C_c	11.08	kN s/m
Out-of-plane damping constant	C_l	0.728	kN s/m

6.2 CORNERING CHARACTERISTICS ON RIGID ROAD

Figure 6.7 shows the simulation used to predict the steady state cornering characteristics on rigid road at 8 km/hr and 18.9 kN vertical load.

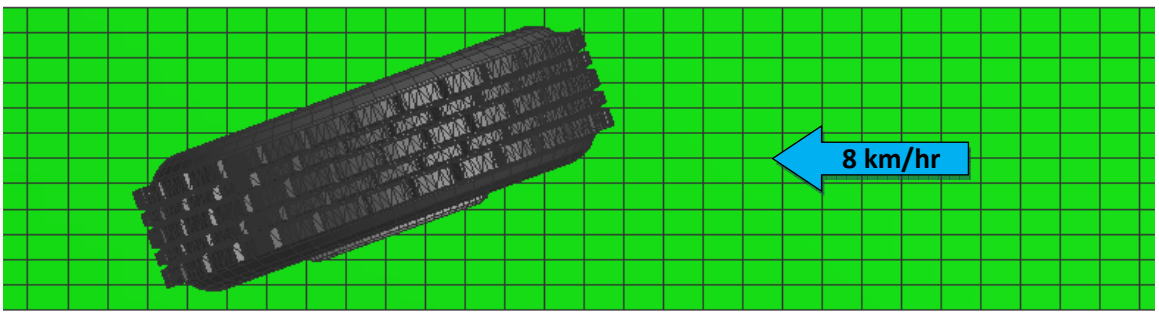

Figure 6.7: Steady state steering test at a slip angle of 20 degrees on rigid road. The tire is fixed and the road is moved with a velocity of 8 km/hr as shown on the figure.

6.2.1 CORNERING STIFFNESS ON RIGID ROAD.

Cornering stiffness (k_f) is defined as the derivative of the lateral force (F_y) with respect to slip angle (α) evaluated at zero slip angle. The cornering stiffness was determined by performing seven steady state steering simulations at a range of slip angles: 0, 1, 4, 6, 8, 12, and 20 degrees. The lateral force for each simulation was plotted with a line connecting the points. Equation 6.5 is used to calculate the slope at zero slip angle, which is estimated as equal to the slope from 0 degrees slip to 1 degree slip.

$$k_f = \left.\frac{\partial F_y}{\partial \alpha}\right|_{\alpha=0} \tag{6.25}$$

Thus, the cornering stiffness is defined as the slope at zero slip angle as shown in Figure 6.8.

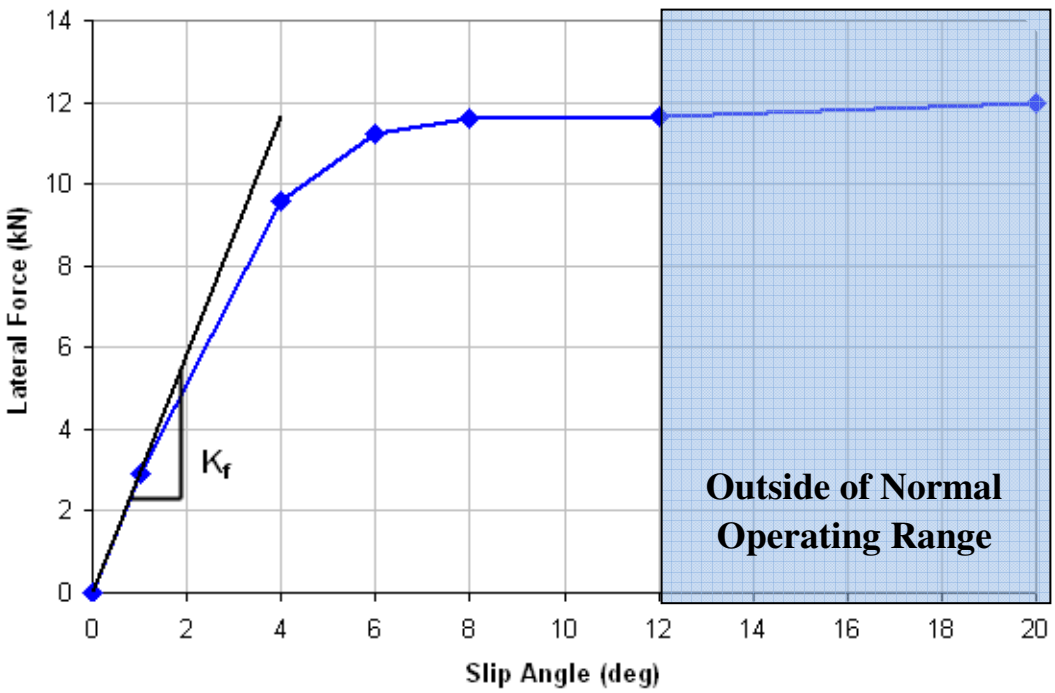

Figure 6.8: Cornering stiffness as a function of slip angle on rigid road for an 18.9 kN vertical load.

A cornering stiffness of 167.2 kN/rad is calculated at tire load of 18.9 kN from the initial slope of the curve in Figure 6.8. The normal operating range for the slip angle of truck tires is usually within 12°, as shown by University of Michigan Transportation Research Institute's (UMTRI) tire testing, and is shaded in blue on Figure 6.8 and Figure 6.9 (Chae, 2006).

6.2.2 SELF-ALIGNING TORQUE STIFFNESS ON RIGID ROAD

The self-aligning torque stiffness (k_M) is the moment on the tire that is generated due to the tendency for the pressure beneath the tire to shift fore or aft during rolling. This moment is produced during turning maneuvers and attempts to counteract the turning forces causing the tire to turn. It is defined as the derivative of the self-aligning moment (M_y) with respect to slip angle (α) evaluated at zero slip angle. The cornering stiffness was determined by

performing steady state steering simulations at a range of slip angles from 0 to 20 degrees. The lateral force for each simulation was plotted with a curve fit through the points. Equation 6.5 is used to calculate the slope at zero slip angle, which is estimated as equal to the initial slope of the curve fit.

$$k_M = \left.\frac{\partial M_y}{\partial \alpha}\right|_{\alpha=0} \tag{6.26}$$

Therefore, the self-aligning torque stiffness is predicted as the slope at zero slip angle as shown in Figure 6.9. A self-aligning torque stiffness of 1.11 kN m/rad is calculated at tire load of 18.9 kN from Figure 6.9.

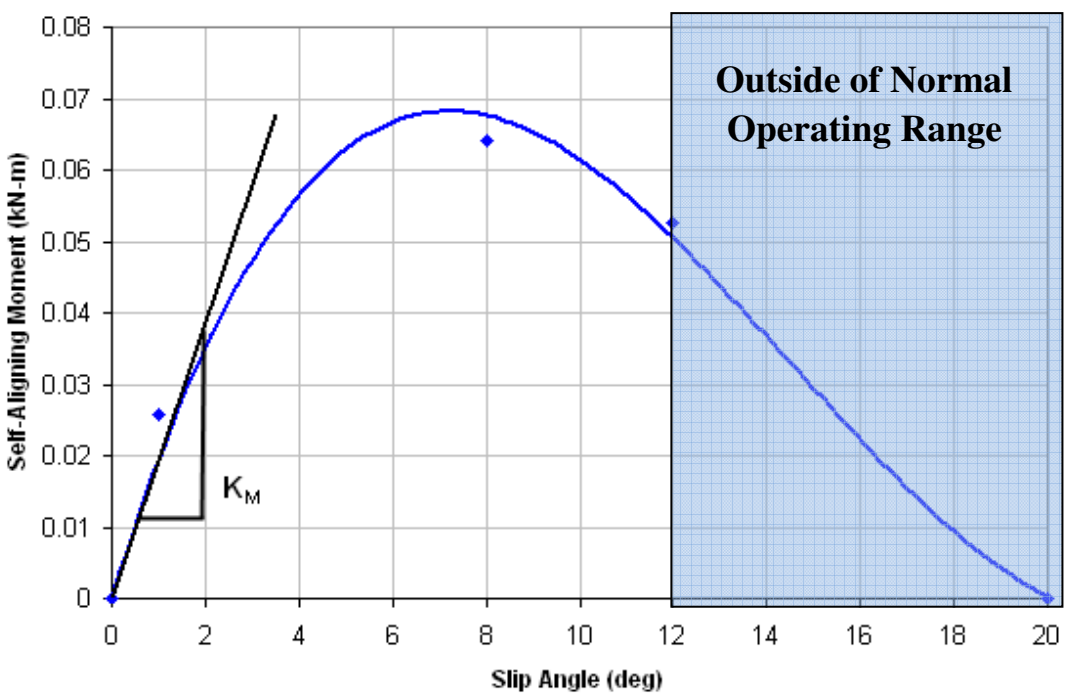

Figure 6.9: Self-aligning moment as a function of slip angle on rigid road for an 18.9 kN vertical load.

6.2.3 RELAXATION LENGTH

The tire contact patch relaxation length (σ) on rigid surface can be calculated from the following equation.

$$\sigma = \frac{k_f}{k_l} = 0.676 \tag{6.27}$$

Where: k_f = the cornering stiffness (167.2 kN/rad) and

k_l = the lateral slip stiffness of the tire, defined in Equation 6.19 (247.525 kN/m).

The relaxation length is dependent on the applied tire load and tire size. However, it is not significantly influenced by other operation conditions, such as speed. Thus, the relaxation length is usually predicted at low tire speeds such as 5 km/hr.

6.2.4 SUMMARY OF OUT-OF-PLANE PARAMETERS ON RIGID ROAD

Table 6.4 is a summary of the symbols, values, and units for each of the out-of-plane parameters calculated for the tire running on rigid road.

Table 6.4: Out-of-plane parameters for the rigid ring model on rigid road for an 18.9 kN vertical load.

Parameter	Symbol	Value	Unit
Translational stiffness of sidewall	k_{by}	787.4	kN/m
Translational damping of sidewall	C_{by}	1.301	kN-s/m
Rotational stiffness of sidewall	$k_{b\gamma}$	276.9	kN-m/rad
Rotational damping of sidewall	$C_{b\gamma}$	0.02295	kN-m-s/rad
Lateral slip stiffness	k_l	247.5	kN/m
Lateral slip damping	C_l	0.728	kN-s/m
Cornering stiffness	k_f	167.2	kN/rad
Self-aligning moment stiffness	k_M	1.11	kN-m/rad
Relaxation length	σ	0.676	m

6.3 DETERMINATION OF ADDITIONAL OUT-OF-PLANE PARAMETERS FOR NEW OFF-ROAD RIGID RING MODEL

The recommended rigid ring model for soft soil, shown in Figure 4.4 and Figure 6.10 below, has already been developed in Chapter 4, therefore only the calculations and tests performed to determine the out-of-plane parameters will be presented in this section.

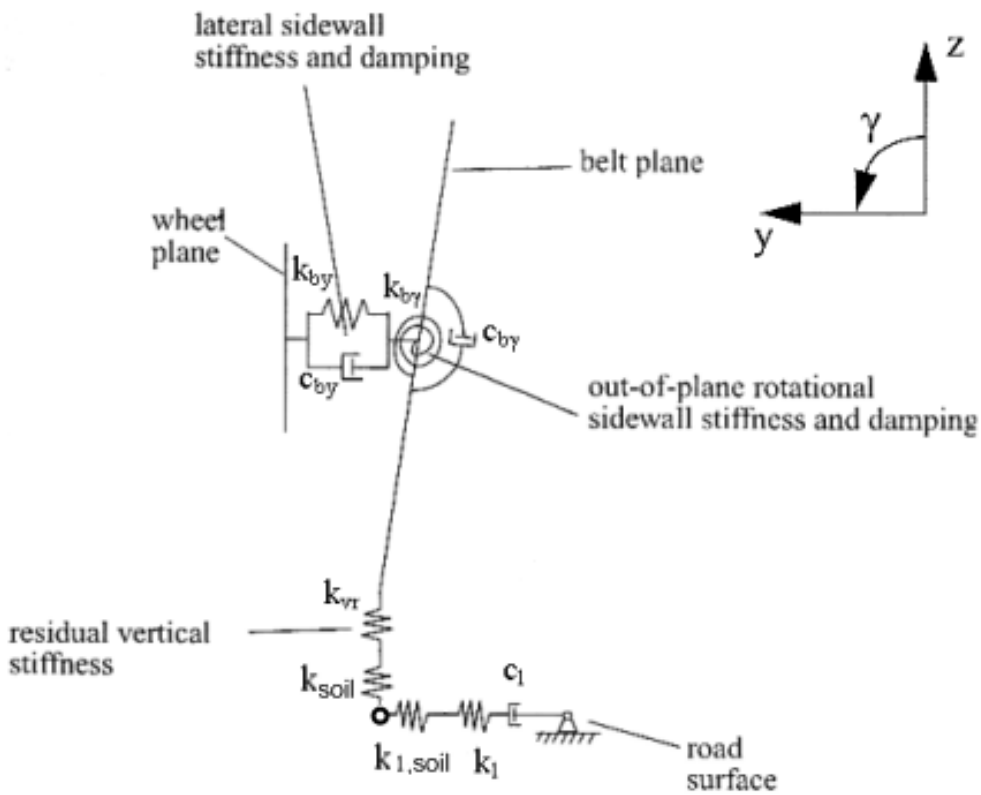

Figure 6.10: Recommended out-of-plane rigid ring model and parameters for soft soil.

6.3.1 DETERMINATION OF LATERAL SLIP STIFFNESS, $k_{l,soil}$, AND DAMPING CONSTANT, $C_{l,soil}$, ON SOFT SOIL

The lateral slip stiffness ($k_{l,soil}$) and damping constant ($C_{l,soil}$) of the tire at the contact area at a vertical load of 18.9 kN can be determined by the lateral free vibration test. In this test, a lateral load of 5.0 kN is applied as shown in Figure 6.11 and suddenly released. The steady state lateral displacement and transient state of damping response of the tire are observed in Figure 6.12.

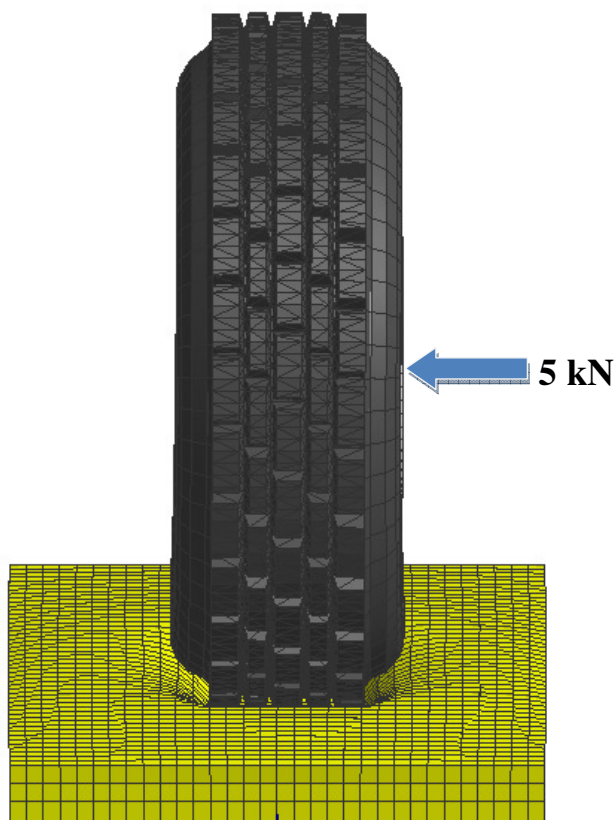

Figure 6.11: Lateral excitation at tire spindle.

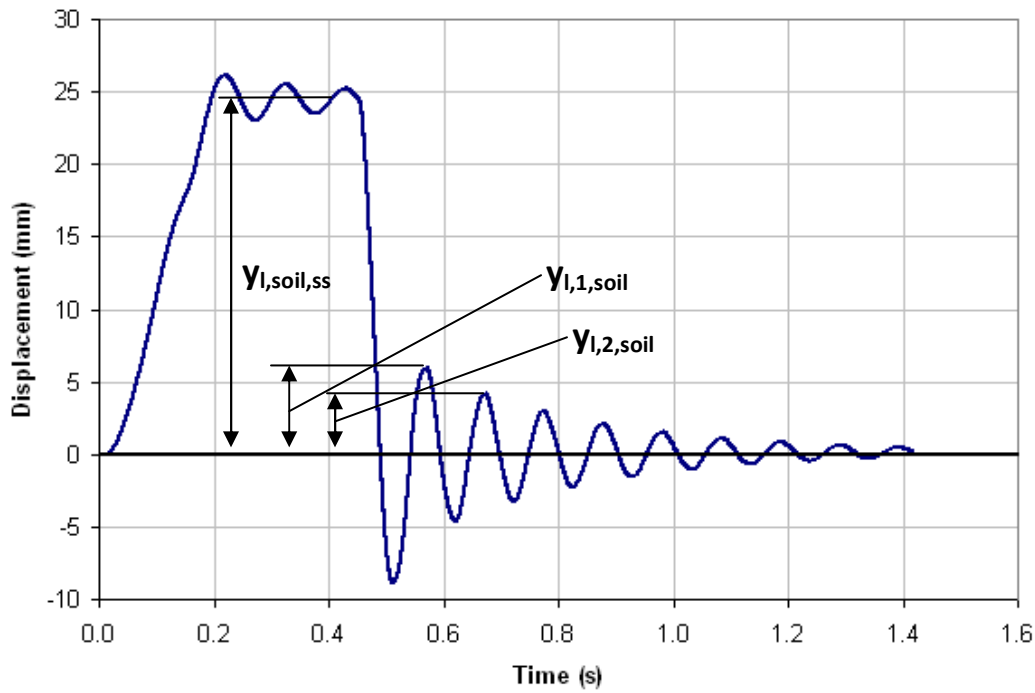

Figure 6.12: Lateral free vibration test results on soft soil for a vertical load of 18.9 kN.

Figure 6.12 shows the lateral displacement of 24.8 mm due to the applied lateral force of 5.0 kN on the tire center. Using the applied force and the lateral displacement, the out-of-plane slip stiffness ($k_{l,total,soil}$) of the tire at the contact can be calculated using Equation 6.28. The equivalent lateral stiffness of the soil, $k_{l,soil}$, can then be calculated using Equation 6.29 and the known values for $k_{l,tot,soil}$ and k_l.

$$k_{l,tot,soil} = \frac{Lateral\ Force}{Lateral\ Displacement} = \frac{5\ kN}{0.0248\ m} = 201.6\ kN/m \qquad (6.28)$$

$$\frac{1}{k_{l,soil}} = \frac{1}{k_{l,tot,soil}} - \frac{1}{k_l} \qquad (6.29)$$

Where: k_l = lateral stiffness of tire on rigid road (247.5 kN/m), and

$k_{l,soil}$ = equivalent lateral stiffness of the soil (1087.1 kN/m).

When the applied lateral forces are quickly removed, the tire undergoes out-of-plane translational vibration as seen in Figure 6.12. The logarithmic decrement of the angular displacements is adopted to calculate the out-of-plane slip stiffness and damping at the contact area. From Figure 6.12, two neighboring peak points are selected to calculate damping constant.

Lateral displacement $y_{l,1,soil} = 5.97$ mm at time $t_1 = 0.5680$ second,
Lateral displacement $y_{l,2,soil} = 4.20$ mm at time $t_2 = 0.6727$ second.

Then, the logarithmic decrement (δ) becomes

$$\delta = \ln\left(\frac{y_1}{y_2}\right) = \ln\left(\frac{34.978\ mm}{32.932\ mm}\right) = 0.352 \tag{6.30}$$

From Equation 6.31, the dimensionless damping ratio (ξ) is found to be 0.0544.

$$\xi = \frac{\delta}{\sqrt{4\pi^2 + \delta^2}} = \frac{0.}{\sqrt{4\pi^2 + (0.)^2}} = 0.0544 \tag{6.31}$$

The damped period of vibration ($\tau_{d,soil} = t_2 - t_1$) is 0.1047 sec. From Equation 6.32 the damped and undamped natural frequencies, $\omega_{d,soil}$ and $\omega_{n,soil}$, can be calculated as 60.1 rad/sec and 60.0 rad/sec respectively.

$$\tau_{d,soil} = \frac{2\pi}{\omega_{d,soil}} = \frac{2\pi}{\omega_{n,soil}\sqrt{1-\xi^2}} \tag{6.32}$$

Where: $\omega_{d,soil}$ = Damped natural frequency,
$\omega_{n,soil}$ = Undamped natural frequency.

Therefore, the critical damping constant ($C_{c,soil}$) can be obtained by using Equation 6.33 with the mass of the tire and rim (m_{wheel}, 106.8 kg).

$$C_{c,soil} = 2 * m_{wheel} * \omega_{n,soil} = 12.816\ kN\ s/m \tag{6.33}$$

Then, the out-of-plane slip damping constant at the contact area ($C_{l,soil}$) is calculated from the following equation.

$$C_{l,soil} = \xi * C_{c,soil} = 0.697\ kN\ s/m \tag{6.34}$$

Table 6.5 shows the parameters used for the calculation of the out-of-plane slip damping constant at the contact area.

Table 6.5: Parameters used in the calculation of the out-of-plane slip damping constant.

Parameter	Symbol	Value	Unit
Logarithmic decrement	δ	0.352	-
Dimensionless damping ratio	ξ	0.0544	-
Damped period of vibration	τ_d	0.1047	s
Undamped natural frequency	ω_n	60.0	rad/s
Critical damping constant	$C_{c,soil}$	12.816	kN s/m
Out-of-plane slip damping constant	$C_{l,soil}$	0.697	kN s/m

6.4 CORNERING CHARACTERISTICS ON SOFT SOIL

The cornering characteristics of a tire running on soft soil are determined using a number of simulations to measure the lateral forces over a range of slip angles from 0° to 20°. The slip angle of a wheel is the angle between the longitudinal axis of the wheel and its direction of travel. A slip angle greater than 0° will generate a force on the tire in the lateral direction, which is referred to here as the lateral force.

6.4.1 CORNERING STIFFNESS ON SOFT SOIL

Figure 6.13 shows an example of the steady state steering simulations used to predict the steady state cornering characteristics on soft soil for a vertical load of 18.9 kN (4250 lbs) and a velocity of 8 km/hr.

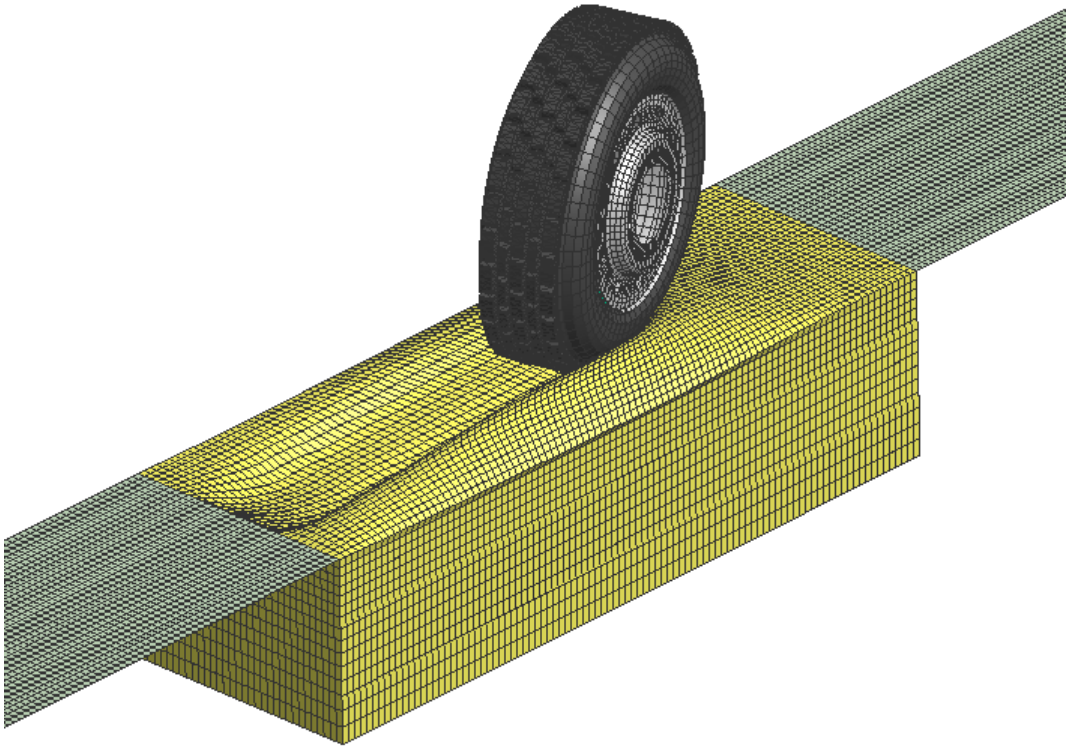

Figure 6.13: Steady state steering test at a slip angle of 20° on soft soil.

The cornering stiffness ($k_{f,soil}$) is defined as the derivative of the lateral force ($F_{y,soil}$) with respect to slip angle (α_{soil}) evaluated at zero slip angle:

$$k_{f,soil} = \left.\frac{\partial F_{y,soil}}{\partial \alpha_{soil}}\right|_{\alpha=0} \tag{6.35}$$

Thus, the cornering stiffness, $k_{f,soil}$, is calculated as 59.8 kN/rad from the slope of the linear curve fit at zero slip angle as shown in Figure 6.14.

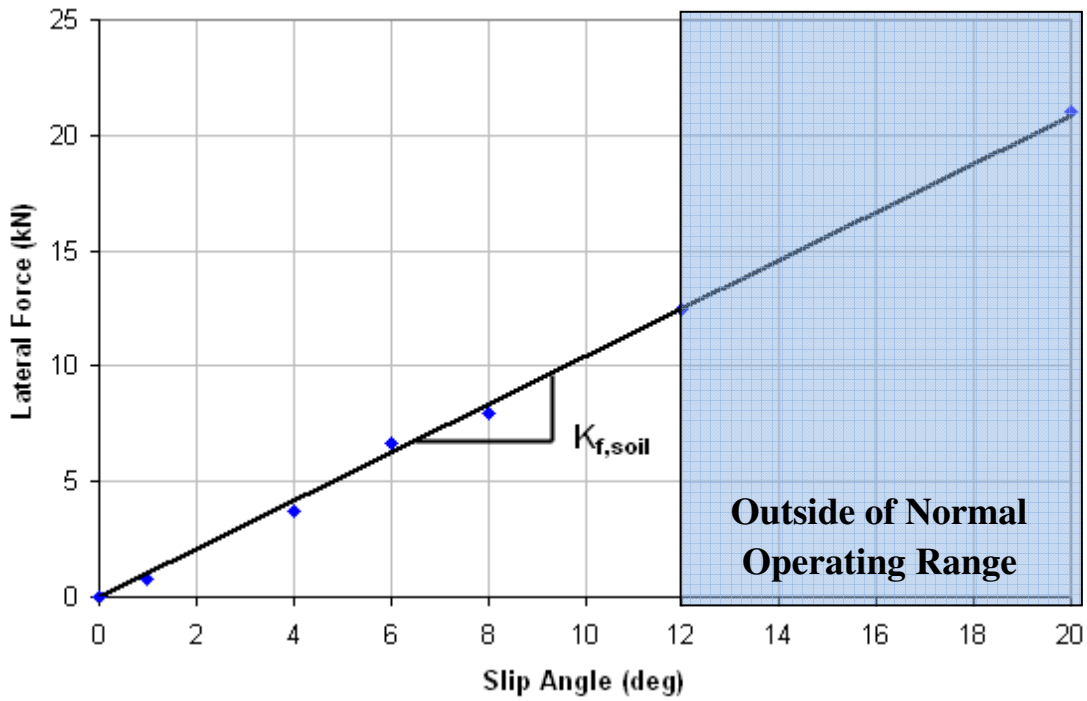

Figure 6.14: Cornering stiffness on soft soil for an 18.9 kN vertical load.

6.4.2 SELF-ALIGNING MOMENT STIFFNESS ON SOFT SOIL

Self-aligning moment stiffness ($k_{M,soil}$) is defined as the derivative of the self-aligning moment ($M_{y,soil}$) with respect to slip angle (α_{soil}) evaluated at zero slip angle.

$$k_{M,soil} = \left.\frac{\partial M_{y,soil}}{\partial \alpha_{soil}}\right|_{\alpha=0} \tag{6.36}$$

Therefore, the self-aligning torque stiffness is predicted as the slope at zero slip angle as shown in Figure 6.15. A self-aligning torque stiffness of 11.1 kN-m/rad is calculated at tire load of 18.9 kN from Figure 6.15. The shaded areas in Figure 6.14 and Figure 6.15 shows the normal operating range for the slip angle of truck tires, which was determined by tire testing at UMTRI (Chae, 2006).

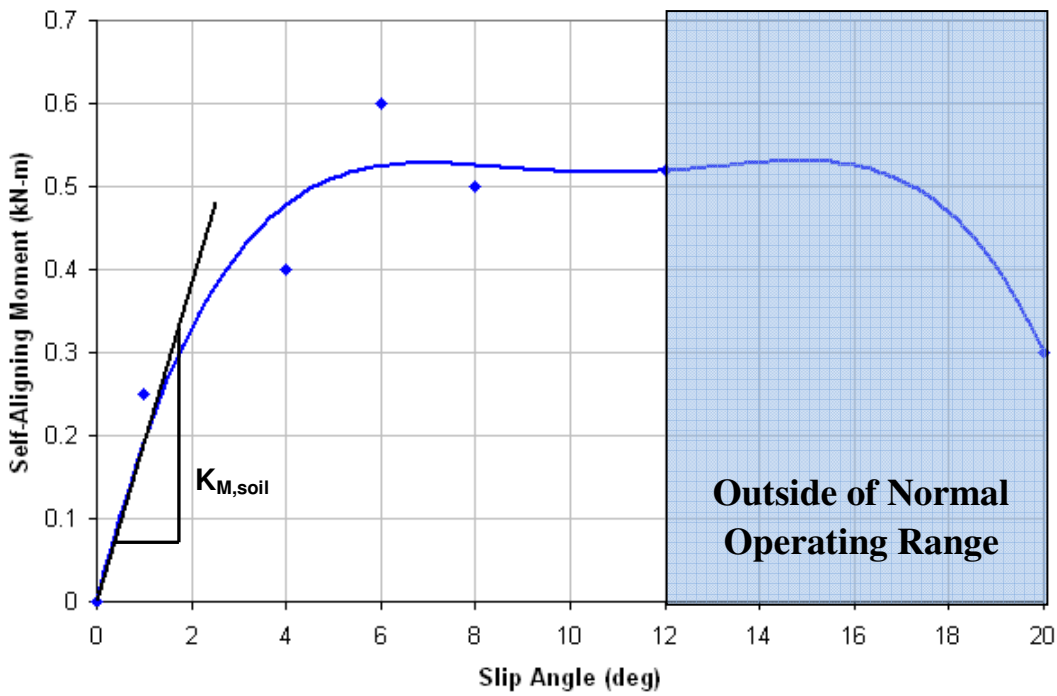

Figure 6.15: Self-aligning moment as a function of slip angle on soft soil for a vertical load of 18.9 kN.

6.4.3 RELAXATION LENGTH ON SOFT SOIL

The relaxation length (σ_{soil}) on soft soil is calculated by the following equation.

$$\sigma_{soil} = \frac{k_{f,soil}}{k_{l,total,soil}} = 0.297 \tag{6.37}$$

Where: $k_{f,soil}$ = the cornering stiffness, and

$k_{l,total,soil}$ = the lateral slip stiffness of the tire.

The relaxation length is dependent on the applied tire load and tire size. However, it is not significantly influenced by other operation conditions, such as speed, but we expect will be affected by the type of surface that the tire is running over. Thus, the relaxation length is usually predicted at low tire speeds such as 5 km/hr.

6.4.4 SUMMARY OF OUT-OF-PLANE RIGID RING MODEL PARAMETERS ON SOFT SOIL

All the out-of-plane characteristic parameters of the rigid ring tire model have been calculated by performing the appropriate virtual FEA tire tests, and the parameters are summarized in Table 6.6 and are valid for an 18.9 kN vertical load.

Table 6.6: Out-of-plane parameters of the rigid ring model on soft soil for an 18.9 kN vertical load.

Parameter	Symbol	Value	Unit
Translational stiffness of sidewall	$k_{by,soil}$	787.4	kN/m
Translational damping of sidewall	$C_{by,soil}$	1.301	kN-s/m
Rotational stiffness of sidewall	$k_{b\gamma,soil}$	276.8	kN-m/rad
Rotational damping of sidewall	$C_{b\gamma,soil}$	0.02295	kN-m-s/rad
Equivalent soil lateral stiffness	$k_{l,soil}$	1078.1	kN/m
Lateral slip stiffness	$k_{l,total,soil}$	201.6	kN/m
Lateral slip damping	$C_{l,soil}$	0.697	kN-s/m
Cornering stiffness	$k_{f,soil}$	59.8	kN/rad
Self-aligning moment stiffness	$k_{M,soil}$	11.1	kN-m/rad
Relaxation length	σ_{soil}	0.297	m

CHAPTER 7

CONCLUSIONS AND FUTURE WORK

7.1 CONCLUSIONS

A new off-road rigid ring model has been successfully developed. The rigid ring parameters for a Goodyear RHD 315/80R22.5 truck tire have been determined for both the on and off-road rigid ring models using Finite Element Analysis (FEA) simulations. Trends in the contact forces, contact patch, self-aligning moment, have also been established. The model is expected to be valid in the range of slip angles of less than 12°, which is within the range for normal driving conditions as determined by tire testing data from the University of Michigan Transportation Research Institute (Chae 2006).

The results show that, in general, for a tire running on a sandy loam the motion resistance coefficient is approximately three times higher than on rigid road. The longitudinal slip stiffness, k_k, is about a factor of four lower for sandy loam than for rigid road. This indicates that the available tractive force on sandy loam is about one-fourth of the available tractive force on rigid road. Interestingly, the longitudinal, or tractive force, appears to continue to increase with slip on sandy loam, while the tractive forces on rigid road level out after reaching a peak around 20% slip.

The cornering stiffness, k_l, on sandy loam is approximately three times lower than the cornering stiffness on rigid road. This is as expected since the soil is able to deform under a lateral force, resulting in a lower force being transmitted to the tire. While Figure 6.14 shows the lateral force a tire on the sandy loam as increasing linearly with slip angle, this is not believed to be the case. When the model is run at high slip angle it is noticed that the soil begins to 'build up' in front on the tire, causing an additional lateral force due to the pushing of the soil. This additional lateral force is probably exceedingly high due to the use of the lack of proper cohesion modeling in the elastic-plastic soil model, which would allow the soil elements to separate from each other during shear.

7.2 RECOMMENDATIONS FOR FUTURE WORK

The linear elastic plastic soft soil model used in this thesis provides some of the characteristics of a soil, but misses many others. Hysteresis effects and damping effects, for example, are not a part of an elastic plastic model. The linear elastic-plastic soil acts like a spring at stresses below the yield stress, and is permanently deformed at stresses above the yield stress. A Drucker-Prager or Mohr-Coulomb yield criterion model would be a better choice, however, software limitations make implementing such a model difficult at best. Nonetheless, the linear elastic-plastic model is a good model to approximate soft soil. To improve the model's accuracy even further Smooth Particle Hydrodynamics (SPH) could be used to represent the soil as individual particles, however, this requires a large amount of computer processing power and may prove to be too costly. If parameters such as cohesion, moisture content, and internal friction angle can be included, the model should more accurately represent soil.

The soil parameters used in this thesis were obtained from multiple sources. No single source was able to provide all of the properties required, therefore averages and approximations were taken from various sources for similar types of soils. Triaxial soil testing on an actual soil of interest is recommended in order to achieve the best possible parameters for a specific soil type.

The friction coefficient, μ, was chosen as a generic value of 0.8 on both rigid road and soft soil. To improve the accuracy of the forces obtained from the FEA simulations, physical experiments should be performed to test the actual friction coefficient on the modeled surfaces. A test rig allowing force measurement while a tire is dragged across a particular surface should be sufficient to determine a dynamic μ. An ideal setup would also allow the addition of different weights to determine how the dynamic μ varies with vertical force on the tire.

The lateral slip model, which comes from Pacejka and Zegelaar, should be re-investigated. A new test may be developed that more intuitively models the slip behavior of the tire. The

current tests seem to combine the effects of the lateral stiffness of the tire with the lateral slip in a way that does not make physical sense.

Further sensitivity analysis on the element sizes in the models should be performed to ensure convergence. Since all of the FEA simulations in the thesis have been run on a workstation class PC it was impossible to decrease element size beyond a certain point. Simulations taking longer than three weeks to run were simply too time consuming for the time allotted for this research. Improvements in processor speeds and the number of processors available would allow these models to be further analyzed.

Finally, the shear characteristics of the soil should be determined and compared with published data. These tests have not yet been performed but are to be a part of future work. Further tests should also be performed to study the effect of speed, load, and inflation pressure on the motion resistance coefficient, and these data could be compiled to provide a look-up table for a wide range of situations that a vehicle may encounter.

REFERENCES

Alcock, R. and Wittig, V., "An Empirical Method of Predicting Traction," *Journal of Terramechanics,* Vol. 29 no. 4/5, pp. 381-394, 1992.

Allison, D. J., and Sharp, R. S., (1997), "On the low Frequency in-plane forced Vibrations of Pneumatic Tire/Wheel/Suspension Assemblies," International Colloquium on Tire Models for Vehicle Dynamic Analysis, Proceedings of the Second International Colloquium on Tire Models for Vehicle Dynamic Analysis, pp. 151-162.

Allen II, J. R., (2007), "Rigid Ring Quarter-Vehicle Model for Durability and Ride Comfort Predictions," M.S. Thesis, The Pennsylvania State University, University Park, PA.

Al-Shayea, N.A., Mohib, K.R., and Baluch, M.H., "A Plastic-Damage Model for Stress-Strain Behavior of Soils," *International Journal of Damage Mechanics*, Vol. 12, pp. 305-329, 2003.

Bekker, M. G. "Introduction to Terrain-Vehicle Systems," The University of Michigan Press, Ann Arbor, 1969.

Bekker, M. G. "Off-The-Road Locomotion: Research and Development in Terramechanics," The University of Michigan Press, Ann Arbor, 1960.

Bekker, M. G. "Theory of Land Locomotion," The University of Michigan Press, Ann Arbor, 1956.

Brixius, W. W. "Traction Prediction Equations for Bias Ply Tires," ASAE Paper No. 87-1662. ASAE, St. Joseph, MI 49085, 1987.

Bruni, S., Cheli, F., and Resta, F., (1997), "On the Identification in Time Domain of the Parameters of a Tire Model for the Study of In-plane Dynamics," International Colloquium on Tire Models for Vehicle Dynamic Analysis, Proceedings of the Second International Colloquium on Tire Models for Vehicle Dynamic Analysis, pp. 136-150.

Captain, K. M., Boghani, A. B. and Wormley D. N, (1979), "Analytical Tire Models for Vehicle Dynamic Simulation," *Vehicle System Dynamics,* Vol. 8.

Chae, S., Öijer, F., El-Gindy, M., Trivedi, M., and Johansson, I., (2005), "In-Plane and Out-of-Plane Dynamic Response Predictions of a Truck Tire Using Detailed Finite Element and Rigid Ring Models," 2005 ASME International Mechanical Engineering Congress and Exposition, Proceedings of IMECE'05, Paper No. IMECE2005-79083, Nov. 5-11, FL.

Chae, S., (2006), "Nonlinear Finite Element Modeling And Analysis of a Truck Tire," Ph.D. Thesis, The Pennsylvania State University, University Park, PA.

Chang, Y.P., El-Gindy, M., Streit, D., (2003), "Literature Survey of Transient Dynamic Response Tire Models," *Heavy Vehicle Systems*, Vol. 10, No. 1-2, pp. 86-111, 2003

Davis, D. C, (1974), “A Radial-Spring Terrain-Enveloping Tire Model,” *Vehicle System Dynamics*, Vol. 3.

Fervers, C. W. "Improved FEM Simulation Model for Tire-Soil Interaction", *Journal of Terramechanics*, Vol. 41, pp. 87-100, 2004.

Goodyear, (2008), “Goodyear Truck Tyres Technical Data Book”, Retrieved on July 1, 2009. <http://eu.goodyear.com/middle_east_en/images/GO2318_TTDB_1-32%20LUX-ENG_tcm195-10683.pdf>.

Grahn, M., “Predictions of Sinkage and Rolling Resistance for Off-The-Road Vehicles Considering Penetration Velocity”, *Journal of Terramechanics*, Vol. 28, No. 4, pp. 339-347, 1991.

Guo, K., (1993), “Tire Roller Contact Model for Simulation of Vehicle Vibration Input,” SAE Technical Paper No. 932998.

Guo, K., (1998), “A Model of Tire Enveloping Properties and Its Application on Modeling of Automobile Vibration System,” SAE Technical Paper No. 980253.

Hiroma, T., Wanjii, S., Kataoka, T., and Ota, Y. "Stress Analysis Using FEM on Stress Distribution Under a Wheel Considering Friction with Adhesion Between a Wheel and Soil", *Journal of Terramechanics*, Vol. 34, No. 4, pp. 225-233, 1997.

Idaho OnePlan, (2009), “Soil Triangle”, The Idaho Association of Soil Conservation Districts, Retrieved July 1, 2009. <http://www.oneplan.org/Images/soilMst/SoilTriangle.gif>.

Janosi, Z. J. "Analysis and Presentation of Soil-Vehicle Mechanics Data", *Journal of Terramechanics*, Vol. 2, No. 3, pp. 69-79, 1965.

Janosi, Z., Hanamoto, B. "Analytical Determination of Drawbar-pull as a Function of Slip for Tracked Vehicles in Deformable Soils", *Proceedings of the 1st International Conference on Terrain-Vehicle Systems*, Turin, 1961.

Karmakar, S. and Kushwaha, R. L. "Soil Viscosity and Yield Stress Measurement Using a Motorized Rheometer", Proc. of the ASABE Meeting Presentation, Paper No. 061094, July 9-12, Portland, OR., 2006.

Kim, S., and Savkoor, A. R., (1997), “The Contact Problem of In-Plane Rolling of Tires on a Flat Road,” International Colloquium on Tire Models for Vehicle Dynamic Analysis, Proceedings of the Second International Colloquium on Tire Models for Vehicle Dynamic Analysis, pp. 189-206.

Loo, M., (1985), “A Model Analysis of Tire Behavior Under Vertical Loading and Straight-Line Free Rolling,” *Tire Science and Technology*, Vol. 13, No. 2, pp. 67-90.

Masad, E., Balasingam, M., and Chameu, J.L., “Stress-Strain Model for Clays with Anisotropic Void Ratio Distribution”, *International Journal for Numerical and Analytical Methods in Geomechanics*, Vol. 22, pp. 393-416, 1998.

Michelin AG, (2009), Michelin AG – Advantages – Bias vs Radial, Retrieved February 24, 2009. <http://www.michelinag.com/agx/en-US/products/advantages/bias_radial/bias_radial.jsp>

Mulungye, R. M., Owende, P. M. O. and Mellon, K. "Finite Element Modeling of Flexible Pavements on Soil Subgrades", *Journal of Materials and Design*, Vol. 28, No. 3, pp. 739-756, 2006.

Okello, J. A. "A Review of Soil Strength Measurement Techniques for Prediction of Terrain Vehicle Performance", *Journal of Agricultural Research*, Vol. 50, pp. 129-155, 1991.

Pacejka, H. B., and Besselink, I. J. M., (1997), “Magic Formula Tire Model with Transient Properties,” International Colloquium on Tire Models for Vehicle Dynamics Analysis, Proceedings of the Second International Colloquium on Tire Models for Vehicle Dynamic Analysis, pp. 234-249.

Schmeitz, A. J. C., Jansen, S. T. H., Pacejka, H. B., Davis, J. C., Kota, N. N., Liang, C. G., and Lodewijks, G., (2004), “Application of a Semi-emphirical Dynamic Tyre Model for Rolling over Arbitrary Road Profiles,” *Int. J. of Vehicle Design*, Vol. 36, Nos. 2/3, pp. 194-215.

Sui, J. and Hirshey, J., (1999), “Evaluation on Analytical Tire Models for Vehicle Vertical Vibration Simulation Using Virtual Tire Testing Method,” SAE Technical Paper No. 1999-01-0786.

Tönük, E., Ünlüsoy, Y.S., “Prediction of automobile tire cornering force characteristics by finite element modeling and analysis”, *Computers & Structures*, Vol. 79, pp. 1219-1232, 2001.

Wallentowitz, H., Köhn, P., Holdmann, P., “Dynamic Properties of Tyres – Testing and Simulation”, SAE Technical Paper 1999-01-0790, 1999.

Wismer, R. D. and Luth, H. J. "Off-Road Traction Prediction for Wheeled Vehicles", *Journal of Terramechanics*, Vol. 10, pp. 49-61, 1973.

Wong, J. “Theory of Ground Vehicles”, John Wiley & Sons, Inc., New York, 2001.

Yong, R. N., Fattah, E. A., Brunsinsuk, P. “Analysis and Prediction of Tyre-Soil Interaction Performance Using Finite Elements”, *Journal of Terramechanics*, v. 15, n 1, Mar, 1978, p 43-63.

Zegelaar, P. W. A. and Pacejka, H. B., (1997), “Dynamic Tyre Responses to Brake Torque Variations,” *Vehicle System Dynamics Supplement*, Vol. 27, pp. 65-79.